**The Thesis Committee for Siddharth Balasubramanian**
**Certifies that this is the approved version of the following thesis:**

# Supplemental Heat Rejection in Ground Source Heat Pumps for Residential Houses in Texas and other Semi-Arid Regions

**APPROVED BY**
**SUPERVISING COMMITTEE:**

**Supervisor:** ______________________________
Glenn Y. Masada

**Co Supervisor:** ______________________________
Tess J. Moon

# Supplemental Heat Rejection in Ground Source Heat Pumps for Residential Houses in Texas and other Semi-Arid Regions


**by**

**Siddharth Balasubramanian, BTech**


**Thesis**

Presented to the Faculty of the Graduate School of

The University of Texas at Austin

in Partial Fulfillment

of the Requirements

for the Degree of

**Master of Science in Engineering**

**The University of Texas at Austin**

**December 2011**

# Dedication

To my Father and Mother for all their love and support.

## Acknowledgements

I would like to thank my co advisers, Dr. Glenn Y. Masada and Dr. Tess J. Moon, who have guided me through the last one and a half years of my research. Their invaluable advice, confidence in my abilities and engagement in thought provoking discussions have resulted in this thesis. I wish to thank Paul Bony, Mike Hammond and Dee Brower of Climate Master for sharing their knowledge from the industry. Expert inputs and in kind support from Paul Ballentine of Solennium, Chris Winland of Good Company Associates and Mel Riser of Tool Works were extremely helpful and I wish to extend my thanks to them. The technical support Austin Energy, Austin Technology Incubator and Texas is Hot is also appreciated.

I would like to thank my colleagues, Jonathan Gaspredes and Jacob Blair, for helping me in various aspects of this thesis. I would also like to thank my friends – Vinay Mohan, Deepjyoti Deka, Arindam Goswami, Columbia Mishra – for making my graduate school experience a wonderful one. Last, but not the least, I must thank my family – father, mother, brother and sister - for all their love and support.

I would like to acknowledge the financial support for this work from the U.S. Department of Energy Office of Energy Efficiency and Renewable Energy, Recovery Act—Geothermal Technologies Program: Ground Source Heat Pump Award No. DE-EE0002803.

## Abstract

**Supplemental Heat Rejection in Ground Source Heat Pumps for Residential Houses in Texas and other Semi-Arid Regions**

Siddharth Balasubramanian, M.S.E

The University of Texas at Austin, 2011

Supervisors: Glenn Y. Masada and Tess J. Moon

Ground source heat pumps (GSHP) are efficient alternatives to air source heat pumps to provide heating and cooling for conditioned buildings. GSHPs are widely deployed in the midwest and eastern regions of the United States but less so in Texas and the southwest regions whose climates are described as being semi-arid. In these semi-arid regions, building loads are typically cooling dominated so the unbalance in energy loads to the ground, coupled with less conductive soil, cause the ground temperature to increase over time if the ground loop is not properly sized. To address this ground heating problem especially in commercial building applications, GSHPs are coupled with supplemental heat recovery/rejection (SHR) systems that remove heat from the water before it is circulated back into the ground loops. These hybrid ground source heat pump systems are designed to reduce ground heating and to lower the initial costs by requiring less number of or shallower boreholes to be drilled.

This thesis provides detailed analyses of different SHR systems coupled to GSHPs specifically for residential buildings. The systems are analyzed and sized for a 2100 $ft^2$ residential house, using Austin, Texas weather data and ground conditions. The SHR systems investigated are described by two heat rejection strategies: 1) reject heat directly from the water before it enters the ground loops and 2) reject heat from the refrigerant loop of the vapor compression cycle (VCC) of the heat pump so less heat is transferred to the water loop at the condenser of the VCC.

The SHR systems analyzed in this thesis are cooling towers, optimized VCC, expanded desuperheaters and thermosyphons. The cooling towers focus on the direct heat rejection from the water loop. The VCC, desuperheater, and thermosyphon systems focus on minimizing the amount of heat rejected by the VCC refrigerant to the water loop. In each case, a detailed description of the model is presented, a parametric analysis is provided to determine the amounts of heat that can be rejected from the water loop for various cases of operation, and the practical feasibility of implementation is discussed. An economic analysis is also provided to determine the cost effectiveness of each method.

# Table of Contents

# List of Tables

# List of Figures

# Chapter 1. Introduction

## OVERVIEW OF GROUND SOURCE HEAT PUMP (GSHP)

Ground source heat pumps (GSHP) can reduce energy consumption for heating and cooling residential homes by up to 40% compared to conventional air-source heat pumps [Fisher and Rees, 2005]. In the cooling mode of operation, an air source heat pump rejects heat from the condenser of the HVAC (Heating, Ventilation and Air Conditioning) system into the ambient air, while a GSHP rejects the heat deep into the ground. The GSHP takes advantage of the nearly constant ground temperature (below 6m/20ft – [EERE, 2011a]), which is lower than the ambient air temperature during summers. The heat extracted from the conditioned space is transferred to water, in the GSHP, or to air, in the air source heat pump, so the lower ground temperatures provide more effective heat transfer than from the air. During the heating mode of operation, heat must be extracted from the ground or air and transferred to the conditioned space, so the higher ground temperatures provide more effective heat transfer than the cold air temperatures of winter. A measure of heat pump performance is the Coefficient of Performance (COP), which is defined as the ratio of energy provided to the building to the energy consumed. The COP for GSHPs is between 3-6 compared to 1.75 – 2.5 for air source heat pumps [EERE, 2011b].

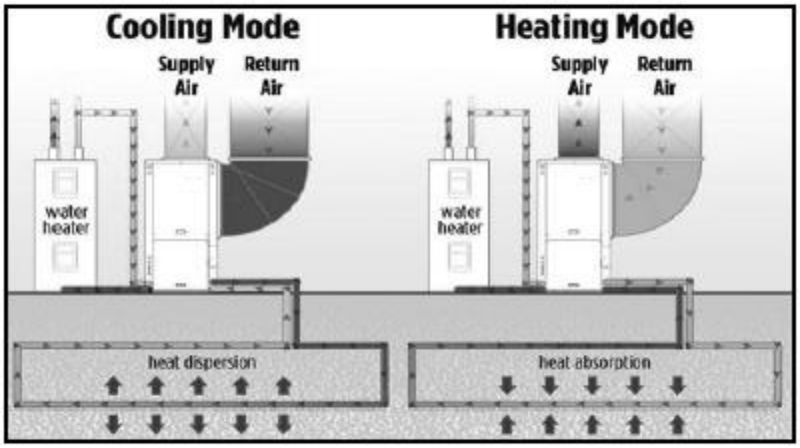


Figure 1-1: Operation of Ground Source Heat Pump (Fiore, G, 2010)

Figure 1.1 shows the two operating modes, cooling and heating, of the GSHP. When the heat pump is operating in the cooling mode, the water removes heat from the condenser and flows into the ground loop where it rejects heat to the ground. In the process, the water cools and is pumped back to the heat pump, and the cycle repeats. In the heating mode, the water in the ground loop absorbs heat from the ground and transfers that heat to the heat pump evaporator, thereby proving heat to the building. In the process, the water loses heat and flows back into the ground, and the cycle repeats.

Figure 1-2 shows possible open and closed loop GSHP systems. Closed loop systems, in which the circulating water flows in a closed loop, have three types of loop configurations: horizontal, vertical and pond lake. In the horizontal configuration, the loops are coiled and placed in shallow trenches 1 to 2m (3.3 to 6.6ft) [Chiasson A. D, 1999] deep. The vertical configuration has vertical boreholes drilled to depths of 80 to

110 m (260 – 360 ft) [OEE, 2009] into the ground. The pond/lake configuration has coiled loops immersed in a body of water near the building. In the open loop system, there are two separate bodies of water; a source and a sink. In this study, the focus is on the vertical borehole configuration since it is the most widely used configuration in Texas and other semi-arid regions.

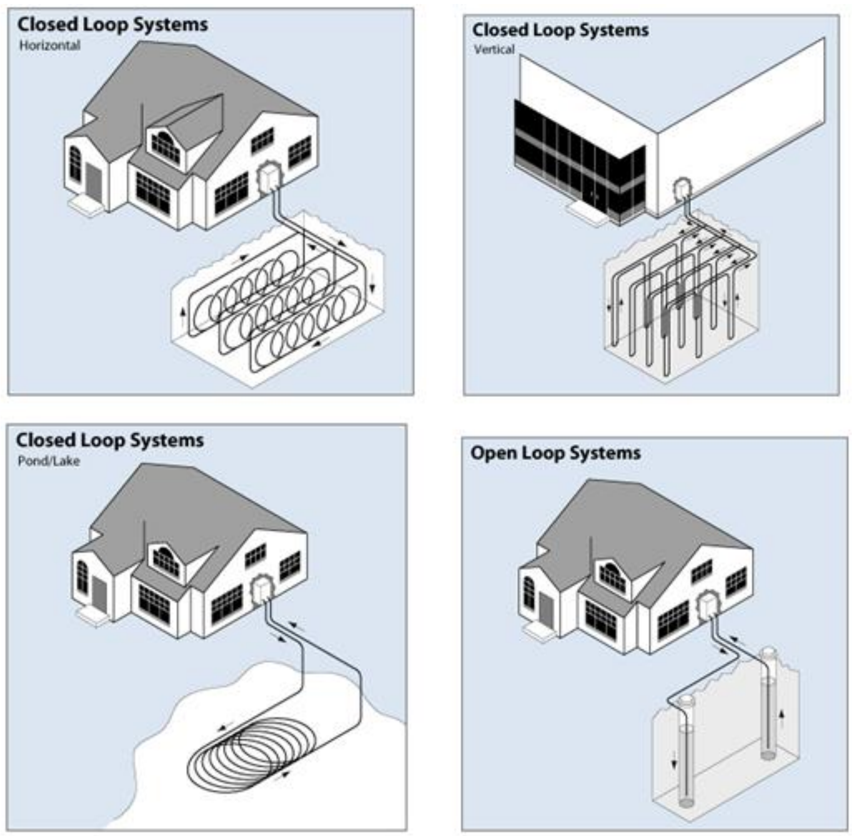


Figure 1-2: Different types of GSHPs [US Dept of Energy, 2011a]

One of the biggest barriers to the installation of GSHPs is that their initial costs are 20 – 40% higher than installing standard air source heat pumps [Kavanaugh and Rafferty 1997]. In Texas, a 90 m (300 ft) borehole installation costs around $ 3,000 and one such borehole is needed for every ton (3.5 kW) of cooling needed [Mike Hammond, 2011]. However, the higher initial costs are offset by the higher operating performance of GSHPs, which leads to lower operating costs.

In hot and semi-arid regions like Texas, the building loads are cooling dominated, which leads to more heat being rejected into the ground (cooling mode) than absorbed out of the ground (heating mode). This net heat into the ground gradually increases the ground temperature and hence, the entering water temperature to the heat pump becomes higher and reduces the EER of the GSHP. EER of a heat pump is defined as the ratio of the cooling provided to the building to the power consumed. The ground heating is exacerbated by the poor soil conductivity properties of the semi-arid regions. The decrease in operating efficiency due to ground heating and the high initial costs are the primary reasons for lower deployment of GSHPs in Texas and other semi-arid regions compared to other parts of the United States.

Employing supplemental heat rejecting devices can reduce the initial costs and reduce ground heating. When coupled with GSHPs, the resulting systems are called Hybrid Ground Source Heat Pumps. Analysis of these systems is the main focus of this thesis.

### HYBRID GROUND SOURCE HEAT PUMPS (HGSHP)

Hybrid Ground Source Heat Pumps (HGSHP) are systems that couple a supplemental heat rejection (SHR) or extraction device to a ground source heat pump. For cooling dominated buildings, a SHR device, such as a cooling tower, is deployed, while for a heating dominated buildings, a supplemental heat extraction device, such as a boiler, is added. When designing GSHPs for cooling dominated regions, the length of the boreholes is sized based on the peak cooling loads, even though the peak loads may last only for a few days. To reduce drilling costs and ground heating, SHR devices are added to reject some of the ground loop heat outside the ground. The most common SHR for commercial buildings uses a cooling tower as shown in Figure 1-3. After removing heat from the heat pump condenser during the cooling mode of operation, the ground loop water flows into the cooling tower, where some of its heat is rejected to the moist air flow of the tower. The cooler water then flows back into the ground where additional heat is rejected to the ground. Determining the division of the amount of heat rejected in the cooling tower and to the ground is a design problem which will be discussed in later sections. [Hackel (2008), Xu (2007), Cullin and Spitler (2010)].

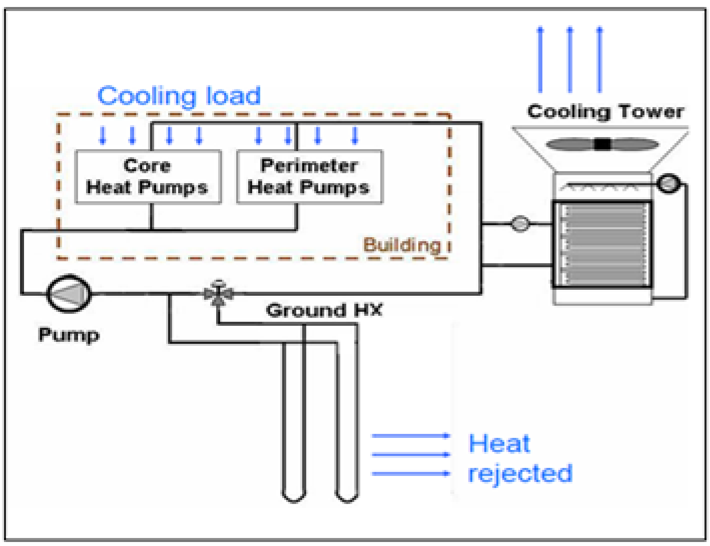


Figure 1-3: Schematic of HGSHP [Hackel, 2008]

An air source heat pump is another commonly used SHR device. This combination is called the dual source heat pump where both air and ground are used as a heat sinks and sources. This combination is convenient since air source heat pumps are the norm for residential home. As a SHR device, the air source heat pump is connected in series with the ground loop. Water leaving the GSHP is sent to the air source heat pump before returning to the ground. The length of the ground loop can be reduced by 130 – 190 ft (39.6 – 57.9 m) per ton of cooling load [DOE Federal Energy Management Program, 2000]. DOE conducted a study on an experimental house located in Fort Stewart, Georgia. A dual source heat pump with a combined cooling capacity of 3 tons was installed. They found a 31% reduction in energy consumption during the cooling season, when compared to energy consumption by a stand-alone air source heat pump. Currently, a company called Global Energy & Environmental Research Inc. (GEER) in Florida manufactures these devices for residential use. These systems are not very popular since cooling towers as SHR systems are more efficient than air source heat pumps in warm climates

Ramamurthy et al (2001) studied HGSHPs using a pond as the SHR device. A section of the water loop was submerged into the pond to reject some heat into the pond before returning to the ground. The study used a 14,205 ft$^2$ (1,319.6 m$^2$) building in Houston. It was found that by using the pond as a SHR device, the 20 year life cycle cost of the HGSHP was reduced by up to 65% when compared to a GSHP.

Cooling towers, dual source heat pumps and pond supplement SHRs have been implemented in various places in the United States. In this thesis, new SHR ideas and systems will be analyzed to reduce ground heating.

**OBJECTIVES**

The objective of this thesis is to develop and assess new supplemental heat rejection systems for residential houses in Texas. The SHR systems investigated are described by two heat rejection strategies: 1) reject heat directly from the water before it enters the ground loops and 2) reject heat from the refrigerant loop of the vapor compression cycle (VCC) of the heat pump so less heat is transferred to the water loop at the condenser of the VCC. The technical feasibility and the cost effectiveness of each method will be analyzed in detail.

A 2100 sq ft (195 sq m) residential house shown in Figure 1-4 will be used as the test case to assess the performance of each SHR system. The GSHP used for the house will be based upon the following conditions: 30 – 45˚C ( 86 – 113˚F) ground loop entering water temperature, 12 gpm (0.748 kg/s) water flow rate, 32.2 ˚C (70˚F) ground temperature and ambient weather conditions for Austin, Texas. Based upon yearly heating loads computed by [Gaspredes, 2011], the heat pump operates in the cooling mode for 2022 hours and in the heating mode for 277 hours.

Figure 1-4: 2100 sq ft Residential House in Texas [Gaspredes, 2011]

The thesis will be divided into four additional chapters, and each chapter will describe the motivation, goal, analysis and results for each SHR system under consideration.

Chapter 3 will focus on cooling towers as SHR devices to reject heat from the water loop of the GSHP for residential homes.

Chapters 4, 5 and 6 will focus on minimizing the heat rejected to the condenser from the refrigerant loop of the vapor compression cycle (VCC) of the heat pumps. The heat rejection potential is higher in the refrigerant loop than from the water exiting the heat pump since the refrigerant temperature at the compressor discharge is in the range 50 - 70˚C (122 – 158˚F), as opposed to the water temperatures in the range of 30 – 45 ˚C ( 86 – 113˚F). Chapter 4 will analyze the modification of the VCC required to reduce the total heat rejected to the condenser. This analysis will include optimizing VCC parameters, such as suction superheat, condenser subcooling and mass flow rate of refrigerant.

Chapter 5 will assess the use of desuperheaters to function beyond extracting heat for heating domestic hot water. The maximum operating limits of the desuperheater will be analyzed to reject as much heat from the refrigerant as possible.

Chapter 6 will assess the use of thermosyphons, a gravity driven heat pump, to extract heat from the refrigerant loop. These thermosyphons are normally used in cold climates to freeze the ground in winter and are effective due to the temperature difference between the ground and the ambient air during the winter. In our application, we analyze the effectiveness of thermosyphons in hot climates

Chapter 7 summarizes the findings of this thesis on the technical and economic analyses of various SHR devices.

# Chapter 2. Cooling Tower

## INTRODUCTION

Cooling towers are devices used to transfer heat from a working fluid by evaporation of water flowing external to the working fluid. Closed wet cooling towers that are used in this analysis use three fluids: working fluid water, spray water and air. The working fluid to be cooled flows through the pipes of the cooling tower. Spray water is injected downward over the rows of pipes and is collected at the bottom to be re-circulated. Air from a fan is blown upward across the rows of tubes. Heat is transferred from the working fluid to the air by evaporation of the spray water droplets falling on the pipes. Spray water vapor is then entrained by the blowing air, and the air becomes saturated by the time it leaves the top end of the cooling tower. Make-up water is needed to replace the evaporated water. The two main operating costs associated with the cooling tower are the fan power and make-up water.

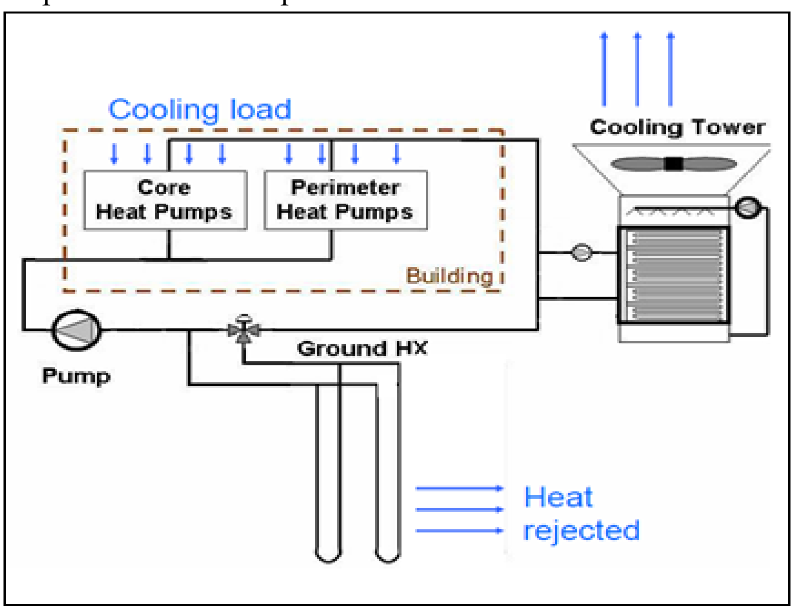


Figure 2-1: Schematic of HSGHP using a Cooling Tower [Scott Hackel, 2008]

A hybrid ground source heat pump (HGSHP) is shown in Figure 2.1 with the ground source heat pump integrated with a cooling tower as a supplemental heat rejection (SHR) device to reject some quantity of heat from the ground loop water before entering the ground. In cooling dominated areas cooling towers are used as SHR devices due to their simple mode of operation and low costs. HGSHPs are used to decrease the high fixed cost of drilling by requiring shallower boreholes and to reduce ground heating over long periods of time, which would otherwise decrease the efficiency of the GSHP. Some of the important factors in determining the costs of a HGSHP are: length of boreholes, size of cooling tower and the control algorithm.

## DESIGN OF HGSHP

The design of a HGSHP involves sizing the length of the borehole and then the capacity of the SHR. Figure 2-2 shows a schematic of the balance between the ground loop (borehole) length ratio (length using a HGSHP/length using GSHP only) and the percentage of heat added/rejected by the SHR system for commercial building loads (Cullin and Spitler , 2011). The right hand side of the plot is for cooling-dominated operation and shows the ratio and the percentage of heat rejected by the SHR system. For example, point 2 denotes the case where the SHR system rejects 60% of the total heat and the ratio of the ground loop lengths is 40%.

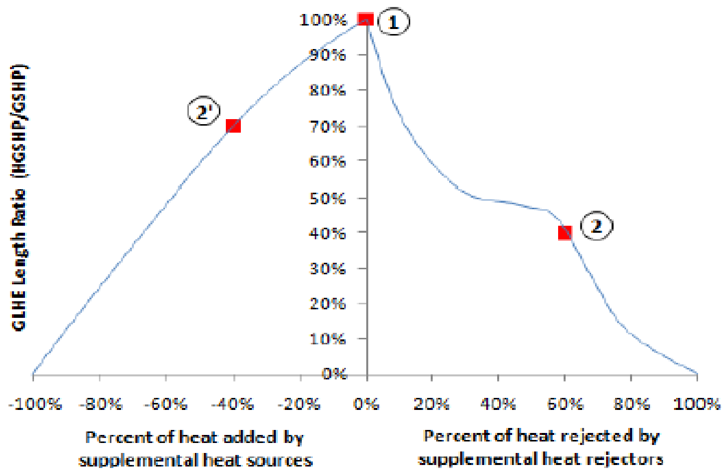


Figure 2-2: GLH Length Ratio vs Percent Heat Rejected by SHR system [Cullin and Spitler, 2011]

Three studies were done on a building in Houston, TX. A 52 storey office building was taken, and three stories of the building were evaluated. The building had a peak heating load of 730 kW (2940 kBtu/h) and a peak cooling load of 819 kW (2794.5 kBtu/h). The number of heating hours in a year was 20 and the number of cooling hours was 1121. The number of boreholes drilled were 120, in a 10 by 12 rectangular grid. The studies by Xu [2007], Hackel et. al [2009] and Cullin and Spitler [2010] are briefly described below.

Xu (2007) used an optimization method to minimize the life cycle cost of the HGSHP over a period of 20 years. In that method, ground loop length and the cooling tower capacity among other parameters (control of the cooling tower) were varied to determine the lowest life cycle cost (LCC). That is, for different ground loop lengths and cooling tower capacities, the LCC were calculated and the minimum among those were the optimized case. With this method, Xu obtained an optimum ground loop length of 5,544 m (18,188 ft) and a cooling tower of size 52 tons (182 kW).

Hackel et al (2009) sized the HGSHP ground loop based on the peak heating load. This ground loop length satisfied some of the cooling needs, and the rest was satisfied by a cooling tower. The resulting ground loop length obtained was 8,061 m (26,446 ft) and a cooling tower capacity of 164 tons (574 kW). The cooling tower was sized to 130% of the unmet cooling load by the ground loop. This was obtained by varying the size of the cooling tower and optimizing the LCC.

Cullin and Spitler (2010) determined the optimal HGSHP design by treating the sizing of the ground loop and the cooling tower as an optimization problem to minimize the error between the desired and the calculated maximum and minimum temperatures into the heat pump. With this strategy, they obtained a ground loop length of 5,769 m (18,920 ft) and a cooling tower capacity of 104 tons (364 kW).

### COOLING TOWER MODEL

Hasan and Siren [2002] developed a detailed cooling tower model for closed wet cooling towers (CWCT). In a CWCT, heat rejection from the working fluid flowing in the tubes is achieved by evaporation of spray water. The working fluid never comes in contact with the spray water to prevent contamination. This type of unit is also called an indirect evaporator. Heat removal from the cooling water is achieved by both sensible heat (convection) and latent heat (evaporation), although the latter dominates. The small quantity of water that evaporates is carried away by the air that blows from below.

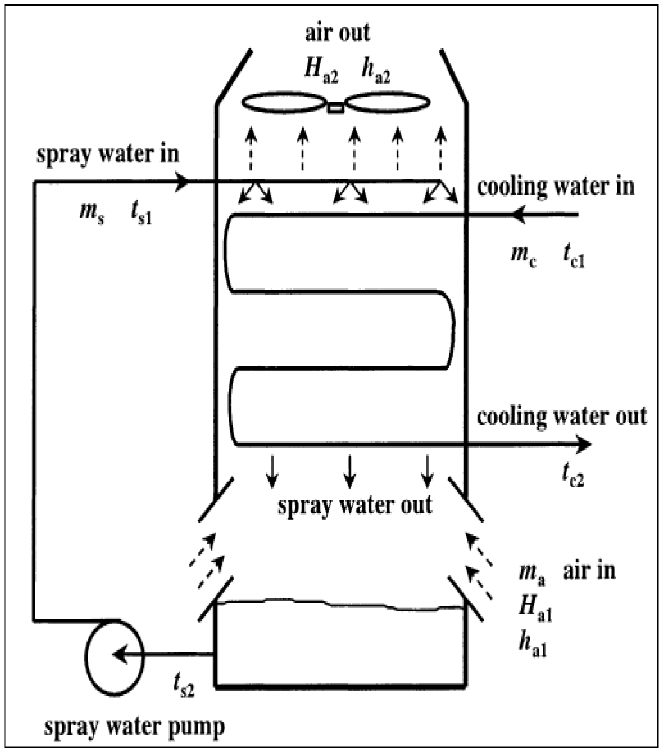


Figure 2-3: Schematic of Cooling Tower for Model [Hasan and Siren, 2002]

Figure 2-3 shows a schematic of the cooling tower. It shows the three fluids and their initial and final conditions as they move from one end of the tower to the other. The exit temperature of the cooling water and the heat rejected, for a given set of conditions (inlet air conditions, mass flow rate of air and spray water), are computed from the governing equations of an elemental control volume cutting across a tube cross-section shown below.

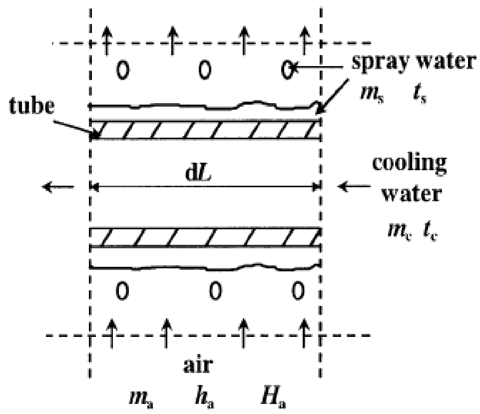


Figure 2-4: Control Volume

Figure 2-4 shows the control volume with inlet conditions of the cooling water, air and spray water.

*<u>Heat Transfer from Cooling Water to Spray Water</u>*

Due to the temperature gradient between the cooling water temperature $(t_c)$ and spray water temperature$(t_s)$, heat transfer occurs through the tube wall. The rate of heat lost by the cooling water $(dq_c)$ is

$$dq_c = m_c C_W dt_c = -U_o(t_c - t_s)dA \tag{2.1}$$

where $(U_o)$ is the overall heat transfer coefficient based on the outer area of the tube and $C_w$ is the specific heat capacity of water contained in the control volume. $U_o$ accounts for the heat transfer coefficient between the cooling water and the internal surface of the wall $(\alpha_c)$, the tube wall thermal conductivity $(k_w)$ and the heat transfer coefficient between the external surface of the wall and the spray water bulk $(\alpha_s)$, which is a function of mass flow rate of spray water.

*<u>Heat Transfer from Air-Water Interface to the Air</u>*

Heat gained by the air stream $(dq_c)$ is due to heat transferred from the air-water interface. It consists of sensible part $(dq_{sn})$ and latent part$(dq_L)$.

$$dq_a = m_a dh_a = dq_{sn} + dq_L \tag{2.2}$$

Substituting for both the heats,

$$dq_a = m_a dh_a = \alpha_i (t_i - t_a) dA + k(H_i' - H_a') h_{fg} dA \tag{2.3}$$

where $\alpha_i$ is the heat transfer coefficient for the air side of the interface, $h_{fg}$ is the latent heat of evaporation of water and $H_i{}'$ is the humidity ratio of saturated moist air at the interface temperature $t_i$ and $k$ is the mass transfer coefficient, which is a function of flow rate of air.

The enthalpy of air and water vapor mixtures is given by

$$h_a = C_H t_a + h_{fg} H_a \tag{2.4}$$

where $C_H$ is the specific heat capacity of humid air which could be considered constant.

Substituting for temperature from Equation (2.4), Equation (2.3) yields

$$m_a dh_a = \left\{ \alpha_i \left[ \frac{( h_i' - h_{fg} H_i')}{C_H} - \frac{(h_a - h_{fg} H_a)}{C_H} \right] + k(H_i' - H_a) h_{fg} \right\} dA \tag{2.5}$$

which is rewritten as

$$m_a dh_a = \left[ \frac{\alpha_i}{C_H} (h_i' - h_a) + k h_{fg} \left(1 - \frac{\alpha_i}{k C_H}\right) (H_i' - H_a) \right] dA \tag{2.6}$$

$(\alpha_i / k C_H )$ is called the Lewis Number $(Le)$, which expresses the relative rates of energy and mass in a system. Le is taken to be 1 for air and water vapor mixtures. Hence Equation (2.6) is simplified to

$$m_a dh_a = k\left(h_i' - h_a\right)dA \tag{2.7}$$

The liquid side of the interface offers a negligible resistance to the heat transfer and hence the interface enthalpy ($h_i'$) in Equation (2.7) could be considered equal to the saturated enthalpy ($h_s'$) at the spray water temperature($t_s$). Therefore, Equation (2.7) is rewritten as

$$m_a dh_a = k(h_s' - h_a)dA \tag{2.8}$$

Equation (2.8) is called the Merkel equation and it shows that the energy transfer can be represented by a process based on the enthalpy difference between air-water interface and the bulk air as the driving force.

*Total Energy Balance of the Control Volume*

The energy balance for the three streams flowing through the control volume is given by

$$dq_a + dq_c + dq_s = 0 \tag{2.9}$$

Expressing the heat transfer in terms of the mass flow rate, specific heat and temperature, Equation (1.9) becomes

$$m_c C_W dt_c + m_a dh_a + m_s C_W dt_s = 0 \tag{2.10}$$

*Spray Water Temperature Distribution*

The spray water temperature varies inside the cooling tower according to the height of the bank of pipes. The assumption is made that heat is transferred only by evaporation. Hence

$$t_{s1} = t_{s2} \tag{2.11}$$

*Mass Balance*

The spray water evaporation is calculated from the mass balance in the Control Volume.

$$m_e = m_a dH_a = k(H_s' - H_a') \tag{2.12}$$

The mass transfer coefficient of air is given by the following relation:

$$k = .065 * m_a^{0.773} \tag{2.13}$$

Hence, the problem can be described based on 5 known values and 5 unknown values give by Table 2.1

Table 2.1: Known and Unknown Values

| Given | Unknown |
|---|---|
| $(m_a)$ | $(t_{s1})$ |
| $(m_w)$ | $(t_{s2})$ |
| $(h_{a1})$ | $(h_{a2})$ |
| $(H_{a1})$ | $(H_{a1})$ |
| $(t_{c1})$ | $(t_{c2})$ |

Five variables are given and the other five are unknown, however there are five equations, (2.1), (2.8), (2.10), (2.11), (2.12), which are solved iteratively to determine the five unknowns. Values of all parameters mentioned in the equation is given in Appendix A.

Each row of pipes in the cooling tower is taken as a control volume element. The procedure starts by guessing values for $h_{a2}$ and $t_{s1}$ in the top row of the tower. Mass balance and energy balance is carried out for each of the rows as one goes down the cooling tower and at row 1, $t_{s2}$ is finally evaluated. For a given $h_{a2}$, $t_{s1}$ is varied until $t_{s1}$ and $t_{s2}$ are equal. Once this is done, the calculated value of $h_{a1}$ at the first row is checked if it is equal to the known value specified in the problem. If not, the initial guess of $h_{a2}$ is changed and iterated again.

**Validation of Model**

The model described by Hasan and Siren [2002] was implemented in MATLAB and verified with experimental results mentioned in the paper. The cooling tower consisted of 12 rows of bank of tubes, each bank with 19 tubes with each tube with an outer diameter of 10 mm (0.39 in). The width of the tower was 0.6 m (1.97 ft) and each tube was 1.2 m (3.94 ft) long. The longitudinal and transverse spacing of the tubes were 0.02 m and 0.06 m, respectively. The nominal data for the cooling tower was: 3 kg/s (396.8 lb/min) air flow rate, 0.8 kg/s (105.8 lb/min) cooling water flow rate, 1.37 kg/s (181.2 lb/min) spray water flow rate, inlet cooling water temperature of 21˚C (69.8 ˚F) and an air wet bulb temperature of 16˚C (60.8˚F).

Figure 2-5 shows the temperature variation of spray water (green color curve) and cooling water (blue color curve). Row 12 refers the highest level of the tower and row 1 refers to the lowest level of the tower. It can be seen that the cooling water enters at 21˚C (69.8˚F) and as it flows along the tubes down the cooling tower, the temperature decreases to 18.3˚C (65˚F). The bulk of the cooling (65%) happens in the top five rows (rows 12 –8). In the top five rows the water temperature decreases by 2 ˚C (3.6˚F), while it cools by only 1.6 ˚C (2.88˚F) in the bottom seven rows (1-7).

It is interesting to see the temperature profile of the spray water. It increases in the top five rows (rows 12 – 8) and then decreases from rows 7 to 1. The initial and final temperatures of the spray water are equal, an assumption made in the model by Equation 2.11. The profile can be explained as follows. In the top few rows of the tower, the air is almost saturated, and hence the cooling water transfers heat to the spray water, thereby increasing the latter's temperature. As the spray water moves down, it evaporates into the air by taking away latent heat. Hence, the temperature of the spray water reduces in the bottom few rows (rows 7 to 1).

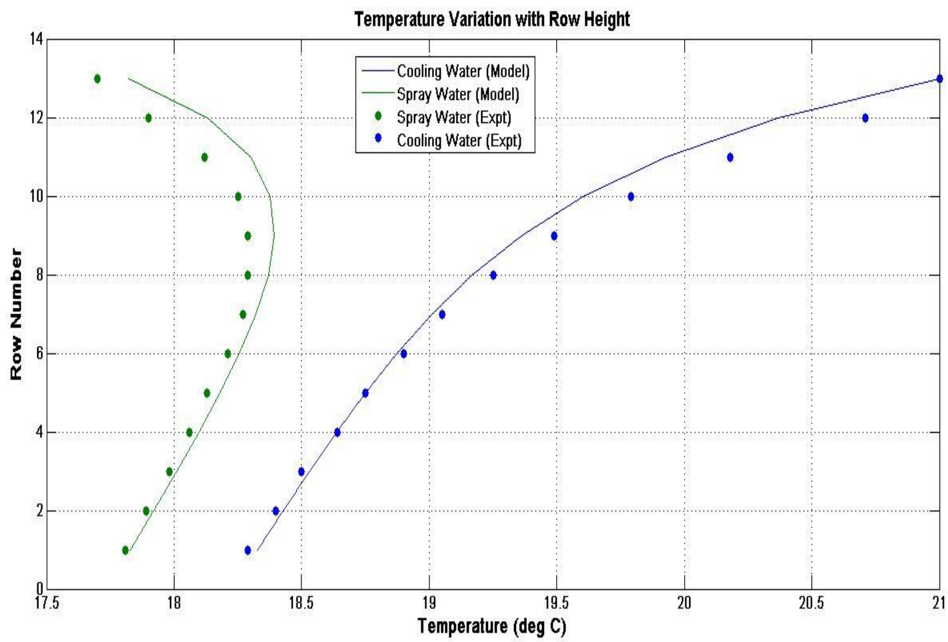


Figure 2-5: Cooling and Spray Water Temperature

Figure 2-6 shows the temperature variation of air with the row height. It is interesting to notice that although heat is being transferred to the air, its temperature decreases as it goes up the tower. Although this seems counter intuitive, it is not. Although the temperature of the air decreases, its water vapor content increases, which leads to a higher enthalpy value as the air rises. Figure 2-7 verifies the increase in enthalpy of air with row height.

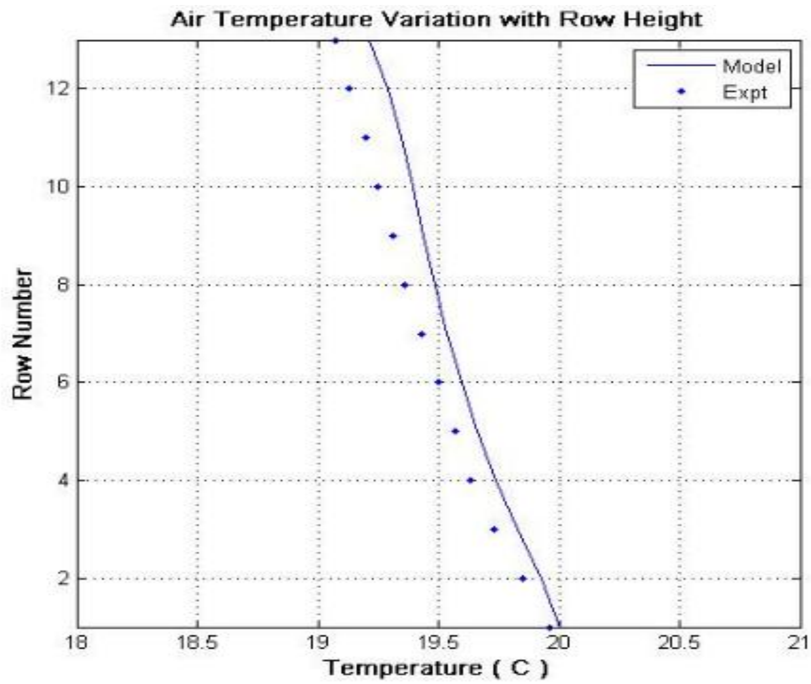


Figure 2-6: Variation of Air Temperature

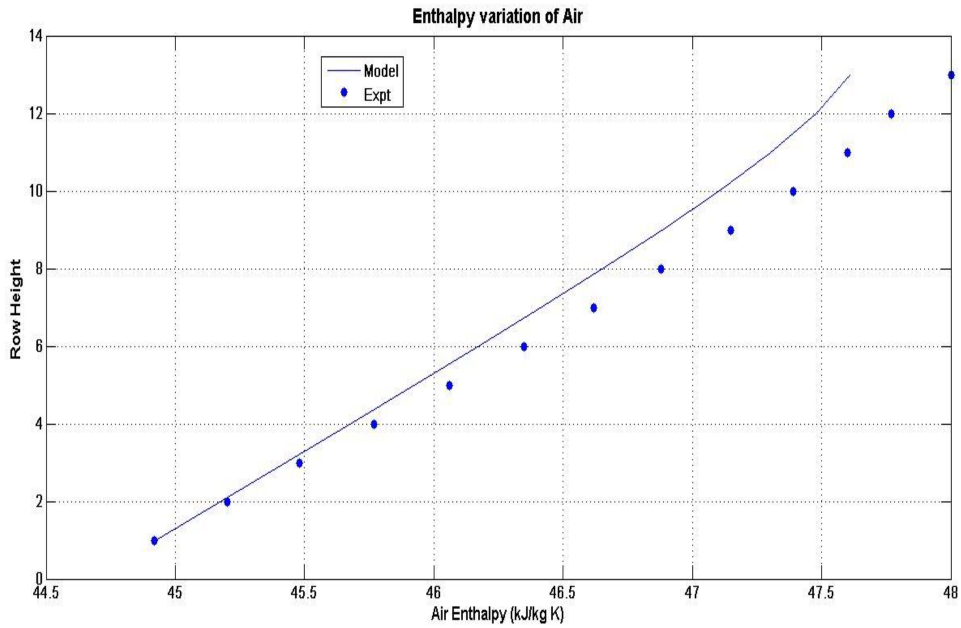


Figure 2-7: Variation of Air Enthalpy

This cooling tower model was selected for our study since it provides the operating values for a small sized cooling tower (9.25 kW / 2.6 tons). Most manufacturers of cooling towers do not have nominal and operating values for sizes less than 5 tons. In a residential application, typical cooling towers capacities are less than 5 tons.

**CONTROL ALGORITHM OF COOLING TOWER**

The control of the cooling tower in a HGSHP is a very important aspect of the entire design. The times at which the cooling tower is started directly impacts the operation and efficiency of the heat pump. Various control strategies have been adopted depending on the ambient temperature conditions, heat pump operating limits (minimum and maximum entering water temperatures) and the operating cost of the cooling tower.

Xu (2007) adopted a strategy where the cooling tower was started when the difference between the heat pump exiting fluid temperature and the ambient wet bulb temperature was greater than 2˚C (3.6˚F). Another control strategy used by Xu but based on a study by Yavuzturk and Spitler (2000) was to operate the cooling tower when the heat pump entering temperature was greater than 32.2˚C (90˚F). Hackel (2008) employed a much more detailed control strategy for the HGSHP system. His control strategy started the cooling tower when the difference between the temperature of the water entering the cooling tower and the ambient wet bulb temperature was greater than

- 27˚F (15˚C) when ambient wet bulb temperature was greater than 70˚F (21.1˚C)
- 23˚F (12.7 ˚C) when ambient wet bulb temperature was between 70˚F (21.1˚C) and 76 ˚F (24.4˚C)
- 20˚F (11.1 ˚C)when ambient wet bulb temperature was greater than 76˚F (24.4 ˚C)

One of the reasons for selecting this algorithm is to ensure that the EWT to the heat pump never was above 95˚F (35˚C), as mentioned by the heat pump manufacturer. This algorithm also resulted in the lowest 20 year life cycle cost of the HGSHP.

The control strategy employed in our analysis was a relatively simple one. The cooling tower was started whenever the ground loop entering water temperature exceeded 35˚C (95˚F) for all ambient air conditions. The reason for choosing this algorithm for all ambient conditions was that the residential building under analysis had significant cooling loads even during winter, which lead to the rise in entering water temperatures.

The next section will discuss our algorithm used to size the ground loops and cooling tower based on the building loads and the ground properties using the GLHEPRO software from Oklahoma State University.

### SIZING OF THE GSHP FOR RESIDENTIAL LOADS

The design of our HGHP includes sizing the ground loop length and capacity of the SHR system using GLHEPRO, and the control algorithm. GLHEPRO is a software program from Oklahoma State University that helps size the length of the ground loop and the SHR capacity based on the building loads, ground and ground loop properties and the configuration of the borehole. The reference computations must size the GSHP without any SHR system. The values shown in the GHLEPRO dialog boxes below reflect the conditions in Austin, Texas for the 2100 ft$^2$ residential house [Jonathan Gaspredes, 2011] described in Chapter 1

Table 2.2: Ground Loop and Ground Properties

| | | | | |
|---|---|---|---|---|
| **Geometry** | | | | |
| Length | 68.6 | m | 225 | ft |
| Borehole Diameter | 127 | mm | 5 | in |
| Shank Spacing | 25.4 | mm | 1 | in |
| Borehole Spacing | 4.572 | m | 15 | ft |
| Configuration | Line of 4 | | | |
| U -Tube ID | 27.33 | mm | 1.076 | in |
| U-Tube OD | 33.4 | mm | 1.315 | in |
| **Thermal Properties** | | | | |
| ***U-Tube*** | | | | |
| Conductivity | 1.333 | W/m/K | 0.225 | Btu/hr/ft/F |
| Capacitance | 1767 | kJ/m^3/K | 22.99 | Btu/ft^3/F |
| ***Grout*** | | | | |
| Conductivity | 0.7443 | W/m/K | 0.43 | Btu/hr/ft/F |
| Capacitance | 3901 | kJ/m^3/K | 58.17 | Btu/ft^3/F |
| ***Ground*** | | | | |
| Conductivity | 0.3895 | W/m/K | 0.77 | Btu/hr/ft/F |
| Capacitance | 1542 | kJ/m^3/K | 26.35 | Btu/ft^3/F |
| Undisturbed Temperature | 21.67 | C | 71.01 | F |
| ***Fluid*** | | | | |

Table 2.3: Ground Loop and Ground Properties

| | | | | |
|---|---|---|---|---|
| Antifreeze | None | | | |
| Convection Coefficient | 1534 | W/m^2/K | 270.2 | Btu/hr/ft^2/F |
| Fluid Factor | 1 | | | |
| Flow Rate per Borehole | 0.1893 | L/s | 3 | GPM |
| **Calculated Borehole Resistance** | 0.2097 | K m/W | 0.3629 | F hr ft/Btu |

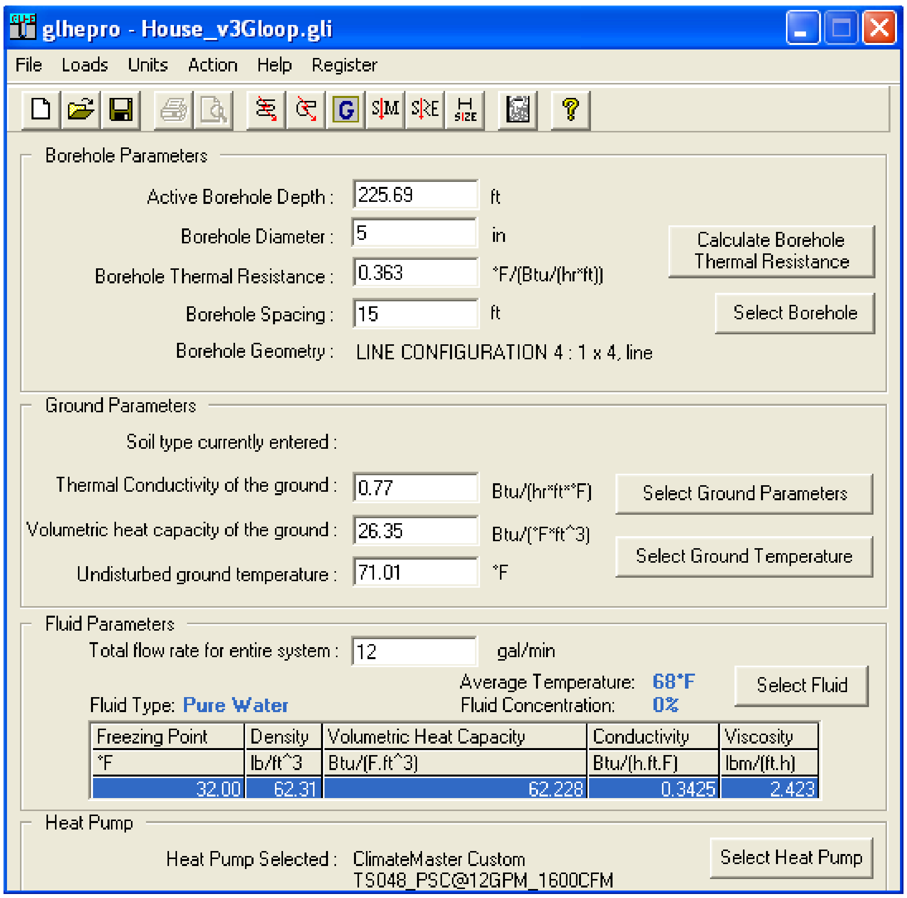


Figure 2-8: Main GLHEPRO Dialog Box

Figure 2-8 shows the main dialog box of the GLHEPPRO software. The basic parameters such as borehole diameter, spacing, configuration and initial guess for the length of the borehole are entered. Soil properties such as thermal conductivity, volumetric heat capacity and the undisturbed temperature are specified in this step. Properties and the flow rate of the fluid through the borehole is also entered.

The borehole thermal resistance is calculated as follows (Refer to Figure 2-9). First the configuration of the borehole (U tube, double U tube or concentric U tube) is selected. Once the configuration is selected the various parameters describing the borehole, such as the inside and outside diameters of the U tube, shank spacing, volumetric flow rate, volumetric heat capacities and the conductivity of the soil, grout and the pipe, and the convection coefficient of the fluid flowing through the borehole, are entered into the dialog boxes. Once all these parameters are entered, the borehole thermal resistance is calculated. The G-functions are automatically updated after the resistances are calculated.

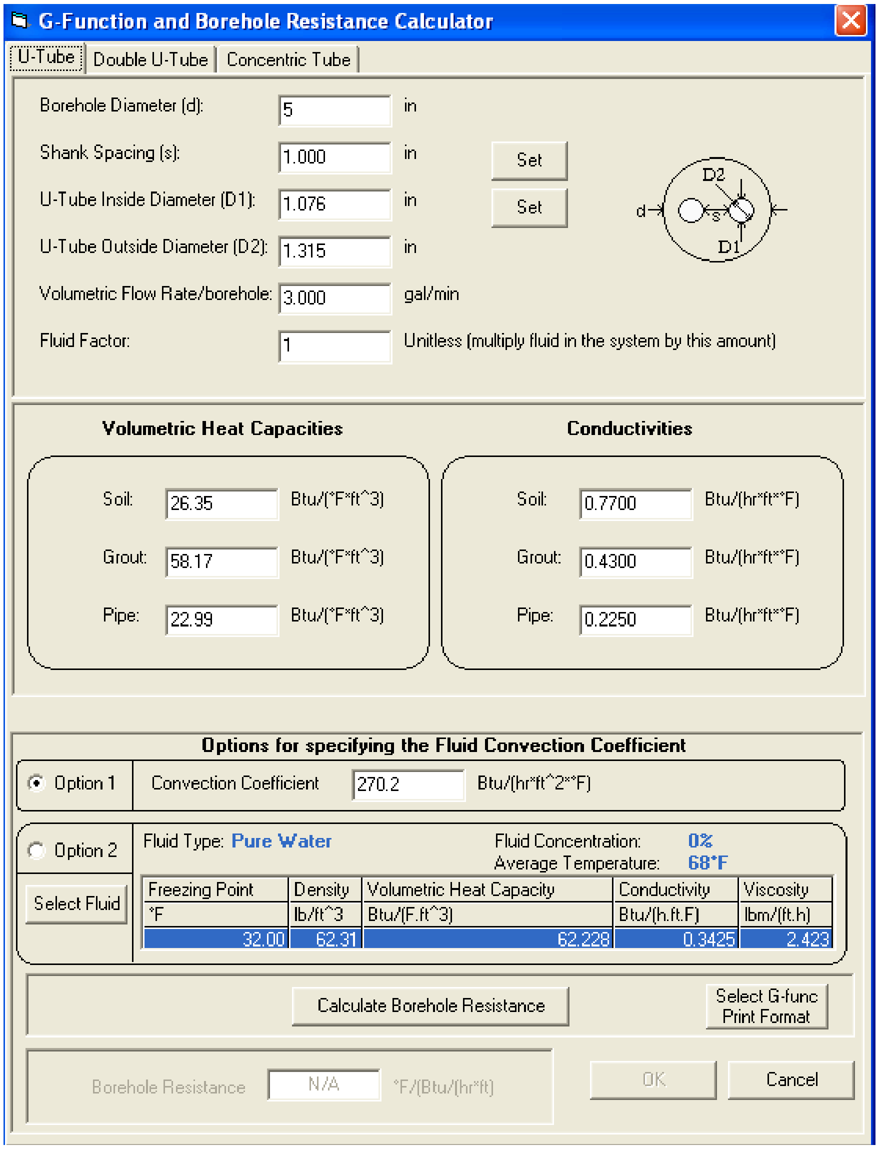


Figure 2-9: G Function Dialog Box

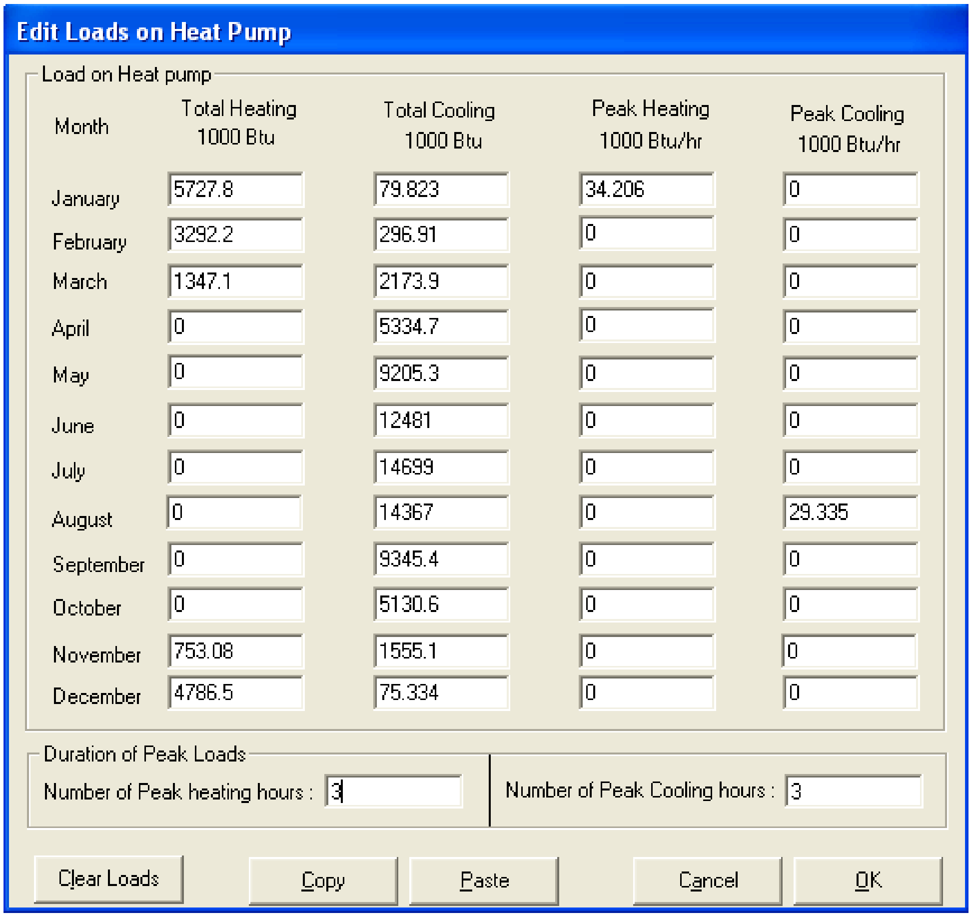

Edit Loads on Heat Pump

Load on Heat pump

| Month | Total Heating 1000 Btu | Total Cooling 1000 Btu | Peak Heating 1000 Btu/hr | Peak Cooling 1000 Btu/hr |
|---|---|---|---|---|
| January | 5727.8 | 79.823 | 34.206 | 0 |
| February | 3292.2 | 296.91 | 0 | 0 |
| March | 1347.1 | 2173.9 | 0 | 0 |
| April | 0 | 5334.7 | 0 | 0 |
| May | 0 | 9205.3 | 0 | 0 |
| June | 0 | 12481 | 0 | 0 |
| July | 0 | 14699 | 0 | 0 |
| August | 0 | 14367 | 0 | 29.335 |
| September | 0 | 9345.4 | 0 | 0 |
| October | 0 | 5130.6 | 0 | 0 |
| November | 753.08 | 1555.1 | 0 | 0 |
| December | 4786.5 | 75.334 | 0 | 0 |

Duration of Peak Loads

Number of Peak heating hours : 3

Number of Peak Cooling hours : 3

Clear Loads | Copy | Paste | Cancel | OK

Figure 2-10: Building Loads

The building loads are entered into the dialog box shown in Figure 2-10 above. The total heat and cooling loads for each month are entered along with the peak heating and cooling loads for the whole year. [Jonathan Gaspredes, 2011]

The minimum and maximum fluid temperatures entering the heat pump are specified as 120˚F (48.9˚C) and 32˚F (0˚C), respectively. These temperatures are based on the heat pump used, Climate Master's TS048_PSC, with an airflow rate of 1200 cfm (0.47 $m^3/s$) and 12 gpm (0.748 kg/s) water flow rate. The duration of the entire simulation (from the starting month to the end month) is entered, and in this case a 10 year run (120 months) is performed.

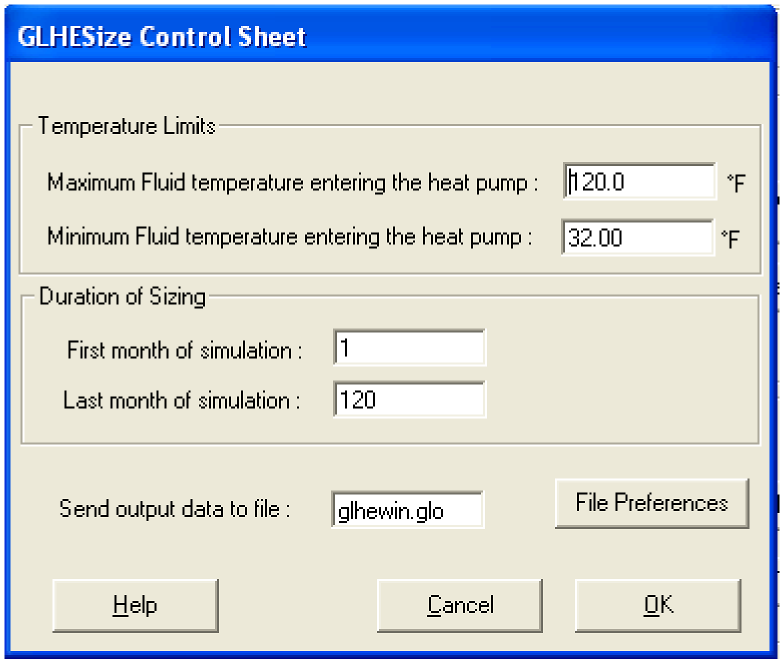


Figure 2-11: Heat Pump Entering Water Temperatures

Once all the parameters have been entered, GLHEPRO computes the length of the ground loop. For the given heating/cooling loads, borehole configuration and ground properties, a borehole depth of 225.69 ft (68.8 m) for each one of the four loops was obtained. The average maximum and minimum temperatures of heat pump entering water temperatures (EWT) calculated were 114.1˚F (45.6 ˚C) and 64.3˚F (17.9 ˚C), respectively (Refer to Figure 2-11).

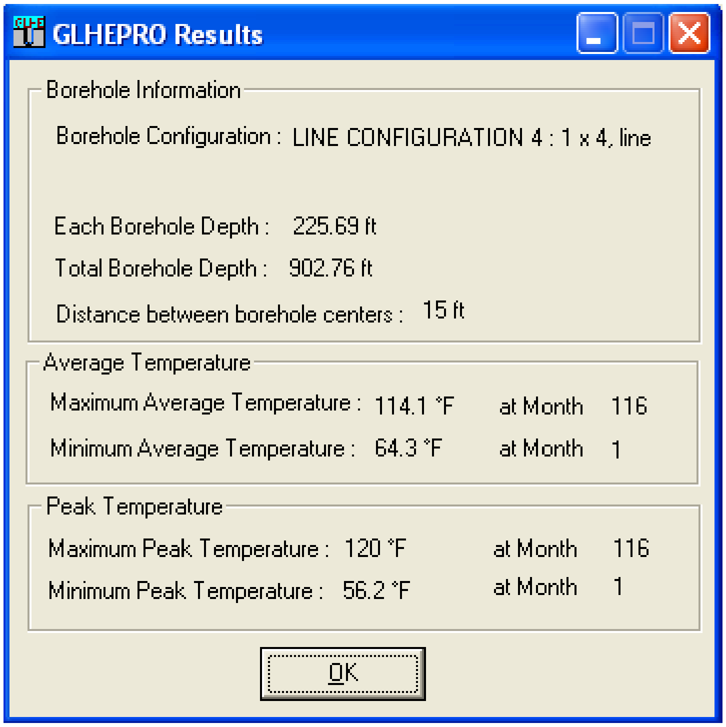


Figure 2-12: Final Result

### SIZING OF HGSHP FOR RESIDENTIAL LOADS

To size the borehole length for the hybrid system, the same procedures as described above was followed. GLHEPro sizes the length based on the peak heating load. The algorithm is based on the premise that the ground loop will be able to satisfy the peak heating load and some of the cooling loads. The remaining loads will be satisfied by the SHR system. At the end, the hybrid sizing option is chosen and GHLEPro calculates the ground loop length and SHR capacity. The output for such a sizing is shown below in Figure 2-13 and yields a ground loop length of 87 ft (26.5 m) for each of the four loops, which is significantly shorter than the 225 ft (68.8 m) obtained in the non-hybrid case. The capacity of the SHR system calculated was 17.2 kBtu/h, which translates to 5 kW and a cooling tower of capacity 1.5 tons.

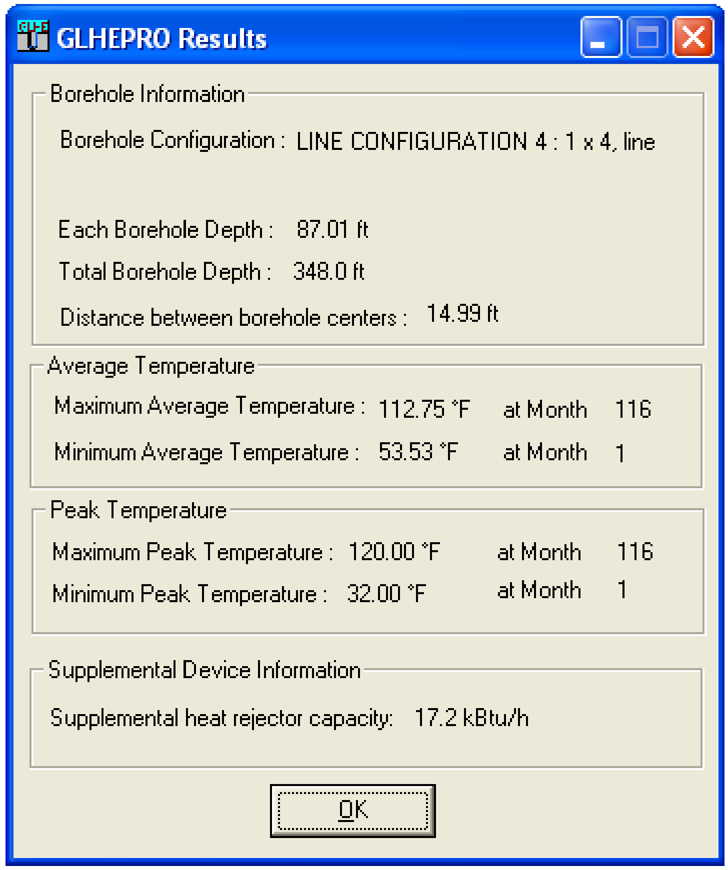


Figure 2-13: HGSHP Sizing Result

Based on the analysis in GLHEPRO, it was found that the cooling tower capacity needed for SHR was 5 kW (1.4 tons). Hence, a cooling tower capacity of 2 tons was chosen and a performance map of its operation was generated with the implemented model. The cooling water flow rate for the residential system is 12 gal/min (0.748 kg/s). The air flow rate of the fan in the cooling tower is 500 cfm (0.23 $m^3$/s). The power rejected, outlet water temperature, and power consumed are computed for a range of input parameters; inlet water temperatures (70 – 120˚F / 32.2 – 48.9˚C), air temperatures (40 – 120˚F / 4.44 – 48.9˚C) and relative humidity (20% - 100%).

## RESULTS

The cooling tower model was coupled with Jonathan Gaspredes' building load and ground loop model [Jonathan Gaspredes, 2011]. The entire model was simulated for a period of 10 years with 2 minute time steps. The simulated data was then averaged for every hour. The figures below show the performance of the HGSHP model and comparisons with results obtained by using only the GSHP [Jonathan Gaspredes, 2011].

Figure 2-14 and Figure 2-15 show the average monthly average temperature of the water entering the ground loop for the HGSHP and the GSHP cases. The green, blue, and red colored plots show the maximum, mean, and minimum water temperatures entering the ground, respectively. Months 1 -12 denote January to December. Figure 2.14 shows that the mean temperatures during the summers are around 32˚C (89.6˚F) and the maximum temperatures are around 34˚C (93.2˚F). There are a few peaks in the maximum temperature plot (indicated by the green color plots) that exceed 35˚C (95˚F). It happens for 68 hours during the ten years of operation of the HGSHP. This happens due to the fact that the cooling tower model does not give valid outputs when the ambient temperature goes below 4.4˚C (40˚F). Note that the average water temperatures do not increase over the 10 years. In contrast, Figure 2.15 shows the average water temperatures entering the ground loop increase over 10 years for the case of GSHP only. The average temperature during the first year summer is around 42˚C (107.6˚F) and after 10 years, it increases to 48˚C (118.4˚F).

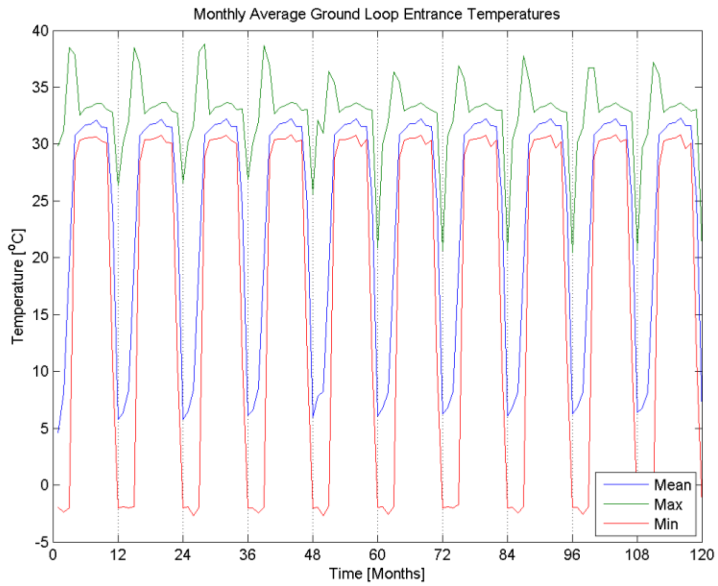


Figure 2-14: Monthly Average Water Temperatures Entering the Ground Loop for HGSHP

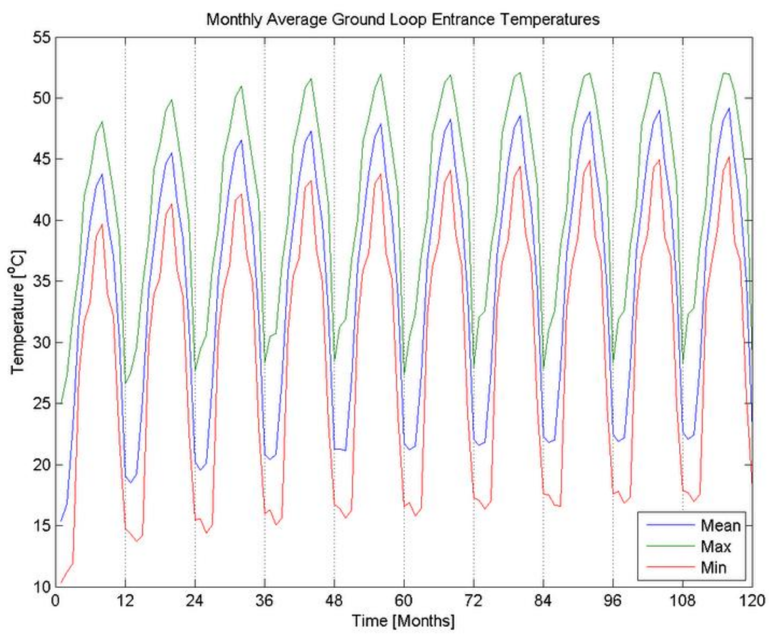


Figure 2-15: Monthly Average Water Temperatures Entering the Ground Loop for the GSHP [Jonathan Gaspredes, 2011]

Figure 2-16 and Figure 2-17 shows the average monthly average heat pump EWT for the HGSHP and the GSHP cases. The profiles are similar to those of the water temperatures entering the ground loop. Figure 2.16 shows that the mean temperatures during the summers are around 30˚C (86˚F) and the maximum temperatures are around 33 ˚C (91.4˚F). Note that the average EWT temperature does not increase over the 10 years. In contrast, Figure 2.17 shows that the average heat pump EWT increase over 10 years, from around 40˚C (107.6˚F) in the first summer to 45˚C (113˚F) in year 10.

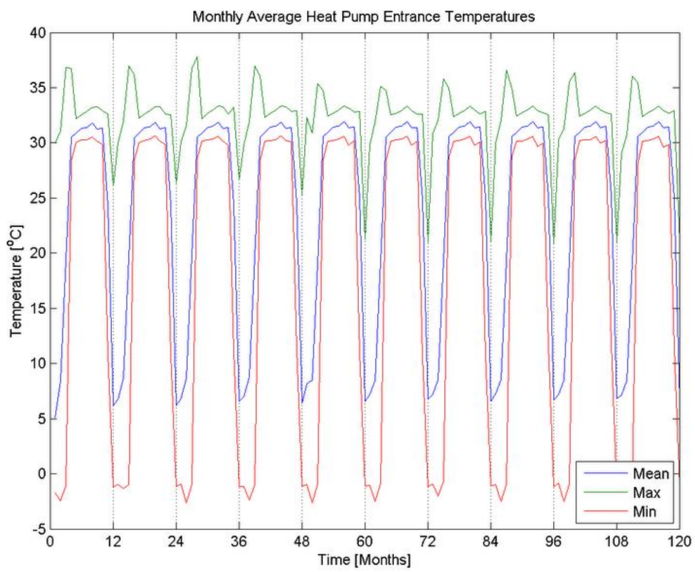


Figure 2-16: Monthly Average Heat Pump EWT for HGSHP

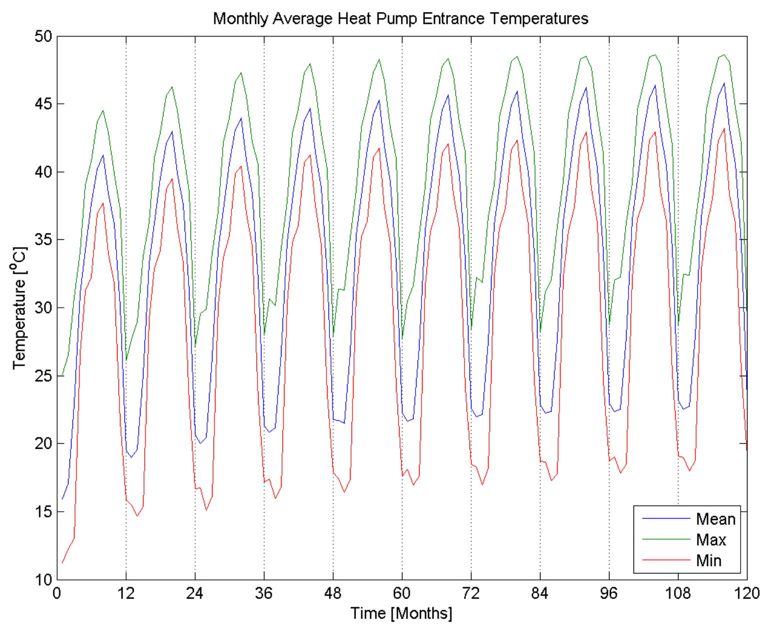


Figure 2-17: Monthly Average Heat Pump EWT for HGSHP

Figure 2-18 and Figure 2-19 show the profiles of COP and the Energy Efficiency Rating (EER) of the heat pump over the 10 year period. EER is the ratio of cooling provided to the power consumed and its units are Btu/Whr . For the HGSHP case of Figure 2-18, the EER is highest during the winter, since the cooling tower operates very efficiently, whenever cooling is needed, because the ambient temperature is low. The EER decreases during the summer months, but remains almost constant. The EER ranges from a minimum of 11.5 to a maximum of 19.5. Note that the minimum value of the EER remains nearly constant over the 10 year period since the cooling tower prevents the ground from heating over 10 years. This is due to the operation of the cooling tower, which prevents the ground from heating up over 10 years.

On the other hand Figure 2-19, shows a slightly different profile for the EER. This is for the case without a cooling tower. First, the minimum EER is 8.6 in the first year for the GSHP only case compared to 11.5 for the case with the cooling tower. Second, the EER keeps decreasing every year. In fact, the minimum EER decreases to 7.5 in the 10$^{th}$ year. This makes the heat pump less efficient when operated over 10 years in comparison to the operation with a cooling tower.

The COP of the heat pump in the heating mode is again different for the two cases. Over the 10 year period, the average value of COP for the GSHP only case increases from an average of 4.5 to 5. This increase is due to ground heating, which enables the heat pump to extract more heat efficiently to heat the building. For the HGSHP case, however, since the ground does not heat up, the average value COP remains constant at 4.

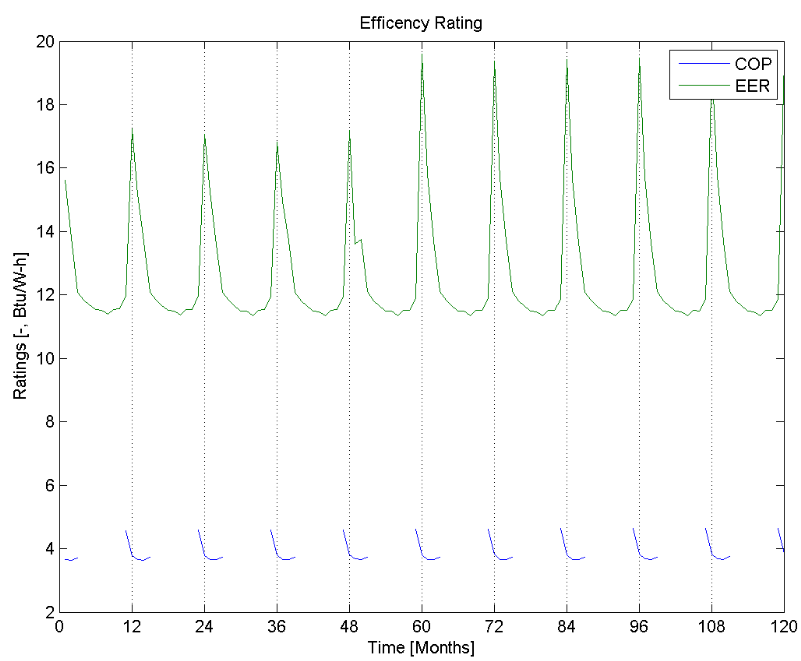


Figure 2-18: COP and EER of Heat Pump for HGSHP

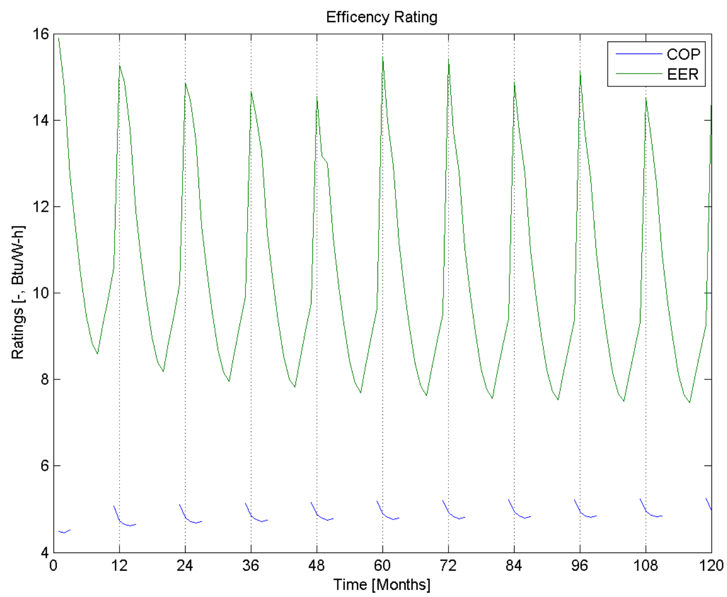


Figure 2-19: COP and EER of Heat Pump for GSHP

Table in Appendix A shows the yearly operation of the cooling tower and the heat pump. It also gives the power rejected by the cooling tower and ground loop for each year of operation.

## ECONOMICS OF GSHP AND HGSHP

Since one of the main reasons for using a cooling tower as a SHR device is to lower costs, an economic analysis was done over 10 years. There were two types of costs, fixed and variable costs. The fixed cost is consists of expenses for the heat pump, installing the borehole, glycol added to water in the ground loop, and the cooling tower. The heat pump cost in both cases will be the same. The variable costs consist of expenses for the power to run the water loop pump, heat pump and the cooling tower and for makeup water in the cooling tower.

The length of the borehole for the GSHP was 225 ft (68.58 m) and that for the HGSHP case was 87 ft (25.5 m). The cost of drilling the borehole was \$ 10/ft [Mike Hammond, 2011]. Ethylene glycol was added to the water to prevent freezing and that cost was \$ 0.12/ft [Mike Hammond]. Cooling towers of sizes smaller than 5 tons are normally not manufactured. However, a company called Allied Thermal Systems in Austin, TX makes cooling towers for residential use. The cost associated with a 2 ton cooling tower was \$ 800 (\$ 400/ ton) [Mac Word, 2011].

Based on the building loads computed for the 2100 $ft^2$ house [Gaspredes, 2011], the heat pump ran for a total of 2022 hrs in the cooling mode and 277 hrs in the heating mode for one year. However, over a period of ten years, the heat pump ran in the cooling mode for 18,928 hours and in the heating mode for 3,564 hours. The total time the heat pump ran was 22,392. This was the same amount of time the pump also ran. For the GSHP, the energy consumed by the heat pump over 10 years was 98,216 kWhr (average power of 4.38 kW) and the energy associated with pumping the water through the ground loop was 9,493 kWhr (average power of 0.42 kW). For the HGSHP, the power consumed by the heat pump over 10 years was 77,864 kWhr (265,682 kBtu) and the power associated with pumping the water through the ground loop and the cooling tower was 11,957 kWhr (407,98 kBtu). The cooling tower fan that was used was a 200 cfm, 170 W power one. The power required to run the cooling tower for 18,458 hrs over ten years (1845.8/yr) was 9,137 kWhr (31,176 kBtu). The electricity rate used was the average value in Texas - \$0.1082/kWhr [EIA, 2011]. The total quantity of make-up water needed to operate the cooling tower was 71,700 gallons and the price of water was taken from the City of Austin Water Rates [Appendix A].

Table 2.4: Economic Comparison of GSHP and HGSHP for 10 Years of Operation

| | **GSHP** | **HGSHP** |
|---|---|---|
| **Fixed Cost** | $ 9,115 | $ 4,322 |
| - **Borehole ($10/ft)** | $ 9007 | $ 3,480 |
| - **Ethylene Glycol ($ .12/ft)** | $ 108 | $ 42 |
| - **Cooling Tower ( $ 400/ton )** | $ 0 | $ 800 |
| **Variable Cost** | $ 11,643 | $ 10,852 |
| - **Heat Pump ($.1082/kWh)** | $ 10,617 | $ 8,417 |
| - **Makeup Water** | $ 0 | $ 154 |
| - **Fan ($.1082/kWh)** | $ 0 | $ 988 |
| - **Pumping ($.1082/kWh)** | $ 1,026 | $ 1,293 |
| **Total Cost (10 yrs)** | $ 20,758 | $ 15,174 |

Table 2.4 shows the cost comparison of using a GSHP and a HGSHP over 10 years. The heat pump cost was not included since it is the same for both cases. The total cost of operation of HGSHP was $ 15,174, which was 26.9% lower than the cost of operating a GSHP, which was $ 20,758. The major reduction in the cost was due to the difference in drilling costs for the two borehole length. The cost of drilling four boreholes, each of length 87 ft (25.5 m), in HGSHP case was only $ 4,322 compared to $ 9,115, for drilling four boreholes, each of length 87 ft (25.5 m), in the GSHP case, which gave a 61.3% cost reduction. Although a cooling tower added $800 in fixed cost and $1142 in variable cost to the total cost of the HGSHP, the 52.6% reduction in the fixed cost more than offset those additional expenses.

The operating cost for the HGSHP was 6.8% lower than that for a GSHP ($ 10,852 compared to $ 11,643) due to the 20.7% reduction in running the heat pump in the hybrid case. Although there was a reduction in costs due to less time of operating the heat pump in the hybrid case, the power and make-up water consumed by the cooling tower added $ 1,052 to the operating costs ($ 988 for the fan operation and $ 154 for the make-up water).

## CONCLUSIONS

There are great advantages to using a cooling tower as a SHR device. The HGSHP reduces ground heating over the 10 year period compared to using a GSHP. It was found that during summer months, the water temperature entering the ground loop does not increase over time and remains around 32˚C (89.6˚F) due to the heat rejected by the cooling tower. The cooling tower rejected 82 % of the total heat rejected by the heat pump. This result directly impacts the heat pump EWT, since it also remains relatively constant at around 30˚C (86˚F) during summers over the 10 year period. Since the heat pump EWT does not increase, the EER profile remains constant with a value about 11.5 during the summers for during the 10 year period. In contrast, the temperatures of the water entering the ground loop and the heat pump increase over the 10 year period, and the EER decreases over time. The COP, however, remains constant at around 4 in a HGSHP compared to an increase from 4.5 to 5 in a GSHP.

The performance of the heat pump improved with a cooling tower, and the cost comparison associated with the HGSHP is very favorable. The 10 year cost of operating a HGSHP was 26.9% lower than that of a GSHP. This savings is mainly due to the reduction in drilling costs in a HGSHP, which overshadows the additional operating costs of the cooling tower, and the improved efficiency of the heat pump that leads to a reduction in operating costs. Hence, based upon performance and cost, the cooling tower is a very viable and economical SHR system.

# Chapter 3. Optimization of Vapor Compression Cycle

## Background of Vapor compression cycle (VCC)

The last chapter focused on using cooling towers to reject heat from the water loop before it enters the ground. This chapter investigates the potential of rejecting heat from the refrigerant loop of the Vapor Compression Cycle (VCC). The VCC is made up of four stages: evaporation, compression, condensation and expansion. Its p-h thermodynamic cycle is show in Figure 3.1. The liquid refrigerant enters the evaporator at point 4. As it moves through the evaporator, at constant pressure $P_e$, the refrigerant removes heat from the conditioned space and its enthalpy increases. The refrigerant then enters the compressor suction at point 1 from where it is compressed to high pressure and superheated vapor. The refrigerant at the compressor discharge is denoted at point 2, where it then enters the condenser. As it passes through the condenser, at constant pressure $P_c$, the refrigerant loses heat to either the air (air source heat pumps) or water (ground source heat pump) and becomes a subcooled liquid. This liquid refrigerant from the condenser at point 3 is then expanded through an expansion valve and the cycle repeats. This chapter focuses on the portion of the cycle that provides subcooling in the condenser (shown in Figure 3.1 as $\Delta T_{sub}$) and superheat in the compressor suction (shown in Figure 3.1 as $\Delta T_{sup}$) and discharge.

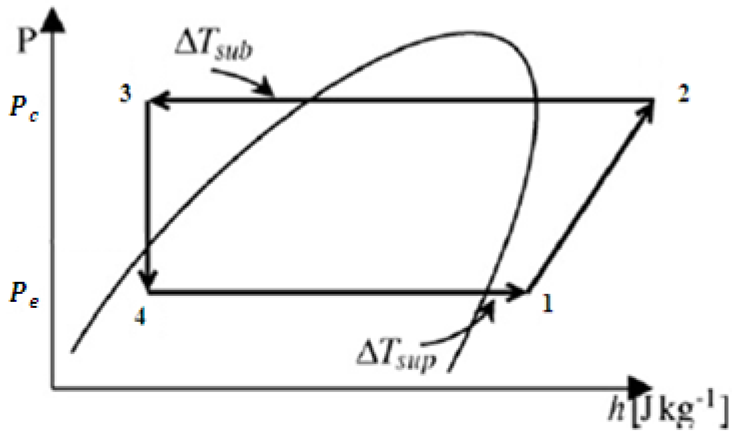


Figure 3-1: P-h diagram of VCC

**INTRODUCTION**

In the cooling mode, the VCC removes heat from the conditioned space at the evaporator to maintain a set point room temperature, and the heat pump water loop removes heat at the VCC condenser. On the ground loop side, the heat rejected to the condenser increases the water temperature entering the ground and subsequently increases the ground temperature. The evaporator and condenser heat loads are coupled. The condenser conditions of the VCC depend upon the ground loop water temperature entering the heat pump (EWT) and water flow rates. Figure 3-2 shows the range of VCC operating points for an EWT of 90˚F (32.2˚C) for Climate Master's Model TS048 heat pump. For a three gpm (0.187 kg/s) water flow rate and 90˚F EWT, the Climate Master data specifies a cooling load rating of 14.06 kW (47.9 kBtu/h) and condenser heat rejection of 16.14 kW (55.1 kBtu/h) . Although this rating is specified by Climate Masters, the heat rejected varies according to the operating points as shown in Figure 3.1.

| Entering Water Temp °F | Water Flow GPM/ ton | Suction Pressure PSIG | Discharge Pressure PSIG | Superheat | Subcooling | Water Temp Rise °F | Air Temp Drop °F DB |
|---|---|---|---|---|---|---|---|
| 90 | 1.5<br>2.25<br>3 | 138-148<br>137-147<br>136-146 | 396-416<br>374-394<br>352-372 | 7-12<br>7-12<br>7-12 | 7-12<br>6-11<br>4-9 | 19.2-21.2<br>14.3-16.3<br>9.3-11.3 | 18-24<br>18-24<br>18-24 |

Figure 3-2: Operating Points of TS 048 Heat Pump (Climate Master)

The research question is posed as follows: can the VCC cycle's thermodynamic parameters be optimized to minimize the heat rejected to the condenser for every cooling load requirement, and thereby minimize the water loop temperature before it returns to the ground? In practice, the use of mechanical control valves and single- or two-speed compressors limit the system's ability to control the suction superheat, condenser subcooling and the mass flow rate of refrigerant. Electronic control valves can be used in to optimize the operation of a VCC (Qureshi and Tassou (1996), He et al. (1998)). In the following sections, different optimization schemes are presented and analyzed to determine the best possible operating conditions for a residential VCC.

### APPROACH BY LARSEN AND THYBO (2002)

In most analysis of VCCs, the objective is to minimize the power consumed by the compressor, but taking a broader picture, power is also consumed by the condenser fans, blower in the evaporator and other control valves. Larsen and Thybo (2002) minimized power consumption from two devices, the compressor and the condenser fan, for a given cooling load. The reason for focusing on these two components is that the power consumed by the compressor and the condenser fan are inversely related. Note that the study was for an air source heat pump. Figure 3-3 shows the compressor power consumption as a function as the pressure ratio (Compressor discharge to Compressor

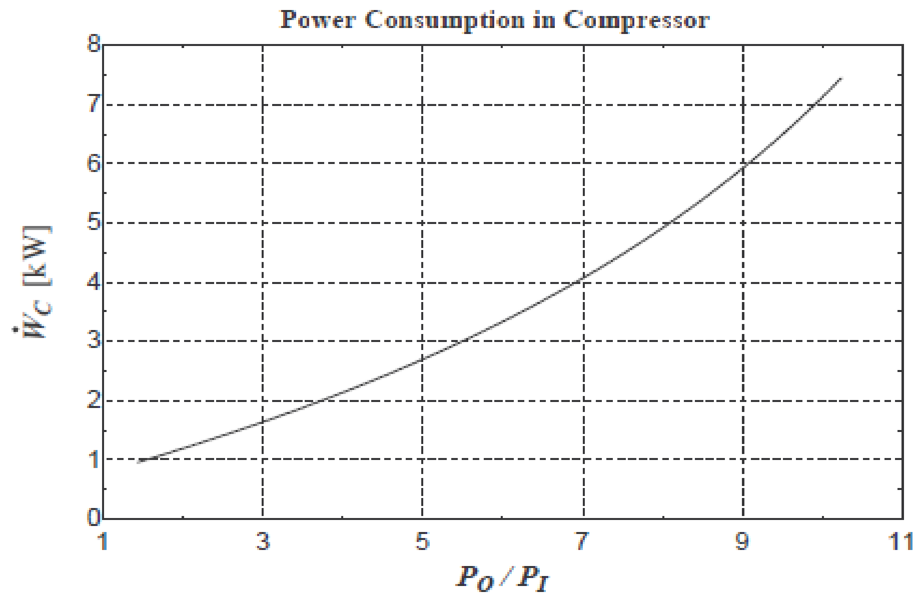


Figure 3-3: Power Consumption in Compressor

suction pressure –($P_o/P_I$) ). For a given suction pressure, the compressor work increases with increased discharge pressure. One way to reduce compressor work is to reduce the discharge pressure. For instance, by reducing the pressure ratio from five to three, the compressor power can be reduced by 30%.

Reducing the compressor discharge pressure would require a higher condenser fan speed to reject the heat for a given ambient temperature, which leads to increased power consumption in the condenser section. Figure 3-4 shows the variation of power consumed by the condenser fan as a function of the pressure ratio ($P_o/P_I$) for different ambient temperatures. As expected, for a given pressure ratio the power consumed is less for a lower ambient temperature. It can be inferred that during cooler days, total power consumption can be reduced by lowering the discharge pressure.

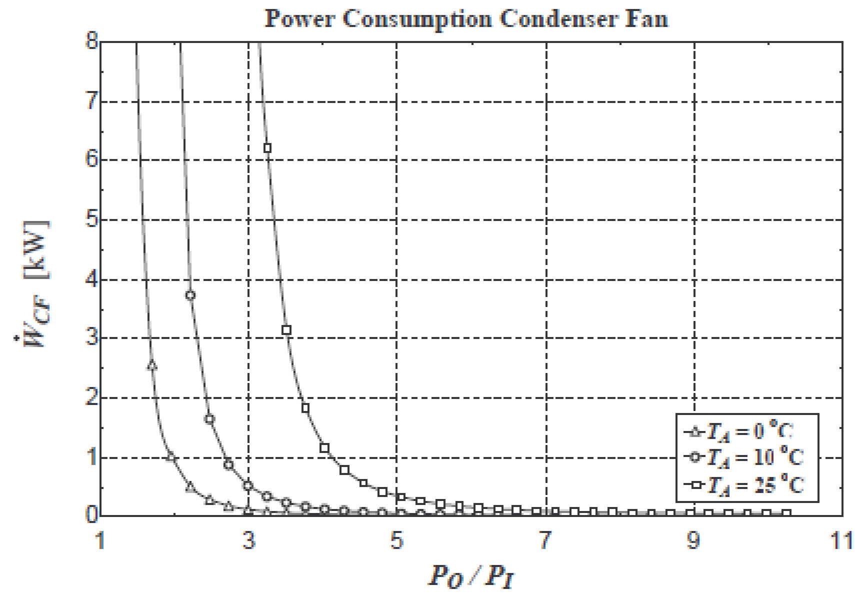


Figure 3-4: Power Consumption in Condenser fan

The objective of investigating the compressor and fan powers was to reduce the total power consumption by varying the compressor discharge pressure for a given ambient temperature, evaporating temperature, suction superheat and condenser subcooling. This is a simple one degree of freedom problem, with compressor discharge pressure as the only variable. The case investigated by Larsen and Thybo was for a cooling load of 8 kW (27.3 kBtu/h), ambient temperature of 25˚C (77˚F), evaporating temperature of 0˚C (32˚F), suction superheat of 10˚C (50˚F) and condenser subcooling of 5˚C (41˚F). Keeping the condenser pressure for the 25˚C (77˚F) ambient temperature as reference, it was found that by reducing the condenser pressure from 1,363 kPa to 751 kPa (197.7 – 108.9 psi), total power consumption could be reduce by 10% for 15˚C (59 ˚F) ambient temperature, 15% for 10˚C (50˚F) ambient temperature and up to 30% for an ambient temperature of 0˚C (32˚F). Since we were not concerned about the power consumed by the condenser fan, a different model was reviewed that focused solely on the compressor work and condenser heat rejection.

### MODEL BY JAIN AND ALLEYNE (2011)

Jain and Alleyne (2011) developed a VCC optimization model to be used to improve performance of refrigeration systems used in trucks. The model had five degrees of freedom or five parameters of the cycle: three enthalpies $\{h_1, h_2, h_3 = h_4\}$, and either one of the three properties $\{P_1, P_3, T_1\}$. These four parameters are sufficient to describe the thermodynamic cycle. However, external conditions affect the conditions of the cycle; cooling load $\{\dot{Q}_L\}$, compressor work $\{W_s\}$ and the mass flow rate of refrigerant$\{\dot{m}\}$. The fifth parameter, the refrigerant mass flow rate is referred to as the dynamic variable. In other optimization models (Larsen and Thybo (2002) and Larsen et al (2003)) the degrees of freedom considered were only thermodynamic conditions and not dynamic ones. The reason why dynamic DOFs are chosen less often is due to the added requirement for hardware changes to the VCC cycle. If the mass flow rate is to be varied, the control valves must be changed from mechanical to electronic actuation.

The objective function used by Jain and Alleyne was unique in that they optimized two terms, performance and efficiency, in a weighted objective function. The performance term was the difference between the desired and actual cooling load. The efficiency term was exergy destruction. While energy is always conserved in a system, exergy is not. In irreversible systems exergy is always destroyed in amounts proportional to the entropy generated. Exergy destruction provides a measure of how efficiently heat is transferred in both the evaporator and the condenser. Exergy destruction is small (entropy generated is low) when the temperature difference between the refrigerant and the ambient temperature is small.

They considered a refrigeration system with a load of 15.3 kW (52.2 kBtu/h) and using the above described objective function, they achieved a 52.5% increase in COP compared to the nominal case. There were, however, some constraints that were not applied and the optimization results showed two-phase conditions at the compressor suction and at the flow through the expansion valve. In practice there is superheat at the compressor suction to prevent floodback and there is subcooling at the expansion value to maintain stable operation. Hence, the next model was studied.

### JENSEN AND SKOGESTAD MODEL

Jensen and Skogestad studied the optimization of the VCC for a storage building with an air source heat pump. They considered a storage building where the VCC operated between a cold medium of air inside the building at $T_c = -12^{\circ}C$ (10.4˚F) and ambient air outside the building at $T_H = 25^{\circ}C$ (77˚F). Cooling load for the building was 20 kW (6.82 kBtu/h )and the compressor efficiency was 95%. Heat transfer coefficients $(U)$of the evaporator and the condenser were 1000 and 500 $Wm^{-2}K^{-1}$, respectively. The refrigerant was ammonia.

In this study, five thermodynamic variables of the VCC were varied to minimize compressor work. Figure 3-5 shows the pressure-enthalpy diagram of an ideal VCC cycle. $\Delta T_{sub}$ and $\Delta T_{sup}$ are the subcooling and superheat, respectively. The five input variables of the VCC to be determined in the optimization are:

Condenser Pressure $(P_c)$

Evaporation Pressure $(P_e)$

Condenser Subcooling $(SC)$= $\Delta T_{sub}$

Suction Superheat $(SH)$=$\Delta T_{sup}$

Mass Flow Rate $(m)$

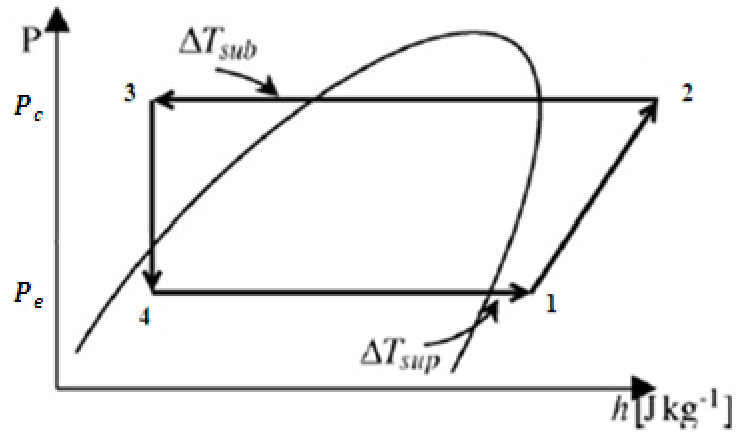


Figure 3-5: P-h Diagram of an Ideal Vapor Compression Cycle

Three other parameters, areas of the evaporator $A_{evap}$ and condenser $A_{cond}$ and the pinch point of the heat exchangers, also affect the compressor work. The pinch point of the heat exchanger is the minimum temperature difference between the refrigerant exit temperature and the air inlet temperature, for an air-source heat pump, or the entering water temperature, for a ground-source heat pump. Jensen and Skogestad (2007) minimized compressor work but used the heat exchanger areas or pinch points as constraints in two different optimizations based on what they call, Design and Operation. In the Optimal Design, the minimum pinch points $(\Delta T)$ of the heat exchangers are specified and the heat exchanger areas are computed. This effectively means selecting the best heat exchanger for a specified pinch point. In the Optimal Operation, the maximum heat exchanger areas are specified and the pinch points are computed. The Optimal Operation case is when heat exchanger has already been selected and one is trying to achieve the best performance out of the heat exchangers.

The objective function (performance index) used was:

Minimize Compressor Work

$$W_s = \dot{m}_r(h_2 - h_1)$$

The five variables are subjected to the following constraints:

Cooling Load: 20 kW

$$\dot{m}_r(h_1 - h_4) = 20\ kW \text{ (6.82 kBtu/h)}$$

Heat Balance at the Condenser

$$\dot{m}_r(h_3 - h_2) = UA_{condenser}(T_{rsat} - T_{air})$$

where $UA_{condenser}$ is the heat transfer coefficient times the area of the condenser heat exchanger, $T_{rsat}$ is the condensing temperature of the refrigerant and $T_{air}$ is the temperature of air. This heat exchanger is an air source heat exchanger.

Heat Balance at the Evaporator

$$\dot{m}_r(h_1 - h_4) = UA_{evaporator}(T_{revap} - T_{room}) \tag{3.1}$$

where $UA_{evap}$ is the heat transfer coefficient times the area of the evaporative heat exchanger, $T_{revap}$ is the evaporating temperature of the refrigerant and $T_{room}$ is the temperature of the room.

0°C Minimum Superheat

$$T_1 > T_{1sat}$$

where $T_{1sat}$ is the temperature of saturated vapor.

0°C Minimum Subcooling

$$T_3 < T_{3sat}$$

where $T_{3sat}$ is the temperature of saturated liquid.

The optimization was performed for two cases as described before. The additional constraints for the heat exchanger parameters, areas and pinch point, for each case are given below:

*Optimal Design*

Constraint on minimum pinch point

$$\Delta T > \Delta T_{min} \text{ (5°C/9°F)}$$

where $\Delta T = T_{r3} - EWT$

*Optimal Operation*

Constraint on the areas of the air source heat exchangers

$$A_{evap} \leq A_{evap\ max}$$

$$A_{cond} \leq A_{cond\ max}$$

The optimal areas obtained in the Optimal Design case are used as the maximum areas for the Optimal Operation constraint.

**UT Model Validation**

The model described in the previous section was implemented using the *fmincon* function in MATLAB. This implemented model shall be referred to as the UT Model. The five thermodynamic variables and the two heat exchanger areas were assigned initial values and then varied using the *fmincon* function of MATLAB. *fmincon* then computes the values for the five variables that minimized the compressor work.

Table 3.1 below shows the results of the UT Model in comparison with those of Jensen and Skogestad for the Optimal Design case; the agreement is very good. Recall for the Optimal Design case the minimum pinch points of 5 ˚C (9 ˚F) (for the heat exchangers were specified and the areas computed. The computed evaporator area agrees well with that of the paper, while the condenser area is 11.7% larger. The computed values for both the subcooling and superheat were 0 ˚C, which is not common in real applications. From this case, we get the best design values of the heat exchanger areas for the given pinch point (5˚C / 9˚F). The minimum value for compressor work ($W_s$) is 4.516 kW (15.4 kBtu/h).

Table 3.1: Optimization Results: Optimal Design Case for 5˚C Pinch Point

| | **UT Model** | **Jensen and Skogestad** |
|---|---|---|
| **Ws (kW/kBtu)** | 4.516 / 15.41 | 4.648 / 15.86 |
| **Qc (kW/kBtu)** | 20 / 68.24 | 20 / 68.24 |
| **COP** | 4.43 | 4.30 |
| **m (kg/s) / (lb / min)** | 0.0181 / 2.394 | 0.0177 / 2.34 |
| **Superheat (˚C )** | 0 | 0 |
| **Subcooling (˚C )** | 0 | 0 |
| **P_evap (bar)/(psi)** | 2.17/31.47 | 2.17/31.47 |
| **P_cond (bar)/(psi)** | 11.67/169.3 | 11.63/168.7 |
| **Aevap ($m^2$) / ($ft^2$)** | 3.96 / 42.6 | 4 / 43 |
| **Acond ($m^2$) / ($ft^2$)** | 9.72 / 104.6 | 8.7 / 93.6 |

The heat exchanger sizes computed above were for a pinch point of 5˚C (9˚F). Table 3.2 compares the results of the UT VCC model and Jensen and Skogestad models for the Optimal Operation case that constrains the maximum size of the heat exchanger areas but allows the pinch points to vary. The maximum areas of the heat exchangers are taken from the computed areas from the Optimal Design results. Again, the models agree well. The minimum value for compressor work ($W_s$) for this case is 4.418 kW (15.1 kBtu/h).

Table 3.2: Optimization Results: Optimal Operation Case— $A_{evap} \leq A_{max}( 3.96\, m^2)$ and $A_{cond} \leq A_{max}(9.72\, m^2)$

| | UT Model | Jensen and Skogestad [3] |
|---|---|---|
| **Ws (kW)/(kBtu)** | 4.4179 / 15.1 | 4.567 / 15.58 |
| **Qc (kW) /(kBtu)** | 20 / 68.24 | 20 / 68.24 |
| **COP** | 4.53 | 4.38 |
| **m (kg/s) / (lb / min)** | 0.0178 / 2.354 | 0.0173 / 2.288 |
| **Superheat (˚C )** | 0 | 0 |
| **Sub-Cooling (˚C ) / (F)** | 4.98 / 8.96 | 4.66 / 8.39 |
| **P_evap (bar)/(psi)** | 2.17/31.47 | 2.17/31.47 |
| **P_cond (bar)/(psi)** | 11.66/169.1 | 11.68/169.4 |
| **Aevap ($m^2$) / ($ft^2$)** | 4 / 43 | 4 / 43 |
| **Acond ($m^2$) / ($ft^2$)** | 9.72 / 104.6 | 8.7 / 93.6 |
| **Pinch Point (˚C) / (˚F)** | 0 | 0.49 |

**Comparing the Optimal Design and Optimal Operation Cases**

Table 3.3 and Table 3.4 compares the results of the two optimization cases. Note that the compressor work of 4.42kW (15.1 kBtu/h) in the Optimal Operation case is less than that of the Optimal Design case of 4.52kW (15.42 kBtu/h), which leads to a higher COP value of 4.53 compared to the 4.43 value of the Optimal Design case. These comparisons show that it is better to constrain the heat exchanger area than to constrain the pinch point. When the pinch point is constrained (5˚C/9˚F in the Optimal Design case), the refrigerant can only be cooled to a temperature that is at least 5˚C (9˚F) greater than the ambient temperature. If the pinch point is not constrained (0˚C pinch point), the refrigerant can be cooled to a temperature that is almost equal to the ambient temperature. The latter case leads to significant subcooling that helps reduce the compressor work. In the former case, compressor work is higher due to the absence of subcooling.

Notice that in the Optimal Design case, both superheat and subcooling values are zero, compared to the Optimal Operation case, where superheat is zero but there is almost 5˚C (9˚F) of subcooling. Also, the refrigerant mass flow rate in the Operation case of 0.0178kg/s (2.354 lb/min) is less than that of the Design case of 0.0181kg/s (2.394 lb/min). The reduction in compressor work of the Operational case is due to non-zero subcooling of the refrigerant entering the evaporator is at a lower enthalpy, and hence the refrigerant is capable of absorbing more heat from the room at a lower refrigerant mass flow rate. This leads to zero superheat needed to extract heat from the room. Zero superheat combined with a lower mass flow rate requires less power from the compressor to compress the refrigerant to the required discharge pressure. Notice that both evaporating (2.17 bar/31.47 psi) and condensing (11.66 bar/169.1 psi) pressures are identical for both cases.

Table 3.3: Comparison of Optimal Design (5C Pinch Point) and Optimal Operation Case — $A_{evap} \leq A_{max}(3.96\ m^2)$ and $A_{cond} \leq A_{max}(9.72\ m^2)$

| | **Optimal Design** | **Optimal Operation** |
|---|---|---|
| **Ws (kW)/(kBtu)** | 4.5162 / 15.41 | 4.4179 / 15.1 |
| **Qc (kW) /(kBtu)** | 20 / 68.24 | 20 / 68.24 |
| **COP** | 4.43 | 4.53 |
| **m (kg/s) / (lb / min)** | 0.0181 / 2.394 | 0.0178 / 2.354 |
| **Superheat (˚C )** | 0 | 0 |
| **Sub-Cooling (˚C ) / (˚F)** | 0 | 4.98 / 8.96 |

Table 3.4: Comparison of Optimal Design (5C Pinch Point) and Optimal Operation Case — $A_{evap} \leq A_{max}(3.96\ m^2)$ and $A_{cond} \leq A_{max}(9.72\ m^2)$

| | | |
|---|---|---|
| **P_evap (bar)/(psi)** | 2.17/31.47 | 2.17/31.47 |
| **P_cond (bar)/(psi)** | 11.67/169.3 | 11.66/169.1 |
| **Aevap ($m^2$) / ($ft^2$)** | 3.96 / 42.6 | 4 / 43 |
| **Acond ($m^2$) / ($ft^2$)** | 9.72 / 104.6 | 9.72 / 104.6 |
| **Pinch Point (˚C)/(˚F)** | 5 / 9 | 0 |

**Application to Residential Building:**

The UT Model, which was validated with Jensen and Skogestad's data, was applied to our 2100$ft^2$ residential building to minimize the compressor work of the VCC. It should be emphasized that the UT model uses an air-source condenser, so the previous optimization results are for an air-source condenser. In this case the VCC operated between the room temperature of 20˚C (68˚F) and ambient temperature of 30˚C (86 ˚F). The refrigerant used for the following study was R 410A and the cooling load was 4 tons (14 kW). Compression efficiency was taken as 65% (Copeland Compressors [4]). The model of the compressor used was Copeland Scroll ZPS40K5E-PFV.

Recall that the Jensen and Stogestad study did not apply constraints on the superheat and subcooling. Our study applies constraints used by heat pump manufacturers. Typical suction superheat settings are 8-20˚F (4.44 to 11.11˚F) [Mike Hammond, 2011] to prevent compressor floodback, a condition where liquid refrigerant from the evaporator enters the compressor which will damage the compressor. Engineers from Climate Master suggest a suction superheat of 8 -18˚F (4.44 to 11.11˚C). The range of values for subcooling is 2 – 6 ˚F (1.11 to 3.33˚C). A minimum value for the subcooling of 2˚F is specified to prevent two-phase refrigerant from being expanded in the expansion valve which would cause valve instability. Hence, the problem can be described as follows:

The objective function (performance index) used was:

Minimize Compressor Work

$$W_s = \dot{m}_r(h_2 - h_1)$$

The five variables were subjected to the following constraints:

Cooling Load: 14 kW/47.78 kBtu/h

$$\dot{m}_r(h_1 - h_4) = 14\ kW \text{(47.7 kBtu/h)}$$

Heat Balance at the Condenser

$$\dot{m}_r(h_3 - h_2) = UA_{condenser}(T_{rsat} - T_{air})$$

where, $UA_{condenser} = 500\ W/K$

Heat Balance at the Evaporator

$$\dot{m}_r(h_1 - h_4) = UA_{evaporator}(T_{revap} - T_{room})$$

where, $UA_{evap} = 1000\ W/K$

Condition on Suction Superheat

$$8^{\circ}\text{F } (4.44^{\circ}\text{C}) < T_1 - T_{1sat} < 18^{\circ}\text{F } (11.11^{\circ}\text{C})$$

where, $T_{1sat}$ is the temperature of saturated vapor.

Condition on Condenser Subcooling

$$2^{\circ}\text{F } (1.11^{\circ}\text{C}) < T_3 < T_{3sat} < 6^{\circ}\text{F } (3.33^{\circ}\text{C})$$

where $T_{3sat}$ is the temperature of saturated liquid.

The optimization was performed for same two cases as described by Jensen and Skogestad. The additional constraints for the heat exchanger parameters, areas and pinch point, for the two cases are given below:

*Optimal Design*

Constraint on minimum pinch point

$$\Delta T > \Delta T_{min} \,(5^{\circ}C/9^{\circ}F)$$

where $\Delta T = T_{r3} - EWT$

*Optimal Operation*

Constraint on the areas of the air source heat exchangers

$$A_{evap} \leq A_{evap\ max}$$

$$A_{cond} \leq A_{cond\ max}$$

As described before, the Optimal Design solution yields values for the heat exchanger areas, which are then used as the maximum area values in the Optimal Operation constraint. The values obtained for the heat exchanger areas in the Optimal Design case were:

$$A_{evap} = 2.78\, m^2 \,(29.9\, ft^2)$$

$$A_{cond} = 6.38\, m^2 (68.6\, ft^2)$$

The results for the optimal design case are shown in

Table 3.5. It is interesting to note that the optimal values obtained for both suction superheat and condenser subcooling are the lowest in their respective ranges (4.44°C/8°F for suction superheat and 1.11°C/2°F for condenser subcooling).

EER (Energy Efficiency Rating) will be used from now on instead of COP for the cooling mode.

Table 3.5: Output for Residential House for Optimal Design Case

| | |
|---|---|
| **Ws (kW) / (kBtu/h)** | 2.56 / 8.73 |
| **EER** | 5.47 |
| **Superheat (kW) / (kBtu/h)** | 2.77 / 9.45 |
| **Superheat as % of load** | 19.78 |
| **$P_{cond}$ (kPa)/(psi)** | 2191.7 / 317.7 |
| **$P_{evap}$ (kPa)/ (psi)** | 1100.0 / 159.5 |
| **SH (˚C ) / (˚F)** | 4.44 / 8 |
| **SC (˚C ) / (˚F)** | 1.11 / 2 |
| **m (kg/s) / (lb/min)** | 0.0807 / 10.67 |
| **$A_{evap}$ ($m^2$) / ($ft^2$)** | 2.78 / 29.9 |
| **$A_{cond}$ ($m^2$) / ($ft^2$)** | 6.38 / 68.6 |
| **$T_1$ (˚C ) /(˚F)** | 15 / 59 |
| **$T_3$ (˚C ) / (˚F)** | 35 / 95 |

The results of the Optimal Operation case are shown below in Table 3.6 and Table 3.7

.

Table 3.6: Output for Residential House for Optimal Operation Case

| | |
|---|---|
| **Ws (kW) / (kBtu/h)** | 2.38 / 8.12 |
| **EER** | 5.89 |
| **Superheat (kW) / (kBtu/h)** | 2.58 / 8.8 |
| **Superheat as % of load** | 18.43 |
| **$P_{cond}$ (kPa)/(psi)** | 2135.9 / 308.9 |
| **$P_{evap}$ (kPa)/ (psi)** | 1100.5 / 159.5 |
| **SH (˚C ) / (˚F)** | 4.44 / 8 |

Table 3.7: Output for Residential House for Optimal Operation Case

| | |
|---|---|
| **SC (˚C ) / (˚F)** | 3.33 / 6 |
| **m (kg/s) / (lb/min)** | 0.0781 / 10.31 |
| **$A_{evap}$ ($m^2$) / ($ft^2$)** | 2.78 / 29.9 |
| **$A_{cond}$ ($m^2$) / ($ft^2$)** | 6.38 / 68.6 |
| **$T_1$ (˚C ) /(˚F)** | 15.05 / 59.09 |
| **$T_3$ (˚C ) / (˚F)** | 31.74 / 89.1 |

The most interesting result is that the computed suction superheat is the lowest value of its constrained range, and the computed subcooling is the highest value of its constrained range. These results are logical and can be explained as follows; with a high value of subcooling, the entering enthalpy of the refrigerant to the evaporator is low which enables the refrigerant to absorb more heat with a smaller mass flow rate. Hence, a lower superheat is needed to provide cooling. This combination of low superheat, reduced mass flow, and maximum subcooling decreases compressor work and hence increases EER. The temperature at the exit of the condenser is 31.74˚C (89.1˚F), which gives a pinch point of 1.74˚C (3.13˚F). This is lower than the 5˚C (9˚F) that was assumed for the optimal design case, and hence leads to a lower compressor work.

Table 3.8 shows the compressor work, EER and superheat (kW) at the compressor discharge for different values of compressor suction superheat (C) for a 65% compressor efficiency and 3.33˚C (6˚F) subcooling. The data shows that as the suction superheat increases: 1) compressor work increases and hence the EER decreases, and 2) superheat (kW) at the compressor discharge, which ultimately has to be rejected into the condenser, increases. From these results, one can infer that to reduce the heat rejected to the condenser, the superheat at the compressor must be reduced by either decreasing the suction superheat or increasing compressor efficiency. In general, the model shows that a 1˚C (1.8 ˚F) decrease in suction superheat decreases heat rejected into the condenser by

0.11 kW (.375 kBtu/h) . By reducing the suction superheat from 4.4˚C to 0˚C (8 – 0 ˚F), the heat rejected into the condenser is reduced by 20.1%. However, as mentioned previously, current industry guidelines recommend a minimum 4.44 ˚C (8 ˚F) of suction superheat to prevent floodback. Zero suction superheat could be accomplished with the addition of a flooded evaporator, which is commonly used in Europe, but very rarely used in the United States.

Table 3.8: Variations of Compressor Work and Compressor Discharge Superheat with Suction Superheat (C)

| | **Suction Superheat (˚C)** | | | | |
|---|---|---|---|---|---|
| | **0** | **4.44** | **6** | **8** | **10** |
| **Ws (kW) / (kBtu/h)** | 1.90/ 6.48 | 2.38/ 8.12 | 2.54/ 8.66 | 2.76/ 9.42 | 3.00/ 10.23 |
| **EER** | 7.39 | 5.89 | 5.5 | 5.08 | 4.67 |
| **Heat rejected in Condenser (kW) / (kBtu/h)** | 15.9/ 54.3 | 16.38/ 55.9 | 16.54/ 56.4 | 16.76/ 57.2 | 17/ 58 |
| **Compressor Discharge Superheat (kW) / (kBtu/h)** | 1.78/ 6.1 | 2.58/ 8.8 | 2.85/ 9.7 | 3.18/ 10.8 | 3.54/ 12.1 |
| **Compressor Discharge Superheat as % of Load** | 12.74 | 18.43 | 20.35 | 22.73 | 25.28 |
| $P_{evap}$ **(kPa) / (psi)** | 1253/ 18.2 | 1102/ 16 | 1051/ 15.2 | 991/ 14.3 | 933/ 13.5 |
| $P_{cond}$ **(kPa) / (psi)** | 2128/ 30.7 | 2136/ 30.98 | 2138/ 31 | 2142/ 31.1 | 2146/ 31.12 |
| $\dot{m}$ **(kg/s) (lb/min)** | 0.0798/ 10.6 | 0.0781/ 10.3 | 0.0775/ 10.25 | 0.0769/ 10.17 | 0.0763/ 10.1 |

Table 3.8 also shows the optimized thermodynamic properties of the VCC. It can be observed that the evaporating pressure of the refrigerant decreases while the condensing pressure increases with an increase in the suction superheat value. The mass

flow rate of refrigerant decreases as the suction superheat value increases. These results make sense since for a given cooling load the enthalpy reduction due to decreased mass flow rate is compensated for by the enthalpy increase due to increased suction superheat. Although the mass flow rate decreases with an increase in suction superheat, the compressor work increases due to the higher range of pressures through which the refrigerant must be compressed.

A flooded evaporator, shown in Figure 3-6, is a device designed like an accumulator to ensure that the refrigerant from the evaporator discharges at saturated vapor condition. Liquid refrigerant enters the flooded evaporator where it takes heat from the conditioned space (cooling mode) and changes into a two phase fluid. Once it exits the flooded evaporator, it enters a surge tank where the vapor rises to the top and the liquid accumulates at the bottom. The liquid level in the surge tank is controlled by a valve that adds liquid refrigerant to the tank. From the surge tank, saturated vapor enters the compressor. Flooded evaporators are used for large industrial chilling stations.

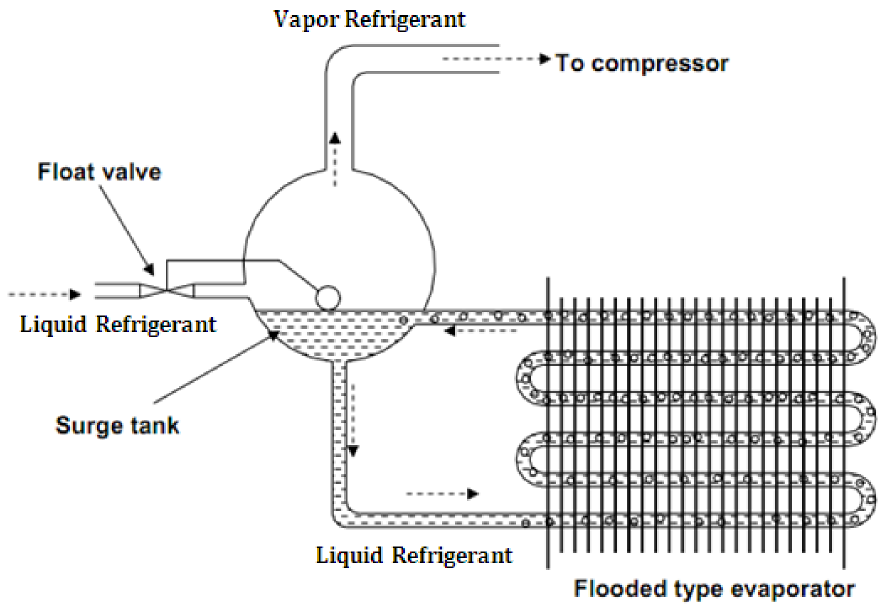


Figure 3-6: Flooded Evaporator [NPTEL – IIT Madras]

Table 3.9 shows the results for the case where the suction superheat is fixed at 4.44˚C (8˚F) (the minimum) and compressor efficiency is varied from 50% to 70%. As expected, the compressor exit superheat increases as the compressor efficiency decreases in a nonlinear fashion; as compressor efficiency decreases, the superheat increases at a much higher rate, and consequently more heat must be rejected by the condenser. This analysis shows compressor efficiency, suction superheat and subcooling values are important variables in the VCC cycle.

Table 3.9: Variations of Compressor Work and Compressor Exit Superheat with Compressor Efficiency at 4.44˚C Suction Superheat

| **Compressor Efficiency (%)** | **70%** | **65%** | **60%** | **55%** | **50%** |
|---|---|---|---|---|---|
| **Ws (kW) / (kBtu/h)** | 2.20/ 7.5 | 2.38/ 8.1 | 2.58/ 8.8 | 2.83/ 9.7 | 3.12/ 10.6 |
| **EER** | 6.36 | 5.89 | 5.42 | 4.95 | 4.48 |
| **Heat rejected in Condenser (kW) / (kBtu/h)** | 16.2/ 55.3 | 16.38/ 55.9 | 16.58/ 56.6 | 16.83/ 57.4 | 17.12/ 58.4 |
| **Compressor Exit Superheat (kW) / (kBtu/h)** | 2.40/ 8.2 | 2.58/ 8.8 | 2.79/ 9.5 | 3.03/ 10.3 | 3.33/ 11.4 |
| **Superheat as % of load** | 17.17 | 18.43 | 19.91 | 21.66 | 23.78 |

Table 3.10 shows the comparison between two cases of suction superheat; the ideal case (0˚C) and the practical minimum case (4.44˚C/ 8˚F). The comparison is also shown for two values of compressor efficiency; 70% and 60%. It can be seen that for compressor efficiency of 70% and with no suction superheat, the compressor work is 20% lower (1.76 kW/ 6 kBtu/h compared to 2.2 kW / 7.5 kBtu/h) than the case with a 4.44˚C/ 8˚F suction superheat. With 60% efficiency, compressor work decreases by 20.1% for the no suction superheat case.

This reduction in compressor work is reflected in the heat rejected into the condenser. Using a compressor with a 70% efficiency rating, the heat rejected into the condenser is lower by 0.44 kW (1.5 kBtu/h) when there is no suction superheat, compared to a 4.44˚C (8˚F) suction superheat. This reduction is 0.52 kW (1.77 kBtu/h) for the compressor with 60% efficiency. It can be inferred that for a low efficiency compressor, it makes sense to have as low a suction superheat as possible to reduce condenser heat rejection.

Table 3.10: Variations of Compressor Work and Compressor Exit Superheat with Compressor Efficiency at 4.44 ˚C Suction Superheat

| **Compressor Efficiency (%)** | **70%** | | **60%** | |
|---|---|---|---|---|
| **Suction Superheat (˚C)/(˚F)** | **0/0** | **4.44/8** | **0/0** | **4.44/8** |
| **Ws (kW) / (kBtu/h)** | 1.76 | 2.20 | 2.06 | 2.58 |
| **EER** | 7.97 | 6.36 | 6.80 | 5.42 |
| **Heat rejected in Condenser (kW) / (kBtu/h)** | 15.76/ 53.8 | 16.2/ 55.2 | 16.06/ 54.8 | 16.58/ 56.6 |
| **Compressor Exit Superheat (kW) / (kBtu/h)** | 1.64/ 5.6 | 2.40/ 8.2 | 1.95/ 6.7 | 2.79/ 9.6 |
| **Superheat as % of load** | 11.75 | 17.17 | 13.91 | 19.91 |

**Coupling with Ground Loop: Water-source Condenser**

All the discussion and results provided above are for air source heat pumps. Since we are interested in implementing ground-source heat pumps, we must replace the air-source condensers with water-source condensers in the previous models. Modeling a water-source condenser is more difficult than modeling an air-source condenser. In an air source condenser, air blows over the heat exchanger and there is a simple formulation to calculate the heat transfer given by:

$$Q_{cond}(Air\ Source\ Heat\ Pump) = UA_{ASHP}(T_{refcond} - T_{air}) \tag{3.10}$$

where $UA_{ASHP}$ is the heat transfer coefficient for the condenser heat exchanger, $T_{refcond}$ is the condensing temperature of the refrigerant and $T_{air}$ is the air temperature blowing across the heat exchanger. This is simple since the heat transfer coefficient for the condenser heat exchanger is typically known. For a water-source condenser heat exchanger the heat transfer coefficient is not known.

A brief description of the parameters and the model are summarized below:

- Cooling Load = 14 kW (4 tons)

- Flow rate of Water in Ground Loop = 12 gpm (.748 kg/s)
- Entering Water Temperature from Ground Loop= 70˚F, 90˚F, 110˚F (21.1, 32.2 43.3˚F)
- Condition Space Room Temp = 21 ˚C (69.8 ˚F)
- Compressor - Copeland Scroll ZPS40K5E-PFV

**Performance Index**– Min $W_s = \dot{m}_r(h_2 - h_1)$

**Constraints**

*Pinch Point*

$$T_3 - EWT > 5^{\circ}C \ \ (9^{\circ}\text{F})$$

This constraint ensures that the refrigerant exit temperature is greater than the EWT by at least 5˚C pinch point [Appendix B].

*Evaporator Exit Temperature*

$$T_1 < 21^{\circ}C/69.8^{\circ}F \text{ (Room Temperature)}$$

*Heat Balance in the Evaporator*

$$\dot{m}_r(h_1 - h_4) = UA_{evap}(T_{room} - T_1) \tag{3.11}$$

where $UA_{evap}$ is the heat transfer coefficient times the area of the evaporative heat exchanger (Appendix), $T_1$ is temperature of the refrigerant at the evaporator exit and $T_{room}$ is the temperature of the room.

*Heat Balance in the Condenser*

$$\dot{m}_r(h_2 - h_3) = UA_{SH}(\overline{T_{r\,SH}} - \overline{T_{w\,SH}}) + UA_{SAT}(\overline{T_{r\,SAT}} - \overline{T_{w\,SAT}}) + UA_{SC}(\overline{T_{r\,SC}} - \overline{T_{w\,SC}}) \tag{3.12}$$

where, in the superheated, saturated and subcooled regions of the condenser, $UA_{SH}$, $UA_{SAT}$, $UA_{SC}$ are the values of heat transfer coefficient times the area; $\overline{T_{r\,SH}}$, $\overline{T_{r\,SAT}}$ and $\overline{T_{r\,SC}}$ are the average refrigerant temperatures; and $\overline{T_{w\,SH}}$, $\overline{T_{w\,SAT}}$ and $\overline{T_{w\,SC}}$ are the average water temperatures, respectively.

Table 3.11: Suction Superheat and Condenser Subcooling in the following Ranges

| **EWT (°C /°F )** | **Superheat (°C / °F )** | **Subcooling (°C / °F )** |
|---|---|---|
| **21.1/70** | 5 – 7.7 / 9 - 14 | 2.8 – 5.5 / 5 - 10 |
| **32.2/90** | 3.9 – 6.7 / 7 - 12 | 2.2 – 5 / 4 - 9 |
| **43.3/110** | 3.9 – 6.7 / 7- 12 | 1.7 – 4.4 / 3 - 8 |

A concentric tube counter-flow heat exchanger between the refrigerant and the water is assumed. The formulation is more complex for a water source condenser since the heat transfer coefficient for the condenser heat exchanger is unknown. Since manufacturers do not reveal the heat exchanger design details, performance data from heat pump performance maps are used to determine the UA (heat transfer coefficient * Area) values of the heat exchanger at different operating conditions. Table 3.12 gives the performance rating of Climate Master's TT 049 model Heat Pump: cooling load, compressor work and the heat rejected in the condenser for three different values of entering water temperature. Figure 8 shows the VCC operating points for five different entering water temperatures. It specifies the range of compressor suction and discharge pressures, suction superheat, and condenser subcooling,

Table 3.12: Rating of TT 049 Heat Pump [Climate Master]

| EWT (˚F)/(˚C ) | Cooling Load (kW)/ (kBtu/h) | Compressor Work (kW)/ (kBtu/h) | Heat Rejected (kW)/ (kBtu/h) | Compressor Efficiency ( % ) |
|---|---|---|---|---|
| 70/21.1 | 15.75/ 53.7 | 2.81/ 9.6 | 18.56/ 63.3 | 64 |
| 90/32.2 | 14.06/ 47.9 | 3.32/ 11.3 | 17.10/ 58.3 | 71.8 |
| 110/43.3 | 12.13/ 41.4 | 4.00/ 13.6 | 16.14/ 55.1 | 69.2 |

| TT049 | | Full Load Cooling - without HWG active | | | | | |
|---|---|---|---|---|---|---|---|
| Entering Water Temp °F | Water Flow GPM/ ton | Suction Pressure PSIG | Discharge Pressure PSIG | Superheat | Subcooling | Water Temp Rise °F | Air Temp Drop °F DB |
| 30* | 1.5 | 112-122 | 187-207 | 22-27 | 14-19 | 20.7-22.7 | 18-24 |
| | 2.25 | 111-121 | 167-187 | 22-27 | 12-17 | 15.5-17.5 | 18-24 |
| | 3 | 111-121 | 147-167 | 23-28 | 11-16 | 10.2-12.2 | 18-24 |
| 50 | 1.5 | 125-135 | 242-262 | 13-18 | 10-15 | 20.9-22.9 | 19-25 |
| | 2.25 | 123-133 | 224-244 | 13-18 | 9-14 | 15.6-17.6 | 19-25 |
| | 3 | 122-132 | 205-225 | 14-19 | 7-12 | 10.2-12.2 | 19-25 |
| 70 | 1.5 | 133-143 | 310-330 | 8-13 | 8-13 | 20.5-22.5 | 19-25 |
| | 2.25 | 132-142 | 290-310 | 8-13 | 7-12 | 15.2-17.2 | 19-25 |
| | 3 | 131-141 | 270-290 | 9-14 | 5-10 | 9.9-11.9 | 19-25 |
| 90 | 1.5 | 138-148 | 396-416 | 7-12 | 7-12 | 19.2-21.2 | 18-24 |
| | 2.25 | 137-147 | 374-394 | 7-12 | 6-11 | 14.3-16.3 | 18-24 |
| | 3 | 136-146 | 352-372 | 7-12 | 4-9 | 9.3-11.3 | 18-24 |
| 110 | 1.5 | 144-154 | 497-517 | 7-12 | 5-10 | 18-20 | 17-23 |
| | 2.25 | 143-153 | 472-492 | 7-12 | 4-9 | 13.3-15.3 | 17-23 |
| | 3 | 142-152 | 447-467 | 7-12 | 3-8 | 8.5-10.5 | 17-23 |

Figure 3-7: Performance Map – Climate Master TT 049 Heat Pump (Source: Climate Master)

The only difference between the method used for water source heat pumps and air source heat pumps is the determination of the $UA$ values, and the following procedure is followed. For three EWTs (70, 90 and 110 ˚F), the average operating points (suction and discharge pressures, suction superheat and condenser subcooling) are taken from the performance map (Figure 3-7). The condenser is divided into three sections:

Superheated, saturated and subcooled. The refrigerant temperatures at the inlet and exit of each section are computed using the average operating points from Figure 3-7.

The condenser is divided into three sections (Figure 3-8) because the refrigerant temperature profile changes across the condenser; decreases across the superheated section, constant through the saturated region and again decreases through the subcooling section. This nonlinear change in refrigerant temperature and associated phase change across the condenser makes the computation of the refrigerant and water conditions more accurate by dividing the condenser into three sections. The water temperature is approximated to increase linearly across the condenser. The computation algorithm is as follows.

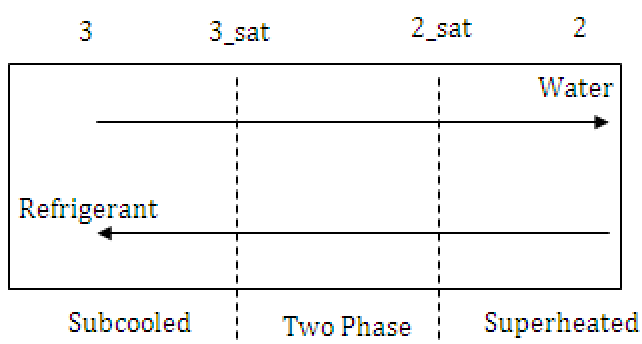


Figure 3-8: Schematic of Condenser Heat Exchanger

- Once the refrigerant temperatures are computed by the optimization model, heat rejected in each section is calculated.
- That heat rejected is used to calculate the water temperature at the exit of each section($T_{3sat}, T_{2sat}, T_2$).
- Average temperatures of the refrigerant and water in each section are computed.
- Average $UA$ values in each section are calculated using the following expressions:

$$UA_{SC} = \frac{Q_{SC}}{(\overline{T_{rSC}} - \overline{T_{wSC}})} \tag{3.13}$$

$$UA_{SAT} = \frac{Q_{SC}}{(\overline{T_{rSAT}} - \overline{T_{wSAT}})} \tag{3.14}$$

$$UA_{SH} = \frac{Q_{SC}}{(\overline{T_{rSH}} - \overline{T_{wSH}})} \tag{3.15}$$

The computed $UA$ values in each section are shown in Table 3.13. These UA values are used to solve the optimization problem as described before.

Table 3.13: UA Values of the Water-Source Condenser (W/K)

| **EWT (°C /°F )** | **Subcooled (W/K)** | **Saturated (W/K)** | **Superheated (W/K)** |
|---|---|---|---|
| **21.1/70** | 87 | 2,217 | 168 |
| **32.2/90** | 77 | 1,904 | 183 |
| **43.3/110** | 84 | 1,794 | 210 |

**RESULTS AND CONCLUSIONS**

The results of the optimization for the three EWTs are shown below. Table 3.14 shows the minimum compressor work that can be attained for each EWT. For each case the suction superheat, condenser subcooling and the mass flow rate of refrigerant is also shown. In all cases, the minimum possible superheat from the specified range gives the minimum compressor work. Likewise, the subcooling values are the maximum possible in the specified range. This again confirms our previous inference that the maximum possible subcooling and minimum possible suction superheat values yield the lowest compressor work, and hence lowest heat rejection into the condenser. EER (Energy

Efficiency Rating) instead of COP is used to describe the efficiency of the VCC in the cooling mode.

Table 3.14: Optimization Results for Water Source Condenser

| **EWT (˚F )/ (˚C )** | **Cooling Load (kW)/ (kBtu/h)** | **Ws (kW)/ (kBtu/h)** | **EER** | **Heat Rejected (kW)/ (kBtu/h)** | **SH (˚C )/ (F)** | **SC (˚C )/ (F)** | **m (kg/s)/ (lb/min)** |
|---|---|---|---|---|---|---|---|
| **70/ 21.1** | 15.65/ 53.4 | 2.89/ 9.9 | 5.46 | 18.64/ 63.6 | 5.00/ 9 | 5.55/ 10 | 0.0806/ 10.67 |
| **90/ 32.2** | 13.96/ 47.6 | 3.15/ 10.7 | 4.44 | 17.21/ 58.7 | 3.88/ 7 | 4.22/ 7.6 | 0.08/ 10.58 |
| **110/ 43.3** | 11.13/ 38 | 3.53/ 12 | 3.15 | 15.66/53.4 | 3.88/ 7 | 4.44/ 8 | 0.0728/ 9.62 |

Table 3.15 shows the comparison of Compressor work, EER and Heat Rejected between the optimization results of the UT Model and Climate Master's performance data. It can be seen that for the 70 F EWT case, the UT Model is less effective than the Climate Master data. The UT model gives a compressor work that is 3.2% lower a COP that is 2.5% lower and heat rejection that is 0.64% higher. The UT model gives more efficient results for the 90 and 110 ˚F EWT cases. The compressor work for the 90˚F EWT case is 5.1% lower and the heat rejected into the condenser is 1% lower compared to the Climate Master data. The EER is 4.7% higher. The performance of VCC for the 110 ˚F EWT case is significantly better than that of the 90 ˚F EWT case. For the 110 F case, the compressor work is lower by 11.8% and the heat rejected is 2.9% lower than the Climate Master data, which leads to a 4% higher EER.

Table 3.15: Comparison between UT Model and Climate Master

| | Ws (kW) / (kBtu/h) | | EER | | Heat Rejected (kW) / (kBtu/h) | |
|---|---|---|---|---|---|---|
| **EWT (°F / °C)** | **Model** | **Climate Master** | **Model** | **Climate Master** | **Model** | **Climate Master** |
| **70/21.1** | 2.88/ 9.8 | 2.81/ 9.6 | 5.46 | 5.60 | 18.64/ 63.6 | 18.56/ 63.3 |
| **90/32.2** | 3.15/ 10.7 | 3.32/ 11.3 | 4.44 | 4.24 | 17.21/ 58.7 | 17.38/ 59.3 |
| **110/43.3** | 3.53/ 12.0 | 4.00/ 13.6 | 3.15 | 3.03 | 15.66/ 53.4 | 16.13/ 55.0 |

This optimization shows that with optimal control of the suction superheat and condenser subcooling, the heat rejected into the condenser can be lowered by as much as 0.46 kW. This heat rejected is lower than the non optimized case by 2.9%. This 0.46 kW reduction in heat rejected to the condenser is equivalent to a reduction in the exit water temperature in the ground loop by 0.15°C. This decrease in temperature is very small.

# Chapter 4. Desuperheaters

## INTRODUCTION

Desuperheaters are devices that use the superheat of the refrigerant at the compressor discharge of the vapor compression cycle to heat domestic water. During the cooling mode of operation, the heat extracted by the desuperheater is a form of supplemental heat recovery since that amount of heat would otherwise be rejected into the condenser. Desuperheaters typically capture 10 – 25 % of the total heat rejected into the condenser (Lee and Jones, 1997). During the heating mode of operation, the heat captured for hot water heating would otherwise be used to heat the house, so the heat pump must run for a longer period to heat the house. For cooling-dominated climates, the desuperheater reduces the heat rejected into the water loop condenser, and hence decreases the amount of heat rejected to the ground. In this chapter, we analyze how an expanded desuperheater can be used as a SHR device to extract as much heat as possible, thereby reducing the heat rejected to the ground.

## BACKGROUND: VAPOR COMPRESSION CYCLE (VCC) IN COOLING MODE

Figure 4-1 shows the ideal thermodynamic P-h diagram of the VCC cycle of the heat pump in the cooling mode with 90F EWT (Entering Water Temperature to the heat pump): G-B is the heat input from the building to be cooled, B-C is the compressor work and reflects its efficiency, C-F is the heat rejected in the condenser, and F-G is the expansion through the expansion valve. C-D is the region where the refrigerant is in a superheated state, and where heat transfer into the desuperheater takes place in a concentric tube heat exchanger.

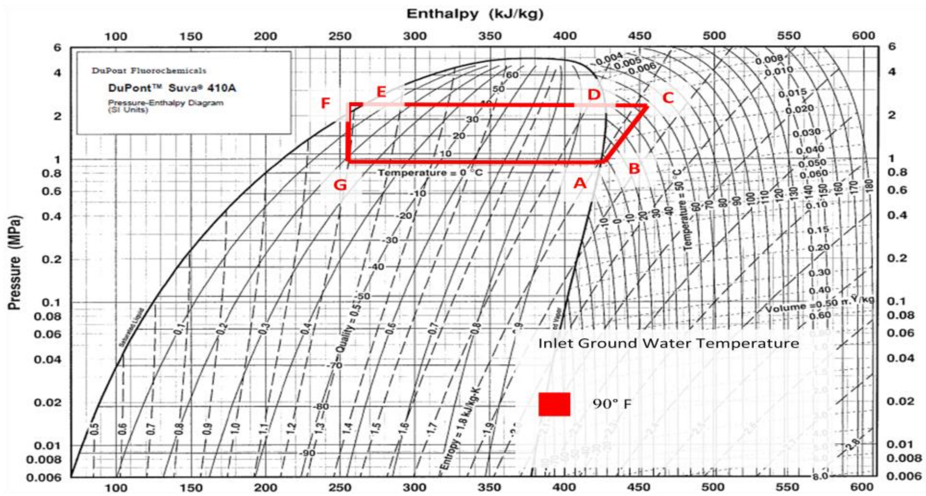


Figure 4-1: Thermodynamic Cycle of Heat Pump in Cooling Mode

For the case of EWT=32.3C (90F), refrigerant 410A and data from Water Furnace Heat Pump, the average enthalpies at C and D are 455.1 kJ/kgK (0.196 kBtu/lb) and 427.1 kJ/kgK (0.184 kBtu/lb), respectively. For a refrigerant flow rate of 0.078 kg/s (10.32 lb/min), the total superheat available is 2.18kW. This amount of superheat represents 15.9% of the cooling load (Table 2). Table 4.1 shows the thermodynamic states for three EWTs, 21.1˚C (70˚F), 32.2˚C (90˚F) and 43.3˚C (110˚F). Table 2 shows the suction superheat A-B and subooling E-F values, and the superheat C-D as a percentage of cooling load for each EWT. The average suction superheat is 6.7 kJ/kg, average condenser subcooling is 9.97 kJ/kg and the average compressor exit superheat is 17.4% of the cooling load (Table 4.2).

Table 4.1: Thermodynamic Values at Different Points of the VCC in Cooling Mode

| 21.1° C (70 °F) EWT | Point A | Point B | Point C | Point D | Point E | Point F | Point G |
|---|---|---|---|---|---|---|---|
| Pressure (MPa) | 0.962 | 0.962 | 1.827 | 1.827 | 1.831 | 1.831 | 0.965 |
| Temperature (°C) | 6.1 | 11.9 | 44.2 | 28.9 | 28.9 | 23.9 | 6.1 |
| Enthalpy (kJ/kg) | 424.2 | 430.9 | 448.7 | 427.5 | 247.1 | 238.5 | 238.5 |
| Pressure (psi) | 139.5 | 139.5 | 265.0 | 265.0 | 265.6 | 265.6 | 140.0 |
| Temperature (°F) | 42.98 | 53.42 | 111.5 | 84.02 | 84.02 | 75.02 | 42.98 |
| Enthalpy (kBtu/lb) | 0.182 | 0.185 | 0.193 | 0.184 | 0.106 | 0.103 | 0.103 |
| 32.2° C (90 °F) EWT | Point A | Point B | Point C | Point D | Point E | Point F | Point G |
| Pressure (MPa) | 0.9894 | 0.9894 | 2.344 | 2.344 | 2.351 | 2.351 | 0.9915 |
| Temperature (°C) | 7 | 12.8 | 57.3 | 38.8 | 38.8 | 38.8 | 7 |
| Enthalpy (kJ/kg) | 424.4 | 431.1 | 455.1 | 427.1 | 264.9 | 254.9 | 254.9 |
| Pressure (psi) | 143.5 | 143.5 | 340.0 | 340.0 | 340.9 | 340.9 | 143.8 |
| Temperature (°F) | 44.6 | 55.04 | 135.1 | 101.8 | 101.8 | 101.8 | 44.6 |
| Enthalpy (kBtu/lb) | 0.182 | 0.185 | 0.196 | 0.184 | 0.114 | 0.110 | 0.110 |
| 43.3° C (110 °F) EWT | Point A | Point B | Point C | Point D | Point E | Point F | Point G |
| Pressure (MPa) | 0.9894 | 0.9894 | 3.102 | 3.102 | 3.111 | 3.111 | 0.9915 |
| Temperature (°C) | 7 | 12.8 | 73.4 | 50.7 | 50.7 | 45.2 | 7 |
| Enthalpy (kJ/kg) | 424.4 | 431.1 | 463.2 | 424.3 | 288.4 | 277.1 | 277.1 |
| Pressure (psi) | 143.5 | 143.5 | 449.9 | 449.9 | 451.1 | 451.1 | 143.8 |
| Temperature (°F) | 44.6 | 55.04 | 164.10 | 123.3 | 123.3 | 113.4 | 44.6 |
| Enthalpy (kBtu/lb) | 0.182 | 0.185 | 0.199 | 0.182 | 0.124 | 0.119 | 0.119 |

Table 4.2: Superheat and Subcooling Values for Cooling Mode

| **EWT ˚C (˚F)** | **Suction Superheat A-B kJ/kg (Btu/lb)** | **Subcooling E-F kJ/kg (Btu/lb)** | **Superheat C-D as % of Cooling Load (cd/gb)** |
|---|---|---|---|
| **21.1 (70)** | 6.7/2.88 | 8.6/3.69 | 11.0 |
| **32.2 (90)** | 6.7/2.88 | 10/4.3 | 15.9 |
| **43.3 (110)** | 6.7/2.88 | 11.3/4.86 | 25.3 |
| **Average** | 6.72.88 | 9.97/4.29 | 17.4 |

## BACKGROUND: VAPOR COMPRESSION CYCLE (VCC) IN HEATING MODE

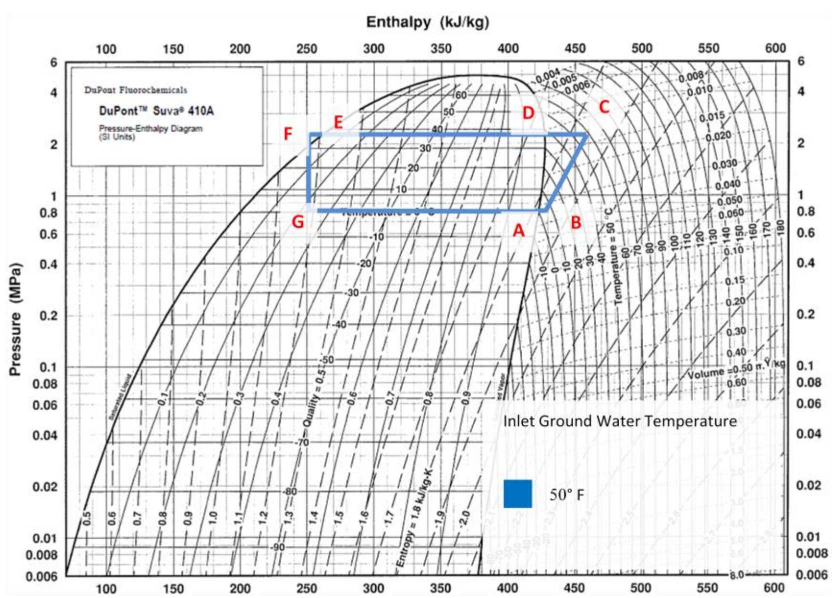


Figure 4-2: Thermodynamic Cycle of Heat Pump in Heating Mode

In the heating mode with 10C (50F) EWT, shown in Figure 4-2 above, G-B is the heat extracted out of the ground loop water entering the heat pump, B-C is the compressor work and reflects its efficiency, C-F is the heat supplied to the building, and F-G is the expansion through the expansion valve. Assuming a 10C EWT, refrigerant

410A and data from a heat pump manufacturer, average enthalpies at C and D are 459.1 kJ/kgK and 426.3 kJ/kgK (0.197 kBtu/lb and 0.183 kBtu/lb), respectively. For a refrigerant flow rate of 0.078 kg/s, the total superheat available is 2.56 kW (8.73 kBtu/h). This amount of superheat is 16.2% of the heating load (Table 4.2). Table 4.3 shows the thermodynamic states for the three EWTs and Table 4.5 shows the suction superheat A-B and subooling E-F values, and the superheat C-D as a percentage of cooling load for each EWT. The average suction superheat is 6.1kJ/kg, average condenser subcooling is 5.0kJ/kg and the average compressor exit superheat is 15.9% of the heating load.

Table 4.3: Thermodynamic Values at different points of the VCC in Heating Mode

| 30 °F EWT | Point A | Point B | Point C | Point D | Point E | Point F | Point G |
|---|---|---|---|---|---|---|---|
| Pressure (MPa) | 0.565 | 0.565 | 2.016 | 2.016 | 2.024 | 2.024 | 0.5666 |
| Temperature (°C) | -10.4 | -4.3 | 57.4 | 32.8 | 32.8 | 30.6 | -10.4 |
| Enthalpy (kJ/kg) | 419.2 | 425.1 | 461.5 | 427.6 | 254 | 250.1 | 250.1 |
| Pressure (psi) | 81.9 | 81.9 | 292.4 | 292.4 | 293.5 | 293.5 | 82.2 |
| Temperature (°F) | 13.28 | 24.26 | 135.3 | 91.04 | 91.04 | 87.08 | 13.28 |
| Enthalpy (kBtu/lb) | 0.180 | 0.183 | 0.198 | 0.184 | 0.109 | 0.108 | 0.108 |
| | | | | | | | |
| **50 °F EWT** | **Point A** | **Point B** | **Point C** | **Point D** | **Point E** | **Point F** | **Point G** |
| Pressure (MPa) | 0.779 | 0.779 | 2.258 | 2.258 | 2.2649 | 2.2649 | 0.7871 |
| Temperature (°C) | -0.7 | 6.1 | 59.1 | 37.3 | 37.3 | 34 | -0.7 |
| Enthalpy (kJ/kg) | 422.35 | 429 | 459.1 | 426.3 | 262.1 | 256.1 | 256.1 |
| Pressure (psi) | 113.0 | 113.0 | 327.5 | 327.5 | 328.5 | 328.5 | 114.2 |
| Temperature (°F) | 30.74 | 42.98 | 138.38 | 99.14 | 99.14 | 93.2 | 30.74 |

Table 4.4: Thermodynamic Values at different points of the VCC in Heating Mode

| | | | | | | | |
|---|---|---|---|---|---|---|---|
| **Enthalpy (kBtu/lb)** | 0.182 | 0.184 | 0.197 | 0.183 | 0.113 | 0.110 | 0.110 |
| | | | | | | | |
| **70 °F EWT** | **Point A** | **Point B** | **Point C** | **Point D** | **Point E** | **Point F** | **Point G** |
| **Pressure (MPa)** | 1.0308 | 1.0308 | 2.4649 | 2.4649 | 2.5388 | 2.5388 | 1.0313 |
| **Temperature (°C)** | 8.3 | 15 | 60.4 | 42 | 42 | 37 | 8.3 |
| **Enthalpy (kJ/kg)** | 424.7 | 432.5 | 456.9 | 426.6 | 270.9 | 261.5 | 261.5 |
| **Pressure (psi)** | 149.5 | 149.5 | 357.5 | 357.5 | 368.2 | 368.2 | 149.6 |
| **Temperature (°F)** | 46.94 | 59 | 140.72 | 107.6 | 107.6 | 98.6 | 46.94 |
| **Enthalpy (kBtu/lb)** | 0.183 | 0.186 | 0.196 | 0.183 | 0.116 | 0.112 | 0.112 |

Table 4.5: Superheat and Subcooling Values for Heating Mode

| **EWT ˚ C (˚F)** | **Suction Superheat A-B kJ/kg (Btu/lb)** | **Subcooling E-F kJ/kg (Btu/lb)** | **Superheat as % of Heating Load (cd/cf)** |
|---|---|---|---|
| **-1.1/30** | 5.9/2.53 | 3.9/1.67 | 16.04 |
| **10/50** | 6.6/2.84 | 6.0/2.58 | 16.16 |
| **21.1/70** | 5.8/2.5 | 9.4/4.04 | 15.51 |
| **Average** | 6.1/2.62 | 6.43/2.77 | 15.90 |

The desuperheater uses the superheat portion C-D of the VCC to heat water. This section showed the amount of superheat that is available when the heat pump is in the cooling and heating modes. These amounts will be used to determine the quantity of hot water that can be generated. The next section describes an analysis by Oak Ridge

National Labs on computing the amount of hot water that can be generated by utilizing the superheat.

### ANALYSIS BY OAK RIDGE NATIONAL LABS

Olszewski and Fontana of Oak Ridge National Labs (1984) performed a detailed analysis of using desuperheaters to generate hot water for domestic use. They took a model house (1800 $ft^2$) and calculated cost savings for a 2 ton heat pump using refrigerant R 22. Figure 4-3 below shows the p-h diagram of the VCC for different operating conditions. For the case shown by the solid line, the refrigerant condenses at a pressure of 257.42 psi (1.774 MPa). The region D-F is the superheated region of the condenser, where the refrigerant cools down from 220˚F (104˚C) at Point D to 150˚F (60 ˚C) at Point F. For this case, the superheat is 31% of the cooling load. For the case shown by the dashed line, the refrigerant condenses at a lower pressure, and hence the available superheat is on an average 20% of the cooling load.

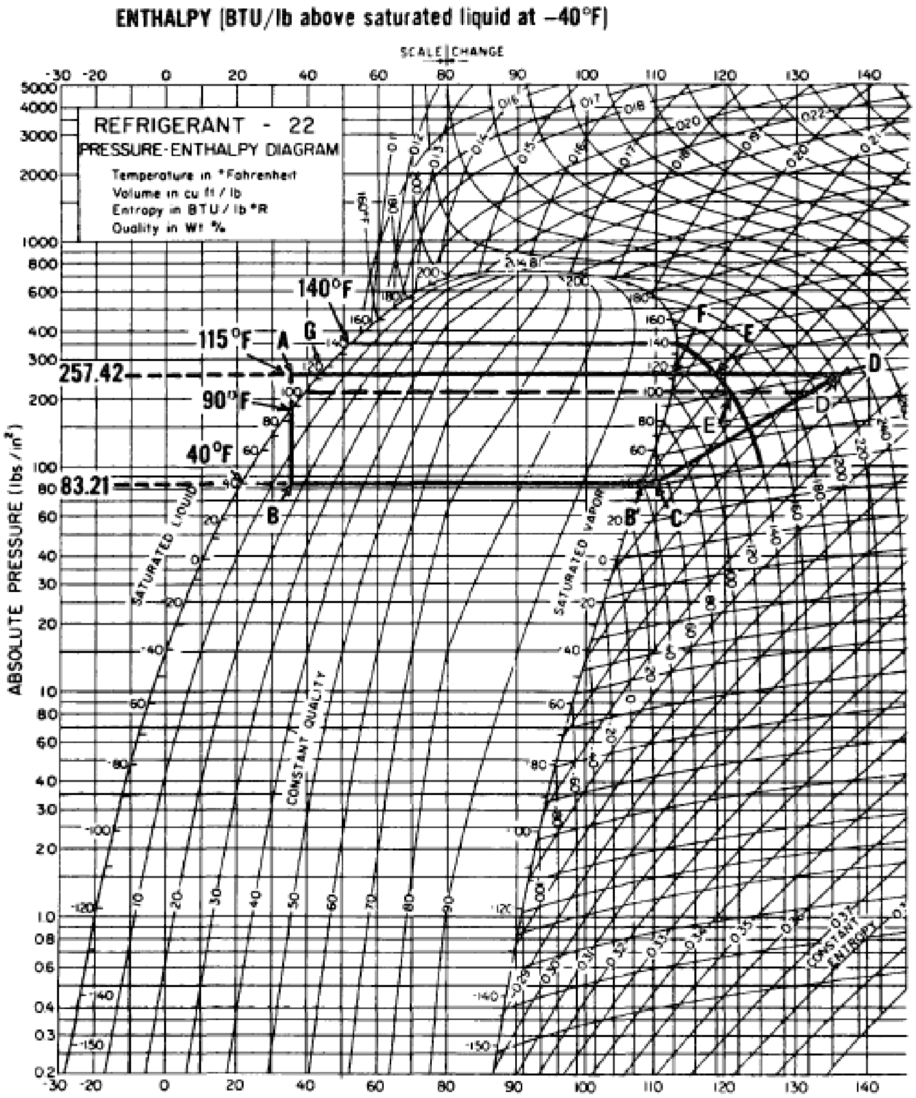


Figure 4-3: P-h Diagram of Heat Pump with R 22 as Refrigerant [Olszewski and Fontana, 1984]

Three cases of hot water consumption were analyzed: 25, 50 and 75 gal/day (1.55, 3.11 and 4.68 kg/s). For each one of the cases, it was assumed that the water could be heated to 140˚F (60˚C). The pinch point associated with the heat exchanger in question was 10°F (5.55°C). Hence, for 75 gal/day domestic hot water consumption, the maximum heat that could be used was given by the equation:

$$Q_{max}\left(\frac{Btu}{h}\right) = 33.88 * (140 - T_{in}) \tag{4.1}$$

where $T_{in}$ was the inlet temperature of water (F) as a function of the location and time of the year.

The superheat heat available from the heat pump was given by:

$$Q_{av}\left(\frac{Btu}{h}\right) = 0.2 * \left(Q_{cyc}\right) * R_s \tag{4.2}$$

where, $Q_{cyc}$ is the heat pump cooling or heating load in Btu/hr and $R_s$ is the fraction of time during an hour the heat pump is switched on.

The analysis was done for 28 different sites. The heating and cooling loads were based on the specific site analyzed, but the domestic hot water usage was assumed to be the same for all sites (three cases - 25, 50 and 75 gal/day). The total energy extracted by the desuperheater was compared to the total energy needed for yearly hot water generation by either gas or electric. The difference between the two values represents the total energy saved. The annual energy savings was found to be a maximum in areas with long summers, where the source of reclaimed heat was mostly from the heat that was going to be rejected into the condenser. It was found that 2,848 kWh of energy per year could be saved if the desuperheater were run in Fort Worth, Texas compared to just 1,616 kWh in Chicago.

The next section will discuss how the method described above will be used to extract heat out from the VCC of a residential house in Austin.

**UT DESUPERHEATER MODEL**

The basic assumption of the Oak Ridge National Lab analysis and the subsequent UT model is that an expanded desuperheater can be designed to remove as much as 100% of the available superheat, while current desuperheater designs remove approximately 20% of the superheat.

The house to be investigated in the UT Desuperheater Model was a 2,100 $ft^2$ ( $m^2$) house located in Austin, TX. It had a 4-ton (14 kW) unit heat pump installed which provided both cooling and heating to the building. The building loads were generated for every two minute time steps for an entire year (Jonathan Gaspredes, 2011). The desuperheater is functional only when the heat pump is operating. The building load data shows that the heat pump was in the cooling mode for 2022 hours and in the heating mode for 277 hours of the year, thus the heat pump was operating for a total of 2279 hours.

From the Background section above, it was calculated that the superheat represented an average of 17.4% of the cooling load and 15.9% of the heating load. The equations used to calculate the total available superheat per year were:

$$SH_{cool}\left(\frac{kBtu}{h}\right) = \sum 0.174 * Q_{cool} \tag{4.3}$$

$$SH_{heat}\left(\frac{kBtu}{h}\right) = \sum 0.159 * Q_{heat} \tag{4.4}$$

$$SH_{total}\left(\frac{kBtu}{h}\right) = SH_{cool} + SH_{heat} \tag{4.5}$$

where $SH_{cool}$ and $SH_{heat}$ are the superheats when the heat pump is in the cooling and heating mode, respectively, $Q_{cool}$ and $Q_{heat}$ are the cooling and heating loads in each time step (two minute steps), respectively, and $SH_{total}$ is the total superheat available in the entire year.

For a 4 ton (14 kW) heat pump, the available superheat during the cooling mode is 8.29 kBtu/hr (2.43 kW) and during the heating mode is 7.58 kBtu/hr (2.22 kW).

The next step was to determine the amount of energy required to heat the water for domestic purposes for three different cases of consumption: 25, 50, and 75 gal/day. The initial temperature of water in all cases was taken to be 72˚F (22.2˚C), which is the same temperature as that of the ground. The water was assumed to be heated to a temperature of 125.6˚F (52˚ C) based on a 10˚F pinch point of the heat exchanger (See Table 4.1 and Table 4.3).

The pinch point was arrived at by first calculating the temperatures of the refrigerant leaving the compressor for each EWT. Point C is the point where the refrigerant exits the compressor. The average compressor exit temperature was then calculated for both the heating and the cooling modes of the heat pump. The minimum average value for the two cases – heating and cooling modes – was calculated to be 135.6 ˚F (57.5˚C). Hence the total heat required per day for each one of the three cases is: 11, 22 and 33 kBtu (11.6 kJ, 23.2 kJ and 34.8 kJ).

For each day, the total superheat that could be extracted when the heat pump was in operation was calculated. With this amount of heat, the quantity of hot water that could be produced each day was calculated for the three cases of domestic hot water consumption. The total number of days that domestic hot water needs could be satisfied by using the desuperheater was also evaluated and plots were generated. There were days when more than the required quantity of hot water was generated. The total additional quantity of water generated in a year and the cost incurred were also calculated.

## RESULTS

As described in the previous section, the buildings loads for a 2,100 ft$^2$ building in Austin were used [Jonathan Gaspredes, 2011]. These loads are building loads for only the first year of operation of the heat pump. This is an assumption since with time, due to ground heating, more heat will be available from the heat pump when the desuperheater is used in the heating mode. Hence, the results shown below are for the first year of operation only and the results will be different if analysis was done for a different year. The superheat available when the heat pump is operating was calculated and shown in Table 4.6 for a year during both heating and cooling modes. Table 5 also shows the amount of energy that can be extracted if only 75% and 50% of the total available superheat were used.

Table 4.6: Energy Extracted by Desuperheater for different Percentages of Available Superheat

| Energy Extracted by Desuperheater per year | 100% of Available Superheat kBtu (kJ) | 75% of Available Superheat kBtu (kJ) | 50% of Available Superheat kBtu (kJ) |
|---|---|---|---|
| During Cooling | 13,228 (13,956) | 9,921 (10,467) | 6,614 (6,978) |
| During Heating | 2,640 (2,785) | 1,980 (2,089) | 1,320 (1,393) |
| Total | 15,868 (16,741) | 11,901 (12,556) | 7,934 (8,370) |

Table 4.7 shows the number of days the desuperheater can satisfy the hot water needs of a house for three different cases of operation: 100%, 75% and 50% utilization of superheat of the VCC. As expected, by utilizing 100% of the superheat, the desuperheater can satisfy the hot water needs 210 days for a house with 75 gal/day requirement, 254 days for 50 gal/day requirement and up to 303 days for 25 gal/day hot water requirement..This means that for the other days, another source must be used to generate the required quantity of hot water. By using 50% of the superheat, the desuperheater can satisfy the hot water needs only for 96, 157 and 254 days for the 75, 50 and 25 gal/day requirement respectively.

Table 4.7: Operation of Desuperheater

| Daily Hot Water Usage (gal/day) | Energy Needed per Day kBtu (kJ) | Number of Days Hot Water Requirements are Met (Days) | | |
|---|---|---|---|---|
| | | 100% Superheat | 75% Superheat | 50% Superheat |
| 75 | 33 (11.6) | 210 | 157 | 96 |
| 50 | 22 (23.21) | 254 | 225 | 157 |
| 25 | 11 (34.8) | 303 | 286 | 254 |

Figure 4-4, Figure 4-5 and Figure 4-6show the quantity of water generated daily for the case where the desuperheater uses 100% , 75% and 50% of the available superheat, respectively. The green line in each case corresponds to the domestic consumption for each case – 75, 50, and 25 gal/day in Figures 4.4-4.6, respectively. It can be seen that most of the days the required hot water needs are met. Moreover, the quantity of hot water generated is much more than needed, especially during the summer. This excess hot water can either be stored or used in other ways.

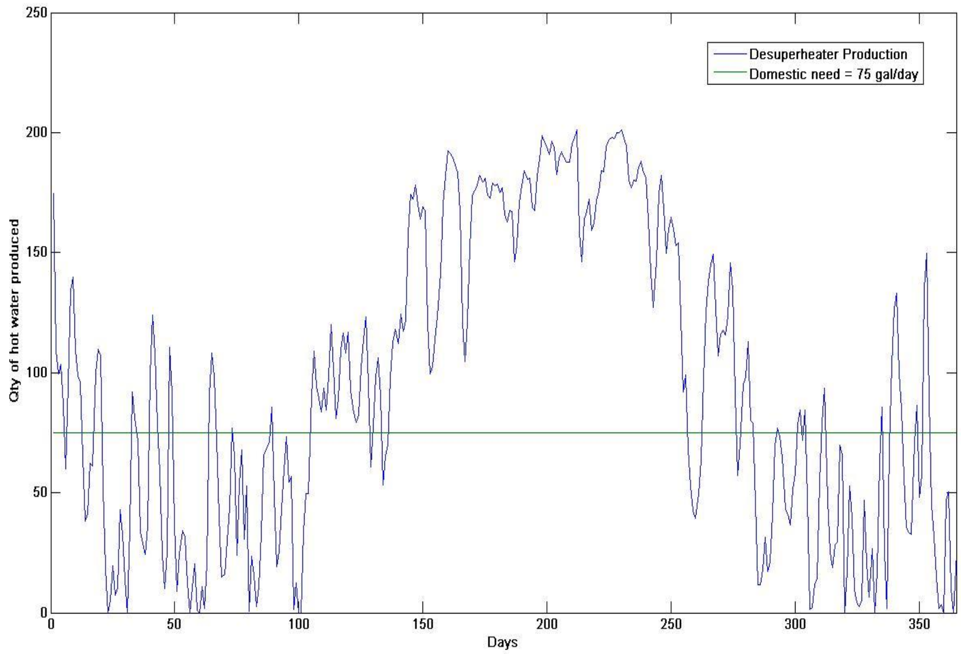


Figure 4-4: Quantity of Hot Water Produced (gallons) using 100% of Superheat

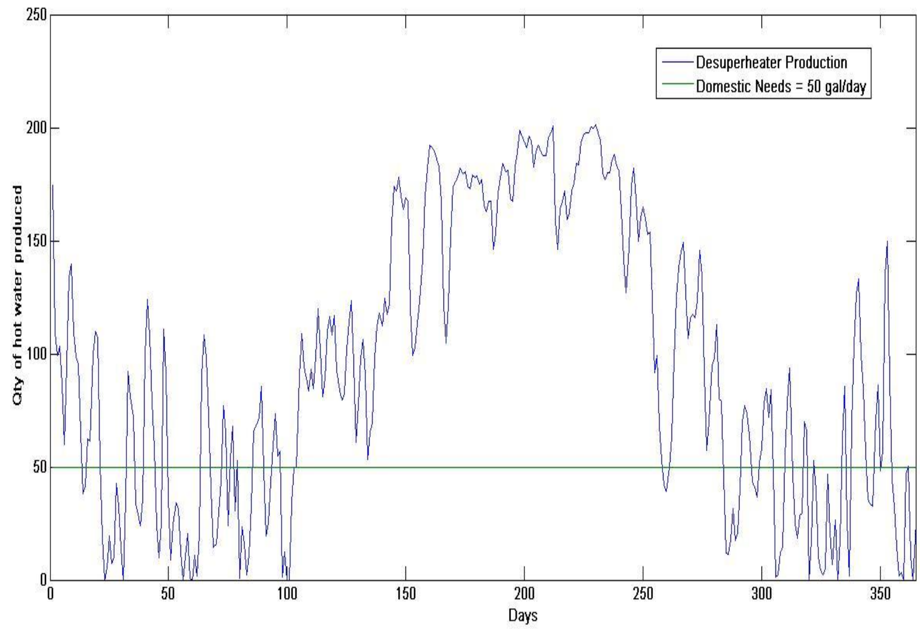


Figure 4-5: Quantity of Hot Water Produced (gallons) using 75% of Superheat

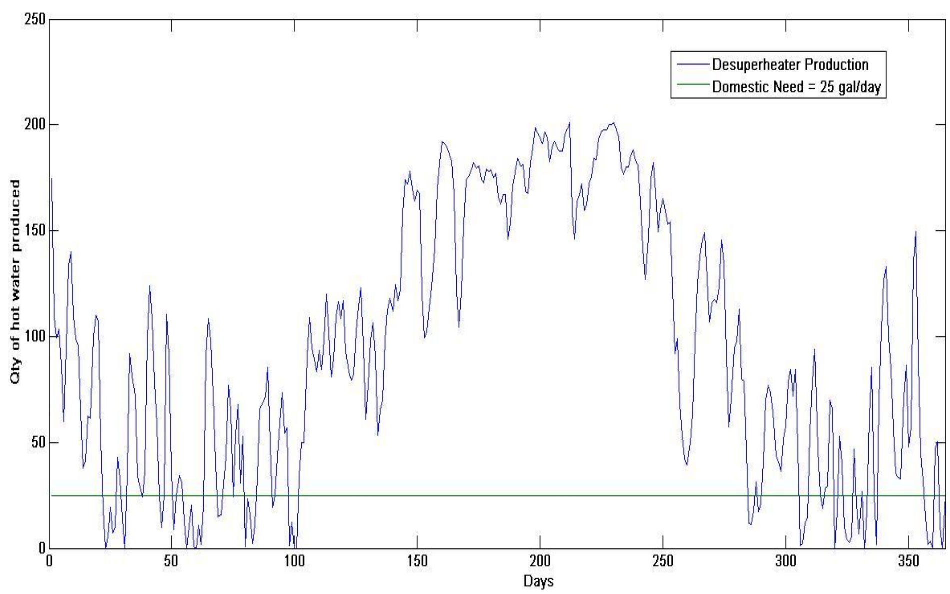


Figure 4-6: Quantity of Hot Water Produced (gallons) using 50% of Superheat

By using the superheat to generate hot water, the heat rejected to the condenser during the cooling mode is decreased, thus reducing the temperature of the water entering the ground. The power rejected to the condenser whenever the heat pump was in cooling mode was calculated by summing the heat rejected for each hour of operation. That power rejected was then averaged over the 2022.2 hours that the heat pump operated in cooling mode. Table 4.8 shows the average power rejected when using the desuperheater in the cooling mode for the three cases. If 100% of the superheat were utilized, an average of 1.91 kW (6.61 kBtu/hr) of power can be rejected, which amounts to reducing the water temperature entering the ground loop by 0.61˚C (1.1˚F). By using 75% of the superheat, 1.43 kW (4.89 kBtu/hr) of power can be rejected, which reduces the water temperature by 0.46˚C (0.82˚F). Using 50% of the available superheat, 0.96 kW (3.23 kBtu/hr) power can be rejected, which reduces the water temperature by 0.31˚C (0.55˚F).

Table 4.8: Power Rejected and Temperature Reduction

| Superheat Utilized (%) | Average Power rejected (kW) | Reduction in Temperature of Water in Ground Loop ˚C (˚F) |
|---|---|---|
| 100% | 1.91 | 0.61 (1.1) |
| 75% | 1.43 | 0.46 (0.82) |
| 50% | 0.96 | 0.31 (0.55) |

### ECONOMIC ANALYSIS OF THE DESUPERHEATER

Turbotec is a company that manufactures desuperheaters (Turbotec Desuperheaters) at a cost of $583 with an additional $1,000 for installation. Table 4.9 shows the additional quantity of water generated annually for the three cases of desuperheater use (100%, 75% and 50% superheat utilization) and three scenarios of domestic hot water consumption. The negative values indicate that the desuperheater alone is not able to satisfy all the hot water needs and that an additional heat source is needed. For example, at 50 gal/day the yearly hot water consumption is 18,250 gal/year. If 100% of the superheat is used, an additional 12,833 gal/year hot water can be generated; at 75% superheat, an additional 6,313 gal/year; and at 50% superheat, no additional hot water can be generated.

Table 4.9: Additional Quantity of Water generated by Desuperheater

| Daily Hot Water Usage (gal/day) | Annual Hot Water Usage (gal/yr) | Additional Qty of Water Heated Utilizing x % of Superheat (gal/yr) | | |
|---|---|---|---|---|
| | | 100% | 75% | 50% |
| 75 | 27,375 | 6,208 | -312 | -6,833 |
| 50 | 18,250 | 12,833 | 6,313 | -208 |
| 25 | 9,125 | 19,458 | 12,938 | 6,417 |

Table 4.10 shows the cost incurred in generating and then using the additional quantity of water generated. It can be seen that the cost in all cases is less than $ 25/ year and hence is cost effective. The water rates are given in Appendix C.

Table 4.10: Cost of Additional Quantity of Water [City of Austin – Water Rates (Appendix A)]

| Daily Hot Water Usage (gal/day) | Cost for additional quantity of water ($/yr) | | |
|---|---|---|---|
| | 100% | 75% | 50% |
| 75 | 7 | 0 | 0 |
| 50 | 14 | 7 | 0 |
| 25 | 21 | 14 | 7 |

## CONCLUSIONS

This analysis computed the total amount of heat that can be extracted from the superheated region of the VCC. An average of 1.91 kW (6.61 kBtu/hr) of power can be rejected and thereby reduce the ground loop water temperature by 0.61˚C (1.1˚F) if 100% of the available superheat were used. The power rejection is 1.43 kW (4.89 kBtu/hr) with 75% superheat utilization and 0.96 kW (3.23 kBtu/hr) with 50% superheat utilization. In all cases, the cost of generating additional hot water is very favorable.

There is one problem with utilizing 100% of the available superheat; the refrigerant loses pressure after it exits the desuperheater and this pressure loss makes it difficult for the refrigerant to move through the entire length of the condenser. Hence, in practical applications, the desuperheater is run only to satisfy the domestic heating needs. Another concern is that when the desuperheater is run in the heating mode, more heat must to be extracted out of the ground, since the heat would normally go to the building, which requires the heat pump to run for a longer time, and hence reduce COP for the same amount of heat provided to the building.

# Chapter 5. Thermosyphon

## INTRODUCTION

Thermosyphons are vertical, two-phase heat pipes that absorb heat from an external source and vaporizes a working fluid at one end of the pipe, moves the working fluid via natural convection to the other end of the pipe, where heat is rejected by convection to an external sink medium, and the working fluid condenses back to the bottom of the pipe. The working fluid is typically a refrigerant (usually ammonia or carbon-dioxide). The pipe is either pressurized or depressurized to keep the refrigerant at its saturated state, and hence constantly evaporating and condensing. There are three parts to a thermosyphon: 1) evaporator, the lowest part of the thermosyphon in contact with the heat source , 2) adaiabtic region, the middle part, and 3) condenser, which is the top part of the thermosyphon.

Thermosyphons rely on the temperature difference between the source temperature and atmospheric sink temperature. Heat absorbed in the evaporator from the external source evaporates the refrigerant. Once it evaporates, its density is lowered and the refrigerant rises due to natural convection. Heat transfer occurs throughout the length of the evaporator. The adiabatic section is at the middle of the thermosyphon and no heat transfer is assumed to occur across this section. As the gaseous refrigerant moves upward, it comes in contact with the condenser wall, whose outer wall is at atmospheric temperature asssuming the thermosyphon top is outdoors. The cylindrical fins around the condenser section remove heat by forced convection with the blowing wind. The gaseous refrigerant then condenses into liquid. This condensate attaches itself to the wall and due to its higher density, it slowly flows downward back to the pool of refrigerant in the evaporator.

Thermosyphons are widely used in Alaska and Tibet to keep the soil (permafrost) below freezing during the winter so that during warmer periods, the soil will remain frozen and still support structures, such as oil pipelines, antennas, and railroad rails. To maintain the structural stability, thermosyphons are installed along the entire length of the structure.


Figure 5-1: Thermosyphons installed next to the Trans-Alaska Pipeline [Source: Alaska Pipeline - Wikipedia]

Thermosyphons can be used in warmer climates. A technology called Frozen Barrier Technology [Frozen Soil Barrier – DOE, 1999] was tested by DOE for containment of radioactive materials under the ground. The objective of this study was to use themosyphons to freeze the ground, and hence create a solid enclosed barrier under the soil to contain the radioactive material. A series of fifty, 30 ft (9.14 m) long thermopiles were installed and to freeze the ground, however, refrigeration systems were deployed to remove heat from the condenser sections. Two separate refrigeration units were used to each drive 25 thermopiles. These units had to be deployed because the ambient climate is warm. With the external power sources consuming 288 kWh (982.7 kBtu) per day, a 12 ft (3.66m) thick frozen soil was ultimately established. Our analysis attempts to use the thermosyphons to extract heat from the superheat portion of the vapor compression cycle, and recognizing the high ambient temperatures, both passive and active operation was investigated to determine the feasibility of using such devices.

The design criteria for selecting a thermosyphon depends on the following variables: quantity of heat to be transferred, the temperatures of the source and sink, temperature difference between the evaporator and the condenser and the wind speed in the region. The thermosyphon must be designed to operate at a pressure such that the refrigerant vaporizes for the amount of heat transferred from the heat source. Forced convection is the main mode of removing heat from the condenser, hence fins are attached around the condenser to maximize the heat transfer. Further, the length of the thermosyphon is important to allow the cycle to operate properly.

## OBJECTIVE

The objective of using themosyphons as a supplemental heat rejection device is to extract heat from the superheat region of the refrigerant loop at the discharge of the compressor. By coiling the refrigerant loop around the evaporator of the thermosyphon or passing the refrigerant loop though a high conducting liquid in contact with the evaporator, heat can be transferred from the refrigerant to the working fluid inside the thermosyphon. Depending on the ambient air and wind conditions, this heat can be rejected from the condenser by either passive or active mode (natural or forced convection). As computed in the chapter on cooling towers, a 5 kW SHR capacity is needed for a residential building with a 4-ton cooling load. Hence, our goal is to design a thermosyphon that can extract up to 5 kW of power from the refrigerant loop.

### EXPERIMENTS BY SHIRAISHI ET AL. (1981)

Shiraishi et al. performed an experiment to investigate the heat transfer characteristics of a two-phase thermosyphon to remove exhaust heat (temperatures < 60 ˚C/140˚F ), which is very common in industrial processes. The experiment was performed to investigate the temperature variation of the working fluid inside the thermosyphon, the wall, and the effect of filling ratio on the temperature profiles. Results of these experiments were used to verify a mathematical model they also developed.

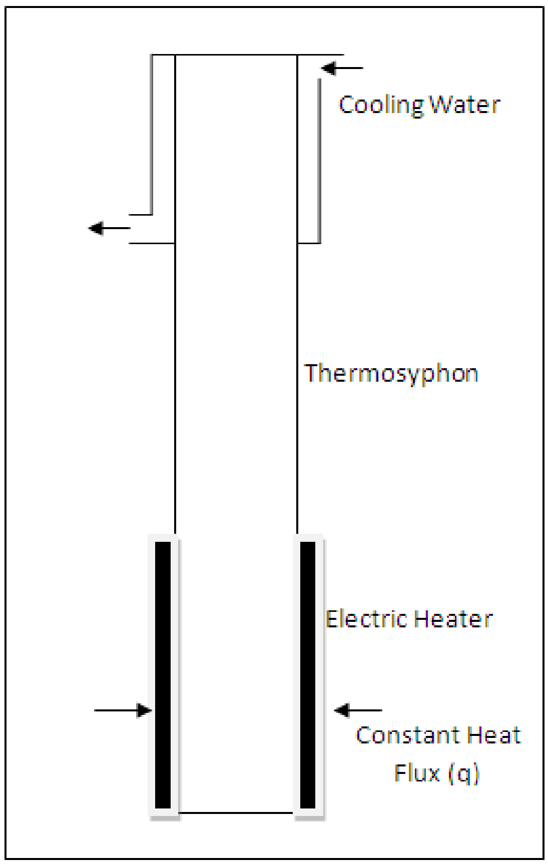


Figure 5-2: Experimental Setup

The thermosyphon used in the experiment Figure 5-2 was made of copper tubing of inner diameter 37 mm (1.41 in) and outer diameter 45 mm (1.77 in) and a total length of 1230 mm (48.43 in). Of this length, the evaporator, adiabatic, and condenser sections were $L_e$=280 mm (11 in), $L_a$=500 mm (19.7 in), and $L_c$=450 mm (17.7 in) long, respectively. An electric resistance heater, insulated with magnesia to fit in special grooves outside the evaporator, provided a constant heat flux condition to replicate an industrial process, where the exhaust gases provide a constant heat flux. The heat sink (condenser) was fitted with circulating water to condense the refrigerant inside the thermosyphon. The working fluid inside the thermosyphon was water, which has a vapor state at 45°C and at a pressure of 9.6 kPa.

The amount of working fluid inside the thermosyphon was varied to determine its effect on performance. A quantity called the filling ratio (F), defined as the ratio of the volume of the working fluid to that of the evaporator volume, is given by:

$$F = \frac{\Pi r^2 L_p}{\Pi r^2 L_e} = \frac{L_p}{L_e} \tag{5.1}$$

where $L_p$ is the height of water pool in the thermosyphon, $L_e$ is the height of the evaporator and $r$ radius of the thermosyphon.

This quantity is introduced for the following reason. The heat exchange process taking place in the portion filled with water ($0 \leq x \leq L_p$) is due to boiling, and for the region above the working fluid ($L_e \leq x \leq L_p$) evaporation takes place in the liquid film of the condensate above the pool of water. The filling ratio indicates the ratio of the amount of heat transferred due to boiling to the amount of heat transferred by evaporation of the fluid.

**Heat Transfer Coefficients**

*Heat transfer in the Condenser*

The working fluid (water) is assumed to be saturated vapor by the time it reaches the condenser, and hence the fluid is in single phase. Then heat transfer is purely to condense the water vapor. The condensate which flows back down along the pipe is assumed to be in laminar flow with respect to the radius of the thermosyphon. Using Nusselt's film condensation theory for a flat plate (Incropera and Dewitt), the condensation heat transfer coefficient $h_c$ is given by

$$h_c \frac{(\nu^2/g)^{1/3}}{k} = (4/3)^{1/3} Re_c^{-1/3} \tag{5.2}$$

$$Re_c = \frac{4 q_c L_c}{\lambda \mu} \tag{5.3}$$

where $\nu$ is the kinematic viscosity of water, $g$ is the acceleration due to gravity, $k$ is the thermal conductivity of water, $\lambda$ is latent heat of vaporization, μ is the dynamic viscosity of water (all in SI units).

*Heat transfer in the liquid pool of the Evaporator*

The heat transfer in the evaporator liquid pool is described as pool boiling. It is different from nucleate boiling since it takes place in closed system where the formation of vapor bubbles has a greater effect on the heat transfer. The empirically-formulated pool boiling heat transfer coefficient $h_p$ is given by Shiraishi et al. (1981):

$$h_p = 0.32 \frac{\rho^{0.65} k^{0.3} C_p^{0.7} g^{0.2}}{\rho_v^{0.25} \lambda^{0.4} \mu^{0.1}} \left(\frac{P}{P_a}\right)^{0.23} q_e^{0.4} \tag{5.4}$$

where $\rho$ is the density of liquid water, $\rho_v$ is the density of water vapor, $P$ is the pressure inside the thermosyphon fluid pool, $P_a$ is the atmospheric pressure, $C_p$ is the heat capacity at constant pressure, $\nu$ is the kinematic viscosity of water, $g$ is the acceleration due to gravity, $k$ is the thermal conductivity of water, $\lambda$ is latent heat of vaporization, μ is the dynamic viscosity of water (all in SI units).

*Heat Transfer in the liquid film of the Evaporator*

The heat transfer process of the falling liquid film is complex and depends on the magnitude of the heat flux applied at the evaporator. At a low evaporative heat flux a continuous liquid film is observed, a phenomena that is well described by Nusselt's condensation theory (Incropera and Dewitt). At a high evaporative heat flux, the film breaks down into droplets which start boiling and leads to a two phase fluid formed on the wall of the condenser. For the latter case, an empirical formulation for the heat transfer coefficient is:

$$h_f \frac{(\nu^2/g)^{1/3}}{k} = (4/3)^{1/3} Re_f^{-1/3} \tag{5.5}$$

$$Re_f = \frac{4 q_e x}{\lambda \mu} \tag{5.6}$$

$$x = L_p + \left(\frac{1}{2}\right) L_f \tag{5.7}$$

where $x$ is the distance measured from the bottom of the thermosyphon, $L_f$ is the distance from the top of the pool level to the top of the evaporator section, $q_e$ is the heat flux at the evaporator and all fluid properties are that of saturated water at 45°$C$/113°F)

**Implementation of Shiraishi's Model**

The following assumptions are made:

- The axial conduction along the length of the tube is negligible
- Constant heat flux is supplied uniformly to the evaporator
- Steady state operation is assumed and all the heat added to the evaporator is taken away from the condenser section.
- The liquid pool level in the evaporator is assumed to be constant, implying that the rate of evaporation is equal to the rate of condensation.
- The saturation pressure - temperature relationship is used in the liquid pool and the vapor just above the pool. It is expressed as:

$$T = f_s(P) \tag{5.8}$$

The primary variables affecting the experiment are the heat flux and the vapor temperature inside the thermosyphon. Although the vapor is at its saturated pressure, the pressure varies along the height of the pool. The pressure at any point at a distance $x$ from the bottom is given by:

$$P(x) = P_v + \rho g(L_p - x) \tag{5.9}$$

Once pressure is known, the temperatures can be determined by the saturation temperature – pressure relation.

$$T_i(x) = f_s\big(P(x)\big) \quad , \quad 0 \le x \le L_p \tag{5.10}$$

$$T_i(x) = f_s(P_v) \quad , \quad L_p \le x \tag{5.11}$$

Since all heat added to the evaporator is taken away at the condenser (e.g. steady-state assumption), the heat flux at the condenser is calculated by:

$$q_c = q_e * (\frac{L_e}{L_c}) \tag{5.12}$$

The heat transfer coefficients for different regions of the thermosyphon are calculated using equations (5.2), (5.4) and (5.5). Using the computed coefficients, the temperature profiles of the inner wall $T_w(x)$ are calculated using the following relations:

$$T_w(x) = T_i(x) + \frac{q_e}{h_p} \quad , \quad 0 \leq x \leq L_p \tag{5.13}$$

$$T_w(x) = T_i(x) + \frac{q_e}{h_f} \quad , \quad L_p \leq x \leq L_e \tag{5.14}$$

$$T_w(x) = T_i(x) \, , \; L_e \leq x \leq L_e + L_a \tag{5.15}$$

$$T_w(x) = T_i(x) - \frac{q_c}{h_c} \quad , \quad L_e + L_a < x \tag{5.16}$$

Knowing the thickness of the wall and conduction across it, the outer wall temperatures are also calculated.

**Validation of Model**

Shiraishi's model was implemented and validated with experimental data. It was run for two cases of filling ratios: 1 (entire evaporator section filled with water) and 0.5. In both cases, a vapor temperature of the working fluid (water) of 45 °C/113 °F (9.6

kPa/0.145 psi) was used to mimic the experimental conditions. A heat flux of $3.4*10^4$ $W/m^2$ was applied along the entire length of the evaporator and the wall and working fluid temperature profiles along the length of the thermosyphon were calculated. In the following figures, the y axis represents distance along the 1.23m (4 ft) length, with the evaporator, adiabatic, and condenser sections represented by 0 - 0.28m (0 - 0.92 ft), 0.28m - 0.78m (0.92 - 2.56 ft) and 0.78m - 1.23m ( 2.56 – 4 ft), respectively.

Figure 5-3 shows the temperatures for a filling ratio = 1. The red line shows the temperature profile of the working fluid inside the thermopsyphon; it is in saturated vapor form at 45˚C/113˚F in both the adiabatic and the condenser section. Since for a filling ratio of 1 the entire evaporator is filled with water, pressure of water increases with the depth, which in turn leads to a higher temperature down the length of the evaporator; this is shown clearly by the linearly increasing temperature from height 0.28m to 0m (0.92 - 0 ft) (bottom of the evaporator). It can be seen from the figure that the model agrees well with the experiments.

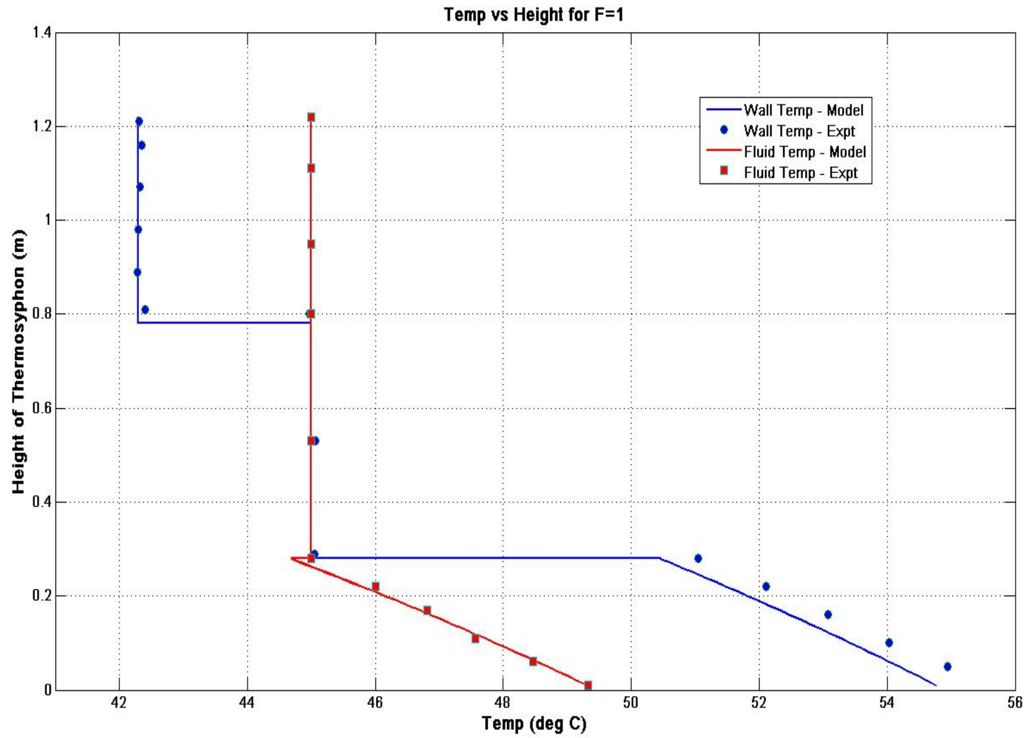


Figure 5-3: Temperature Profile of Working Fluid and Wall for F =1

The blue line corresponds to the wall temperatures. From the bottom of the thermosyphon to the point where the pool ends, the temperature decreases due to a reduction in saturation pressure. The working fluid above the pool is in saturated vapor state, and hence is at a temperature of 45 ˚C (9.6 kPa) throughout the rest of the thermosyphon. Since the temperature of the water in the pool decreases with height, the wall temperature also decreases with height to accommodate the heat flux that is supplied. Although, the temperature difference between the pool and wall temperature appear constant from the figure, it is actually not. This is due to the varying value of the heat transfer coefficient in the water pool (Eq 5.4).

The adiabatic section is assumed to have zero heat transfer, hence the temperature difference between the wall and the working fluid should be zero. The experimental data confirms this assumption. At the condenser section, the heat is transferred from the vapor to the wall, and then to the water outside the thermosyphon. The wall temperature must be lower than the vapor temperature, and experimental data confirms this condition. From the assumptions of steady-state operation and constant heat flux applied at the evaporator section, the heat flux at the condenser was also constant. This led to a uniform wall temperature as can be seen from the experiment too. Figure 4 shows excellent agreement between the model and experiment.

Figure 5-4 shows the results for the case of 0.5 filling ratio. The fluid and wall temperature profile in the pool is similar to that of the previous case.

However, just above the pool and still within the evaporator section (from H=0.14m - 0.28m/ 0.46 – 0.92 ft) the wall temperature increases while the vapor temperature remains constant, even though the heat flux is a constant. The reason for this is the varying heat transfer coefficient just above the pool region (Eq 5.5).

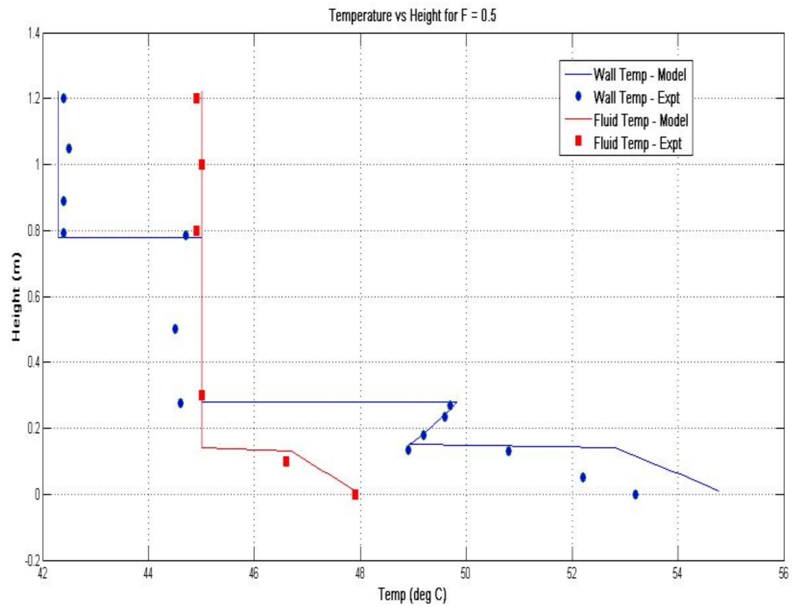


Figure 5-4: Temperature Profile of Working Fluid and Wall for F =0.5

## MODEL DEVELOPMENT FOR THERMOSYPHON AS SHR SYSTEM

To use a thermosyphon as a SHR device, the refrigerant loop can either be designed to coil around the evaporator of the thermosyphon or it can be immersed in a liquid which transfers heat uniformly to the evaporator . The subsequent model assumes that the design of the interaction between the refrigerant loop and the thermosyphon is ideal and provides constant heat flux. The refrigerant at the compressor discharge has temperatures in the range of 40 – 70˚C (104 - 158˚F) (Refer Chapter on Desuperheater). The working fluid in the thermosyphon is ammonia and is pressurized to 1468.3 kPa (212 psi), corresponding to a vaporization temperature of 38.8˚C/101.8˚F. This temperature was chosen low enough to always allow heat transfer between the refrigerant, which is at temperatures greater than 40˚C/104˚F, and the ammonia in the thermosyphon. Since the heat is ultimately dissipated into the atmosphere by convection, the ambient temperature must be less than 38.8°C/101.8°F, and preferably much less than that value for higher heat transfer rates. To improve the effectiveness of convection across the condenser, fins are designed around the condenser (Figure 5-5). In summary, the refrigerant from the VCC is assumed to provide an almost constant heat flux to the evaporator and heat is removed at the condenser by either natural or forced convection.

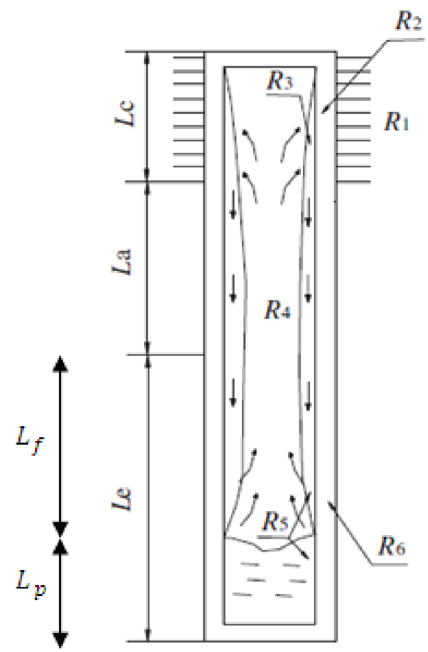


Figure 5-5: Schematic of Thermosyphon (Zhang et al, 2011)

In Shiraishi et al.'s experiment, a known constant heat flux was supplied at the evaporator, and the heat was removed by external cooling water at the condenser. In our case, the value of heat flux at the evaporator is unknown. Hence, we use the heat transferred at the condenser by convection to determine the heat that must be added at the evaporator. At the condenser, there are three modes of heat transfer: convection across the vapor condensing along the condenser walls, conduction through the wall of the thermosyphon and convection across the fins to the outside air. The heat transfer can be written as:

$$Q = \frac{T_v - T_a}{R_1 + R_2 + R_3} \tag{5.17}$$

where, $T_v$ is the temperature of vapor ammonia at 38.8 ˚C/101.8˚F , $T_a$ is the ambient air temperature, $R_3$ is the thermal resistance across condensing ammonia vapor, $R_2$ is thermal resistance across thermosyphon wall and $R_1$ is the thermal resistance across condenser fins. The thermal resistances are given by:

$$R_3 = \frac{1}{\pi D_i L_e h_c} \tag{5.18}$$

where $D_i$ is the internal diameter of the themosyphon, $L_e$ is the length of evaporator and $h_c$ is the heat transfer coefficient given by Eq (4.2).

$$R_2 = \frac{1}{2\pi k_t L_c} \log(\frac{D_o}{D_i}) \tag{5.19}$$

where $D_o$ is the outer diameter of the thermosyphon, $L_c$ is the length of the condenser, $k_t$ is the thermal conductivity of copper.

$$R_1 = \frac{1}{h_a^e \pi D_o L_c} \tag{5.20}$$

where $h_a^e = h_a \frac{D_c(L_c - n\delta) + [\, 2n(\, r_2^2 - r_1^2) + 2nr_2\delta \,]\eta}{L_c D_c}$ (5.21)

$$h_a = 0.1378 \frac{\lambda_a}{D_c} Re_a^{0.718} Pr_a^{1/3} (\frac{s_n}{b_n})^{0.296} \tag{5.22}$$

$$Re_a = \frac{V D_c}{\nu} \tag{5.23}$$

where $\boldsymbol{\lambda}$ is the thermal conductivity of air, $b_n$ is the fin height, $s_n$is the fin spacing, $\boldsymbol{\delta}$ is the fin thickness, $r_2$ is the outer radius of circular fin, $r_1$ is the inner radius of circular fin, $n$ is the number of fins, $Pr$ is the Prandtl Number and $\eta$ is the fin efficiency.

The building that was investigated was a 2,100 ft$^2$ (195 m$^2$) building located in Austin, Texas. It had a 4 ton unit heat pump installed to provide cooling and heating. The building loads were generated for every two minute time steps to cover the entire year (Jonathan Gaspredes, 2011). From the building load data, it was found that the heat pump was in the cooling mode for 2022 hrs and in the heating mode for 227 hrs of the year. The total time the heat pump was operating during a year was 2,249 hrs. The thermosyphon is operated only when the heat pump is in the cooling mode. Further, since the ammonia vapor inside the thermpsyphon is at 38.8˚C (101.84˚F), the heat will be rejected from the condenser only if the ambient temperature is less than 38.8˚C (101.84 ˚F). The model is implemented is as follows. For each time step the mode – heating or cooling – of the heat pump is determined. If the heat pump is in the cooling mode, the ambient temperature of air is taken. For ambient temperatures less than 38.8˚C (101.84 ˚F), Equation (5.23) is used to determine the heat removed from the thermosyphon. The heat removed during the heating mode is zero. Once this is done for all the times steps, the heat dissipated is averaged over every hour and results are plotted.

Table 5.1 shows two thermosyphons manufactured by Arctic Foundations. The heat that can be removed by these thermosyphons for a temperature difference of 20˚C (between the vapor and the air) were in the range 1 – 2.5 kW. Hence appropriately-sized units were used in our analysis. Model 170 SF has a larger condenser section (5.2 m) and model 70 SF has a smaller condenser section (2.4m/7.9 ft). The evaporator section length for both is 5m (16.4 ft).

Table 5.1: Thermosyphon Models by Arctic Foundation Inc [Edward Yarmark Jr, Arctic Foundations]

| Model | Diameter $D_o$ $(mm/in)$ | Length $(m/ft)$ | Condenser Length $L_c$ $(m/ft)$ | Price ($) | Weight $(lbs/kg)$ | Capacity $\frac{W}{m^2}$ / $\frac{Btu}{ft^2}$ |
|---|---|---|---|---|---|---|
| 70 SF | 152/6.0 | 7.4/24.3 | 2.4/7.9 | 2,700 | 310/140.6 | 1000/292 |
| 170 SF | 152/6.0 | 15.2/ | 5.2/17.0 | 3,600 | 625/283.5 | 2500/730 |

**Passive Condenser Case: Natural Convection**

The thermosyphon can be operated in a passive mode, where natural convection of the air dissipates heat at the condenser, or in an active mode, where fans are employed to dissipate heat by forced convection. For the passive case, data for average wind speeds blowing across the terrace of residential buildings in Austin are used for this study, as shown in Table 5.2

Table 5.2: Average Wind Speeds in (m/s) / (ft/min) for different months of the year (Konopacki, S. and Akbari, H)

| Jan | Feb | Mar | Apr | May | Jun | Jul | Aug | Sep | Oct | Nov | Dec |
|---|---|---|---|---|---|---|---|---|---|---|---|
| 1.75/ 344.4 | 2.88/ 566.8 | 2.76/ 543.2 | 3.00/ 590.4 | 2.80/ 551 | 2.50/ 491 | 2.30/ 452.6 | 1.84/ 362.1 | 1.94/ 381.8 | 2.20/ 433 | 2.23/ 439 | 3.01/ 592 |

Figure 5-6 shows the power dissipated by the thermosyphon condenser (170 SF model) in the passive case for different days of the year. Again, the thermosyphon was switched on whenever the heat pump was in the cooling mode when SHR was necessary. The average power rejected by one thermosyphon is 0.52 kW (1.77 kBtu/h). Hence to achieve at least 5 kW (17.1 kBtu/h) of supplemental power rejection 10 units are needed at a total cost of $ 36,000.

It is interesting to note that more heat is rejected during the summer than during winter, although the ambient temperatures are much lower during the winter. This is due to the fact that the thermosyphon is switched on only during the cooling mode of the heat pump, which happens mostly in summer.

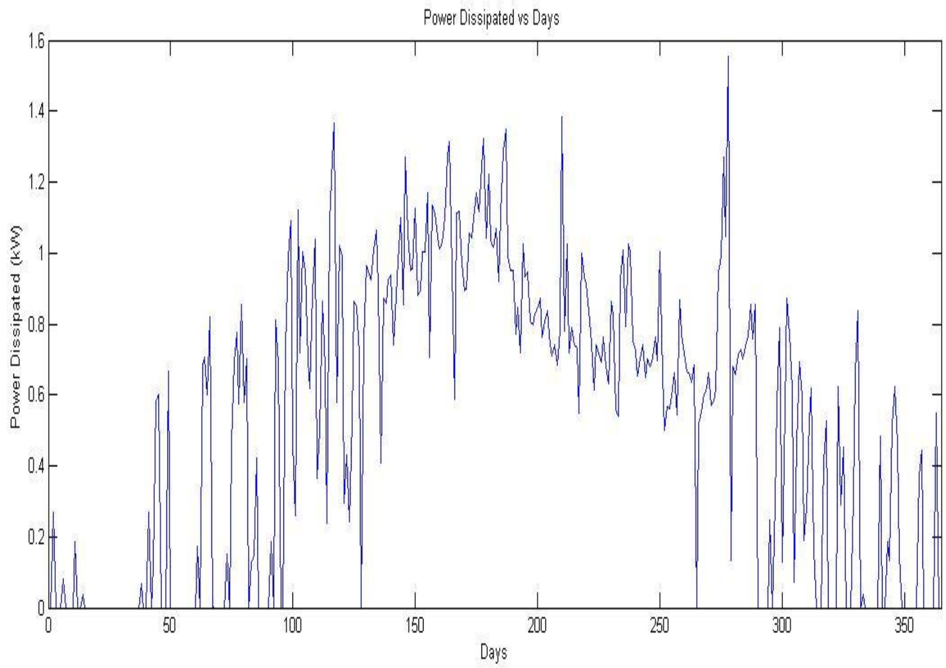


Figure 5-6: Power Rejected vs Days for Thermosyphon Model 170 SF

Figure 5-7 shows the power rejected by the thermosyphon for a single summer day (July 1). It also shows the cooling load for that particular day. It can be seen that the thermosyphon rejects heat only when the heat pump is in the cooling mode. The two profiles don’t match each other since other factors like temperature and wind speeds also play a role in the heat rejection.

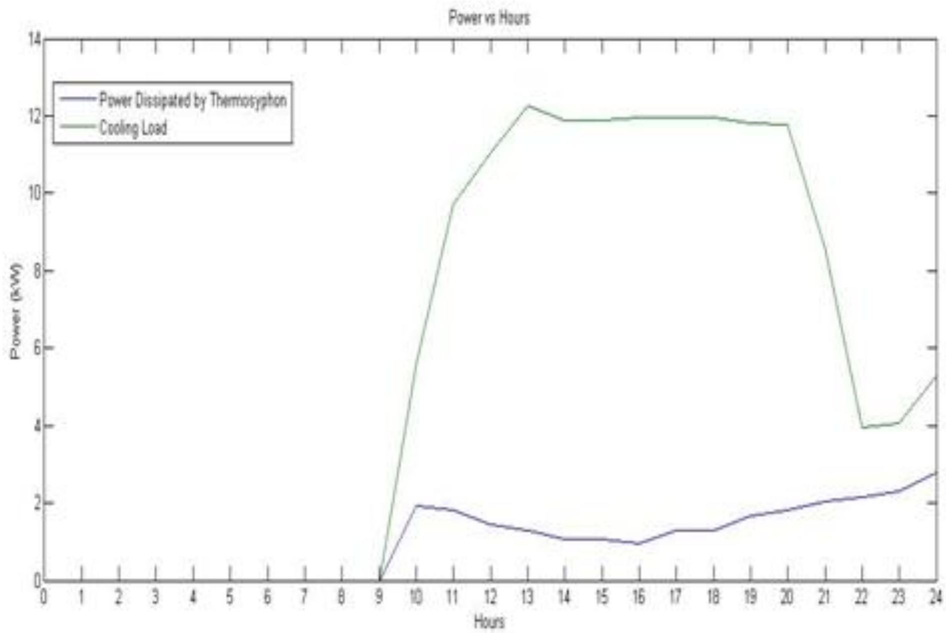


Figure 5-7: Power Rejected on July 1 (Model 170 SF)

Figure 5-8 shows the power dissipated by the thermosyphon condenser (70 SF model) in the passive case for different days of the year. Again, the thermosyphon was switched on whenever the heat pump was in the cooling mode when SHR was necessary. The average power rejected by one thermosyphon is 0.38 kW (1.3 kBtu/h). Hence to achieve at least 5 kW (17.1 kBtu/h) of supplemental power rejection 13 units are needed at a total cost of $ 33,800 (13* $ 2,600).

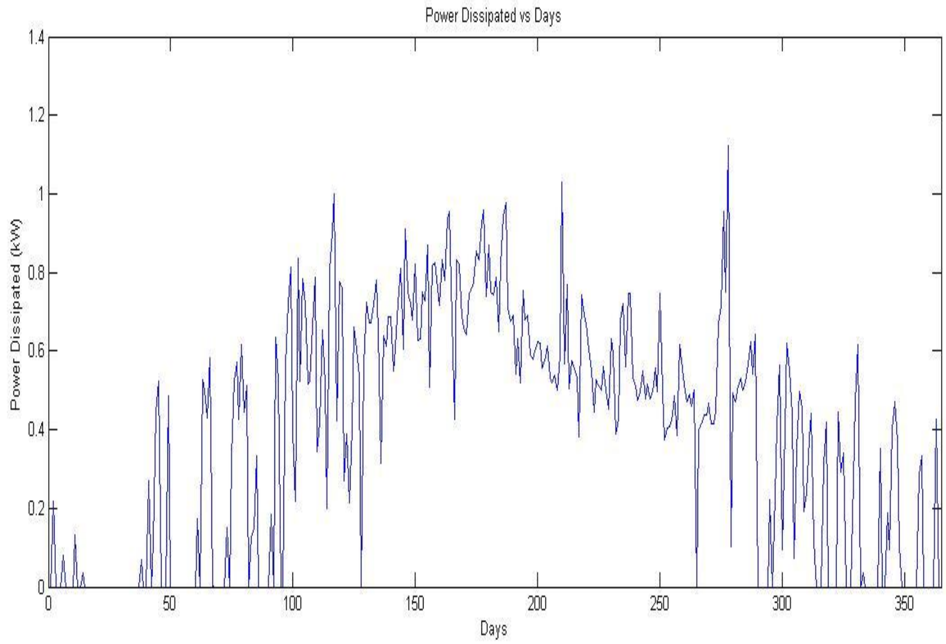


Figure 5-8: Power Rejected vs Days for Thermosyphon Model 70 SF

**Active Condenser Case: Forced Convection**

The active case has fans blowing air across the condenser section to increase heat dissipation. Figure 5-9 shows the power dissipation for the Model 170 SF run with a Climate Control Model WSS 049 fan (10,000 cfm with 1/3 HP consumption-cost $8422). Average power dissipation during cooling mode is 0.68 kW (2.32 kBtu/h), which is slightly higher compared to the 0.52 kW (1.77 kBtu/h) for the passive case. Hence, to achieve 5 kW (17.1 kBtu/h) of heat rejection nine thermosyphons are required, compared to the 10 required for the passive case. The total cost in this forced convection case is the sum cost of the thermosyphons, fans and the operating electric cost, and it is given as:

Total Cost = Cost of Thermosyphon + Cost of Fan + Operating Cost

= $ 3,600*9 + 8,422 + $ 119 (per year) = $ 32,408 + $ 82 (per year)

Operating Electric Cost = Fan Power * Number of Hours * Cost per kWhr =

0.24867*(1977)*$ 0.1082 = $ 54 per year

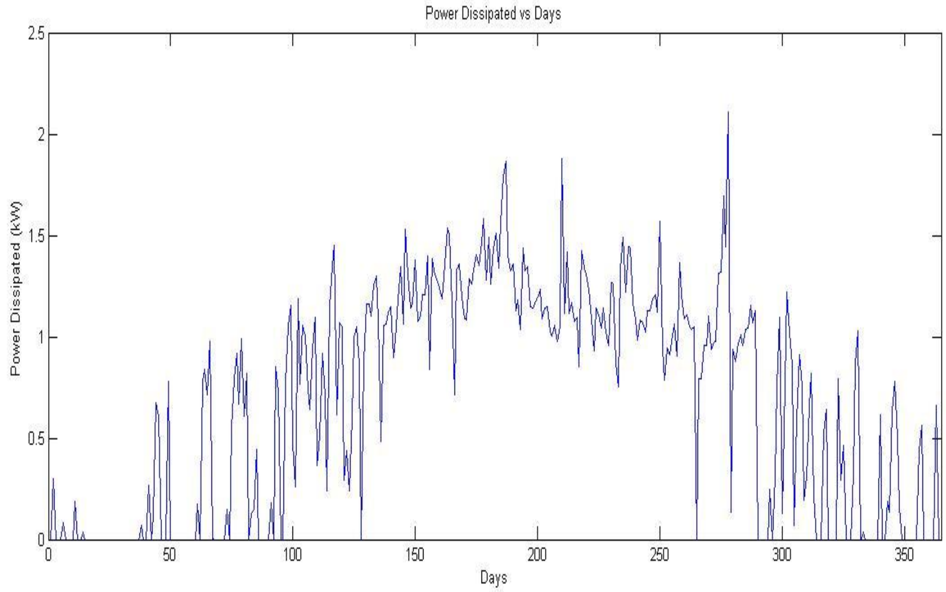


Figure 5-9: Power rejected by Thermosyphon (170 SF model) with Fans

## CONCLUSION

The analysis in this chapter shows that it is prohibitively expensive to install and operate a thermosyphon of the sizes needed to reject 5 kW (17.1 kBtu/h) ; $ 33,800 for the passive case and $ 32,408 for the forced convection case. Further, these types of device have never been deployed or tested for a residential house in a warm climate. The thermosyphons currently used in cold regions like Alaska and Tibet. Hence, the practical feasibility of operation in warm climates is unknown. Another difficulty is the design associated with transferring heat from the refrigerant loop to the thermosyphon. Special piping/coils or liquid pools must be designed for the refrigeration loop at the thermosyphon evaporator, which will add to the total cost. Taking into all these factors into account, it can be concluded that use of thermosyphons as SHR devices is not practical in Texas climates.

# Chapter 6. Conclusions

This thesis analyzed several methods for supplemental heat rejection from a GSHP in a residential house in Texas. While one method for SHR, the cooling tower, is currently used for commercial buildings, this work also applied the strategy to a residential case. Three other SHR methods, optimization of the VCC, expanded desuperheaters, and thermosyphons were analyzed for their technical, economic, and operational feasibility. A summary of findings is provided below.

The cooling tower, as a SHR for a residential GSHP, showed the greatest promise, both in terms of operational and economic feasibility. It was found that adding a 2 ton cooling tower to the GSHP reduced ground heating and increased the ground loop lifetime to over 10 years. This reduction in ground temperature directly improved the performance of the heat pump to keep its EER constant at 11.5 during the summers, in contrast to the GSHP-only case where its EER decreased from 8.5 to 7.5 over the 10 year period. The COP for the HGSHP case, however, remained constant at 4 compared to the GSHP-only case where it increased from 4.5 to 5 due to the increased ground temperatures for the latter case. By far, the biggest advantage of using cooling towers was the cost effectiveness of the HGSHP system. It was found that the 10-year cost of the HGSHP system was 26.9% lower than the GSHP-only case (with savings of $ 5,584) due to two main factors: 1) decreased borehole drilling costs from the shallower boreholes and 2) increased heat pump efficiencies during the cooling periods. Moreover, cooling towers are commonly available and easy to use as a retrofit. Hence, in both performance and cost bases, the cooling tower is a very viable and economical SHR system, even for residential applications.

The next SHR method was the optimization of the VCC by varying the suction superheat, condenser subcooling and mass flow rate of refrigerant. It was found that by using electronic control valves and controlling the previously mentioned parameters, up to 0.46 kW (1.57 kBtu/h) of power could be rejected from the refrigerant loop, which would in turn reduce the heat rejected into the ground. This reduction, however, was limited by the minimum amount of suction superheat that could be attained in practical application (value of 3.88°C/7°F). With advances in control valves and the use of variable speed compressors and flooded evaporators, the SHR potential of this method is very high.

The maximum operating limits of an expanded residential desuperheater was analyzed as a potential SHR device. During the cooling mode of operation, extracting 100% of the available superheat at the compressor discharge would amount to 1.91 kW (6.61 kBtu/h) of heat being removed from the refrigerant loop and thus reducing the water loop temperature rise at the heat pump condenser. This heat can be used to produce hot water, some of which can used to satisfy the domestic needs, while the remaining hot water generated can be stored or used for other purposes. However, using 100% of the superheat will reduce the pressures in the condenser and the effects of this reduction my limit the practicality of this method and must be analyzed further.

The last and probably the most novel idea was the application of thermosyphons to remove heat from the refrigerant loop. Analysis showed that the cost of using this system is prohibitively expensive, costing up to $ 30,000 to reject up to 5 kW (17 kBtu/h) of power during the cooling mode of operation of the heat pump. Another drawback is that while the analysis shows themosyphons to be technically feasible, these systems have not been implemented in warm regions like Texas. Hence, the cost of themosyphons are too large for residential application.

# Appendix A

Parameters used in Cooling Tower Model

$C_a = 1.006\ kJ/kgK$

$C_w = 4.186\ kJ/kgK$

- Table below gives yearly power rejection by cooling tower and heat pump, number of hours of operation and quantity of make-up water consumed.

| Year | Energy Rejected per year (kWhr) | | Total Energy Rejected per Year (kWhr) | Ratio (Cooling Tower/ Heat Pump) | Number of Hours of Operation per Year (hrs) | | Make up Water per Year (gallons) |
|---|---|---|---|---|---|---|---|
| | Cooling Tower | Ground Loop | | | Heat Pump | Cooling Tower | |
| 1 | 23,099 | 5,609 | 28,708 | 80.5 | 1,891 | 1,839 | 7,101 |
| 2 | 23,236 | 5,478 | 28,714 | 80.9 | 1,892 | 1,843 | 7,143 |
| 3 | 23,294 | 5,414 | 28,708 | 81.1 | 1,892 | 1,845 | 7,161 |
| 4 | 23,329 | 5,381 | 28,709 | 81.3 | 1,892 | 1,846 | 7,172 |
| 5 | 23,359 | 5,372 | 28,731 | 81.3 | 1,894 | 1,847 | 7,180 |
| 6 | 23,379 | 5,353 | 28,732 | 81.4 | 1,894 | 1,848 | 7,186 |
| 7 | 23,366 | 5,346 | 28,712 | 81.4 | 1,893 | 1,846 | 7,182 |
| 8 | 23,383 | 5,339 | 28,722 | 81.4 | 1,894 | 1,848 | 7,187 |
| 9 | 23,398 | 5,326 | 28,724 | 81.5 | 1,893 | 1,848 | 7,192 |
| 10 | 23,403 | 5,326 | 28,729 | 81.5 | 1,894 | 1,848 | 7,193 |

City of Austin, Texas – Austin Water Utility Rates

| Quantity (Gallons) | Cost ($) |
|---|---|
| 0 – 2,000 | 1.17 |
| 2,001 – 9,000 | 3.08 |
| 9,001 – 15,000 | 7.92 |
| 15,001 – 25,000 | 10.95 |
| 25,001 – over gallons | 12.19 |

# Appendix B

Operating Points of Heat Pump TT 049 [Climate Master]

| EWT (˚F) / (˚C) | Suction Pressure (kPa)/(psi) | Discharge Pressure (kPa)/(psi) | Suction Superheat (˚F)/(˚C) | Condenser Subcooling (˚F)/(˚C) |
|---|---|---|---|---|
| 70/21.1 | 937.9/136.1 | 1896.6/272.3 | 11.5/6.4 | 7.5/4.2 |
| 90/32.2 | 972.4/141.1 | 2496.6/362.3 | 9.5/5.3 | 6.5/3.6 |
| 110/43.3 | 1013.8/147.1 | 3151.7/457.4 | 9.5/5.3 | 5.5/3.1 |

| Load (kW) /($\frac{\mathbf{kBtu}}{\mathbf{h}}$) | $T_3$ (˚F)/(˚C) | $T_{3sat}$ (˚F)/(˚C) | $T_{2sat}$ (˚F)/(˚C) | $T_2$ (˚F)/(˚C) |
|---|---|---|---|---|
| 15.75 /53.74 | 79.1/26.18 | 86.7/30.38 | 86.7/30.38 | 138.8/59.34 |
| 14.06 / 47.9 | 100.2 /37.84 | 106.6/41.44 | 106.6/41.44 | 161.8/72.10 |
| 12.13 / 41.3 | 119 /48.31 | 124.5/51.41 | 124.5/51.41 | 188.8/87.10 |

| Load (kW) /($\frac{\mathbf{kBtu}}{\mathbf{h}}$) | $T_{w3}$ (˚F)/(˚C) | $T_{w3sat}$ (˚F)/(˚C) | $T_{w2sat}$ (˚F)/(˚C) | $T_{w2}$ (˚F)/(˚C) |
|---|---|---|---|---|
| 15.75 /53.74 | 70/21.10 | 70.3/21.30 | 78.9/26.05 | 80.7/27.03 |
| 14.06 / 47.9 | 90/32.20 | 90.3/32.38 | 97.9/36.61 | 100/37.75 |
| 12.13 / 41.3 | 110/43.30 | 110/43.47 | 116.6/47.01 | 119.2/48.45 |

Pinch Point = $T_w - T_{w3}$ = 5˚C (9˚F)

# Appendix C

Thermosyphon Working Fluid Properties

$T_v = 38^{\circ}C$
$P_{sat} = 1.468\ MPa$
$P_{atm} = 101.325\ kPa$
$\rho_l = 582.96\ kg/m^3$
$\rho_v = 11.36\ kg/m^3$
$Latent\ Heat = 1108.3\ kJ/kg$
$k_l = 0.4517\ W/mK$
$\mu_l = 124.74 * 10^6\ kg/m\ s$
$C_{pl} = 4920.5\ J/kgK$

Thermosyphon Fin Dimensions

$k_t = 401\ W/mK$
$b_n = .01\ m$
$s_n = 0.02\ m$
$\delta = 0.02\ m$
$r_2 = 0.15\ m$
$r_1 = 0.1\ m$
$\eta = 0.6$
$n = 50$

Air Properties

$k_a = .0257\ W/mK$
$\mathrm{Pr} = 0.72$

## Bibliography

Alaska Pipeline - http://en.wikipedia.org/wiki/Trans-Alaska_Pipeline_System

Alex H. W. Lee and J. W. Jones, “Analytical Model of a Residential Desuperheater”, Applied Energy, Vol 57, No4, pp 271 – 285, 1997

Alex H. W. Lee and Jerold W. Jones, “Thermal Performance of a Residential Desuperheater/Water Heater System” Energy Conversion Management, Vol 37, No 4, pp389 – 397, 1996

Chiasson A. D and Yavuzturk C., “A Design Tool for Hybrid Geothermal Heat Pump Systems in Cooling-Dominated Buildings”, ASHRAE Transactions 2009, vol. 115, part 2

City of Austin – Water Rates - http://www.ci.austin.tx.us/water/downloads/approvedservicerates2011waterretail.pdf

City of Austin, Water Rates - http://www.ci.austin.tx.us/water/downloads/approvedservicerates2011waterretail.pdf

Climate Control Fans - http://www.heatcraftrpd.com/products/PDF%5CCC%20Tech%20Bulletins%20Folder%5CCC-TB-C-AIRCOOLED-1-26.pdf

Climate Master – Performance Maps - http://www.climatemaster.com/share/Res_All_Products_CLM/Section_3_TT27.pdf

Copeland Compressors - http://www.emersonclimate.com/en-US/products/compressors/scroll_compressors/copeland_scroll_residential/Pages/CopelandScrollZRK5Compressor.aspx

Cullin, J. R. and Spitler, J. D., “Comparison of Simulation-based Design Procedures for Hybrid Ground Source Heat Pump Systems”, 8th International Conference on System Simulation in Buildings, Liege, December 13-15, 2010

DOE FEMP – Dual Source Heat Pump, Aug 2000 http://www.p2pays.org/ref/43/42888.pdf

EERE, 2011a - Geothermal Technologies Program – http://www1.eere.energy.gov/geothermal/geothermal_basics.html

EERE, 2011b - Geothermal Technologies Program - http://www.energysavers.gov/your_home/space_heating_cooling/index.cfm/mytopic=12640

EIA, 2011 - http://www.eia.gov/state/state-energy-profiles-data.cfm?sid=TX

Fanney A. H and Dougherty B. P., AHSRAE Transactions, 98, 489 (1992)

Fiore, G., “Geothermal: How it works,” http://www.gregfiore.com/s/%20Thermal/.htm, Accessed February 1, 2010.

Fisher, D. E. and Rees, R. J.. Modeling ground source heat pump systems in a building energy simulation program (EnergyPlus). In 9th International IBPSA Conference, pages 311-318, Montreal, Canada, August 2005.

Frozen Soil Barrier – Department of Energy, October, 1999

Gaspredes, Jonathan, “Development of an Integrated Building Load-Ground Source Heat Pump Model as a Test Bed to Assess Short- and Long-Term Heat Pump and Ground Loop Performance” Master’s Thesis, The University of Texas at Austin, 2011

Hackel, S., “Development of Design Guidelines for Hybrid ground-Coupled Heat Pump Systems”, Master’s Thesis, University of Wisconsin, Madison, May 2008

Hackel, S., G. Nellis, and S. Klein. 2009. Optimization of cooling-dominated hybrid ground-coupled heat pump systems. ASHRAE Transactions 115(1): 565-580.

Hasan, A and Siren, K, “Theoretical and computational analysis of closed wet cooling towers and its application in cooling of buildings”, Energy and Buildings, 34, 2002, Pg 477 – 486

He, X. Liu, S., Asada, H., and Itoh, H., “Multivariable Control of Vapor Compression Systems,” HVAC&R Research, vol. 4, no. 3, pp. 205– 230, 1998.

Jain, N. and Alleyne, A.G, “Thermodynamics-Based Optimization and Control of Vapor-Compression Cycle Operation: Optimization Criteria”, American control Conference, June 29 – July 01, 2011

Konopacki, S. and Akbari, H., “ Measured Energy Savings and Demand Reduction from a Reflective Roof Membrane on a Large Retail Store in Austin “http://www.osti.gov/bridge/servlets/purl/787107-U1Gpfp/native/ - Page 22

Larsen, L. and Thybo, C., “Potential energy savings in refrigeration systems using optimal setpoints,” in Conference on Control Applications, 2002.

Larsen, L. and Thybo, C., Stoustrup, J., and Rasmussen, H., “Control methods utilizing energy optimizing schemes in refrigeration systems,” in European Control Conference, 2003.

Mac Word, Allied Thermal Systems - http://www.alliedenergysystems.com/

Mike Hammond meeting, 2011

NPTEL – IIT Madras - http://nptel.iitm.ac.in/courses/Webcourse-contents/IIT%20Kharagpur/Ref%20and%20Air%20Cond/pdf/R&AC%20Lecture%2023.pdf

Office of Energy Efficiency, 2009 - http://oee.nrcan.gc.ca/publications/infosource/pub/home/heating-heat-pump/gsheatpumps.cfm

Olszewski. M. and Fontana. E. C., "Heat Pump Desuperheaters for Supplying Domestic Hot Water – Estimation of Energy Savings and Economic Viability for Residential Applications" – ORNL 1983

Qureshi, T. and Tassou, S., "Variable-speed capacity control in refrigeration systems," Applied Thermal Engineering, vol. 16, no. 2, pp. 103–113, 1996.

Ramamurthy, M., Jin, H., Chiasson, A. D., Spitler, J. D., "Optimal Sizing of Hybrid Ground-Source Heat Pump Systems That Use a Cooling Pond as a Supplemental Heat Rejecter— A System Simulation Approach "

Refrigeration and Air Conditioning", by W. F. Stoecker.

Sayyaadi, H. and Nejatolahi, M., "Multi-objective Optimization of a Cooling Tower Assisted Vapor Compression Refrigeration System," International Journal of Refrigeration, 2010.

Shiraishi, M., Kikuchi, K. and Yamanishi, T., "Investigation of Heat Transfer Characteristics of a Two-Phase Closed Thermosyphon", Heat Recovery Systems, Vol1, pp 287 – 297, 1981

Svensson, M. C. (1994). Studies on on-line optimizing control, with application to a heat pump. PhD thesis. Trondheim: Norges Tekniske Høgskole

Turbotec Desuperheaters - http://www.turbotecproducts.com/EPspecs.html

U.S. Dept. of Energy. Types of geothermal heat pump systems, February 2011a. - http://www.energysavers.gov/your_home/space_heating_ cooling/index.cfm/mytopic=12650.

US Energy Information Administration – http://www.eia.gov/energyexplained/index.cfm?page=electricity_factors_affecting_prices

Water Furnace – Heat Pump Performance Maps - http://www.waterfurnace.com/literature/synergy3d/SC1300YS.pdf

Xu, X., "Simualtion and Optimal Control of Hybrid Ground Source Heat Pump Systems", Doctoral Dissertation, Oklahoma State University, Dec 2007

Zhang, M., Lai, Y., Zhang, J., Sun, Z., "Numerical study on cooling characteristics of two-phased closed thermosyphon embankment in permafrost regions", Cold Regions and Technology, 65, (2011), 203-210

# Vita

Siddharth Balasubramanian was born in Mumbai, India. He completed his schooling in Chennai and then entered the Indian Institute of Technology, Madras to study Mechanical Engineering. After receiving a Bachelors degree in 2009, he went to the University of Texas at Austin, from where he received a Masters degree in Mechanical Engineering (with a specialization in Thermal Fluid Systems) in 2011. He is very passionate about new energy technologies and energy efficiency and plans to pursue a career in these fields. He can be reached at siddharthbala@utexas.edu.

This thesis was typed by Siddharth Balasubramanian